

# Material Characterization in the Microwave Range, When the Materials Become Composite, Reinforced, 3D-Printed, Artificially Mixed, Nanomaterials and Metamaterials

Plamen I. Dankov

Sofia University “St. Kliment Ohridski”, Faculty of Physics

(dankov@phys.uni-sofia.bg)

**Abstract**—The development of new artificial materials is a key issue of the modern world moving toward the 5G communication standard and Industry 4.0. Therefore, the characterization of these materials (determination of their key parameters) plays an important role. The dielectric and magnetic constants and their anisotropy can be measured in the microwave range; as integral characteristics, they give useful information for the whole sample and we have shown how they can depend on the sample composition, structure, inclusion orientation, fabrication technology, conditions for the sample growth and forming, etc. We present in this paper a summary of our concepts, models, measurement methodologies and measurement methods for extraction of the dielectric and magnetic parameters of different artificial materials, as a result of our experience in the material characterization in the Microwave Laboratory of the Faculty of Physics in Sofia University, Bulgaria. A set of useful examples is presented for the determination of the dielectric and magnetic parameters of big groups of artificial materials: reinforced substrates, 3D printed dielectrics, ceramics, multilayer radomes, foams, absorbers, gradient dielectrics and magneto-dielectrics, textile fabrics, metamaterials, carbon-containing materials, fresh plant tissues, plasmas, etc. A special circumstance in this research is the anisotropy of the considered materials (different permittivity and/or permeability in different directions), which is a very informative parameter and gives valuable additional information for the samples. We discuss in this paper the origin of the anisotropy of variety of materials, how to measure this parameter, how to use the anisotropy data in the design and simulations of microwave devices and antennas and how the anisotropy influences their main characteristics.

**Index Terms**—3D-printed dielectrics, absorbers, antenna radomes, artificial dielectrics, carbon-containing materials, ceramics, conductivity, composites, crystals, dielectric anisotropy, ferrites, metamaterials, microwave measurement methods, multiferoics, nano-materials, permeability, permittivity, substrates, textile fabrics

## I. INTRODUCTION

The new materials are a key issue of today's world. The mechanical and chemical engineers together with the physicists can construct now a variety of new artificial materials with quite specific properties, never met before in nature. As we mentioned in the title, the modern materials became reinforced, composite, 3D printed, mixed, nano-sized and meta-materials. First of all, these new materials will play a very important role for the realization of the current trends for automation and data exchange in manufacturing technologies within the modular structured smart factories or so-called fourth industrial revolution Industry 4.0. The second field of the modern materials' implementation is the forthcoming 5G/6G communication standards, which will ensure the ability of machines, devices, sensors and people to connect and communicate with each other via the Internet of Things (IoT) or Internet of People (IoP). The third important area of application of the new materials is the sustainable development of human societies. All these future processes in the development of human civilization explain the needs to develop materials with a variety of new properties and the needs to have reliable ways to characterize these unique properties.

The characterization of materials usually means to specify their properties by different chemical, mechanical, optical, spectroscopic, electric, magnetic and other methods. The determination of the electromagnetic (EM) properties is also important when the new materials can be used in the modern electronics, wired and wireless communications, sensor networks, for specific EM wave propagation, EM compatibility, optical and microwave imaging, etc. The EM properties of materials are connected mainly with their complex dielectric and magnetic constants and related parameters as conductivity, refractive index, wavelength, propagation constants, phase/group velocities of waves, attenuations, penetration depths, cut-off and threshold conditions, etc. in the EM structures, where these materials have been incorporated. Due to these reasons, today many materials, known with some of their traditional applications can be considered as electrodynamic media, e.g. textile fabrics as antenna substrates, bio-tissues as electronic

components, semiconductor structures as sensors for different macroscopic parameters of the environment, etc.

Our laboratory for Microwave material characterization has been orientated to determination mainly of the dielectric (and magnetic) properties of the modern artificial materials: 3D printed dielectrics, reinforced substrates, ceramics, multi-layer antenna radomes, foams, absorbers, gradient dielectrics and magneto-dielectrics, wearable textile fabrics, metamaterials, carbon-containing materials, liquids, fresh plant tissues, plasmas, ferrites, etc. We concentrated our research to determination of their dielectric anisotropy (different permittivity along different directions), which turned out to be a very informative parameter and could be bound with the sample composition, structure, inclusions' orientation, fabrication technology, conditions for sample growth and forming, etc.

In this review article originally published in [1] in two parts, we try to summarize the common issues of our many years' research work for characterization of different materials in the whole microwave range, including the mm-wavelength range. A poster with the same title was presented on the interactive University poster exhibition of the Asia-Pacific Microwave Conference APMC'2018 [2].

The article is conditionally divided into two parts. First of all, we present here a classification of the modern materials from an EM point of view, their main EM parameters and how these parameters could be bounded with the structure, inclusions and used fabrication technology. Especially, we discuss in the first part the origin of the different types of artificial anisotropy with examples. Then we describe the developed in the laboratory variety of measurement methods for characterization of the material parameters in the microwave range (0.5-40 GHz), including several authorship methods. We include also the proposed numerical models for reliable extraction of the material parameters from the obtained measurements results and discuss the basic principles and specific techniques for utilization of the commercial 3D EM simulators as auxiliary tools for extraction of the material parameters of the samples. In the second part of this paper, we illustrate our rich experience in the area of material characterization by presenting a lot of published and new concrete examples for determination of the parameters and specific properties of many commercial and unique artificial materials: reinforced substrates, ceramics and other crystal samples, multi-layer radomes, foams, absorbers, gradient dielectrics and magneto-dielectrics, textile fabrics, 3D printed dielectrics, metamaterials, carbon-containing materials, nano-composites, fresh plant tissues, plasma, ferrites, etc. Finally, we unify the common issues of these examples and present conclusions.

## II. MAIN ELECTROMAGNETIC PARAMETERS OF MATERIALS IN THE MICROWAVE RANGE AND HOW THEY CAN BE USED FOR MATERIAL CHARACTERIZATION AND TECHNOLOGY CONTROL

### A. Classification of Modern Materials

From the electrodynamic point of view, the materials could be characterized on the base of their response on the presence of EM fields in each considered electrodynamic

system, where these materials have been incorporated. This response is determined by the properties of the materials, described by defining macroscopic scalar complex parameters: dielectric constant (permittivity)  $\varepsilon = \varepsilon_r \varepsilon_0 = (\varepsilon'_r - j\varepsilon''_r) \varepsilon_0 = \varepsilon_0 \varepsilon'_r (1 - j\tan\delta_\varepsilon)$  and magnetic constant (permeability)  $\mu = \mu_r \mu_0 = (\mu'_r - j\mu''_r) \mu_0 = \mu_0 \mu'_r (1 - j\tan\delta_\mu)$  of these materials ( $\varepsilon_0, \mu_0$  – absolute material constants of the vacuum;  $\tan\delta_\varepsilon, \tan\delta_\mu$  – dielectric and magnetic loss tangents; details in the next section). The real parts of the relative parameters ( $\varepsilon'_r, \mu'_r$ ) can have as positive, as well as negative values for different materials. Exactly this circumstance is the basis for the nowadays classification of modern materials [3, 4]. First of all, most of the standard dielectrics and some magneto-dielectrics fall in the group of double-positive (DPS or right-hand) materials, for which  $\varepsilon'_r > 0; \mu'_r > 0$ . They still are the most occurring electrodynamic media in modern electronics. The other two media are also well-known from nature: a group of the “epsilon“-negative (ENG) materials –  $\varepsilon'_r < 0; \mu'_r > 0$  and a group of the “mu“-negative (MNG) materials –  $\varepsilon'_r > 0; \mu'_r < 0$ . Many plasma media (ENG) and ferrites (MNG) at certain frequency intervals in external dc magnetic fields fall in the last two groups. The fourth group represents the double-negative (DNG or left-hand) materials –  $\varepsilon'_r < 0; \mu'_r < 0$ ; this is the class of the most rapidly developing engineering artificial materials and negative reflective index metamaterials with very specific and extra-ordinary properties, not existing in nature, which gives us the right to call them 21<sup>st</sup> century electromagnetic and photonic materials, as it is pointed in [5].

### B. Dielectric and Magnetic Properties of Materials

The complex permittivity  $\varepsilon_r$  of the materials in the microwave region varies between the static (dc) value  $\varepsilon_{dc}$  at very low frequencies (including  $\omega = 2\pi f = 0$ ) up to the optical value  $\varepsilon_\infty$  at very high frequencies according to the empirical Cole-Cole model [6], often used to describe the dielectric relaxation in the water and polymers

$$\varepsilon_r \equiv \varepsilon_\infty + \frac{\varepsilon_{dc} - \varepsilon_\infty}{1 + (j\omega\tau)^{1-\alpha}}. \quad (1)$$

Exactly due to this reason the “microwave” complex permittivity  $\varepsilon_{MW} = \varepsilon_r$  of the materials could be enough informative parameter for the relaxation mechanism understanding, specific sample structure, used inclusions and other properties of the materials ( $\omega$  is the angular frequency,  $\tau$  – relaxation time;  $\omega_r = 1/\tau$  – relaxation frequency;  $\alpha$  is a parameter between 0 and 1;  $\alpha = 0$  describes pure Debye relaxation model;  $\alpha > 0$  – stretched relaxation model).

From a more common point of view, the “permittivity  $\varepsilon$  is a measure of how an electric field affects, and is affected by a dielectric medium, and is determined by the ability of a material to electrically polarize in response to the field, and thereby reduce the total electric field inside the material” [7]. It is directly related to electric susceptibility  $\chi_e$ , which is a measure of how easily a dielectric polarizes in response to an electric field. They are related to each other through expression  $\varepsilon_r = (1 + \chi_e)$ , where  $\varepsilon_r$  is a scalar quantity in the simple case of linear, homogeneous and isotropic materials, while

for anisotropic medium, the permittivity is a tensor  $\tilde{\varepsilon}_r$ .

By similar considerations, the permeability  $\mu$  is the degree of magnetization that a material obtains in response to an applied external magnetic field. The relative permeability  $\mu_r = (1 + \chi_m)$  is related to the magnetic susceptibility  $\chi_m$ , which is sometimes called volumetric or bulk susceptibility, to distinguish it from  $\chi_p$  (magnetic mass or specific susceptibility) and  $\chi_M$  (molar or molar mass susceptibility). Again,  $\mu_r$  is a scalar quantity for linear, homogeneous and isotropic magnetic materials, while when the medium is anisotropic (gyrotropic), the permeability is a tensor  $\tilde{\mu}_r$ .

In general, as the permittivity  $\varepsilon_r(\omega)$ , as well as the permeability  $\mu_r(\omega)$ , are not constants; they both can vary with the local position in the medium, sample form (depolarization, demagnetization), the frequency of the fields applied (electric/magnetic), humidity, temperature, and other parameters. In the non-linear media, they may depend on the strength of the electric/magnetic field.

Most of the modern artificial materials could be considered as mixtures between two or more isotropic components. In this case, very important is the homogenization of the resultant material, which can be described by effective (we prefer to use the term “equivalent”) dielectric or magnetic constant ( $\varepsilon_{eq}$ ;  $\mu_{eq}$ ). The process of homogenization is possible to a certain extent degree [8] if the characteristic length of the non-resonant inclusions in the mixture is sufficiently smaller than the wavelength  $\lambda$  at the operating frequency (typically less than  $\lambda/10$  to  $\lambda/1000$ ). There exist many different technologies to mix two dielectrics: series, parallel, series-parallel; layered, dispersed (uniform or random), pillar, impregnated, foamed, woven, knitted, by additive or subtractive technology, etc. The question is how to calculate the resultant effective/equivalent parameters of the mixed material. A set of empirical formulas exist [9]; one of the earlier approximations is the well-known Maxwell-Garnett expression [7], when the mixture is got from small spherical dielectric inclusions of permittivity  $\varepsilon_2$ , embedded in a host environment medium of permittivity  $\varepsilon_1$ .

$$\varepsilon_{eq} = \varepsilon_1 + 3V_2\varepsilon_1 \frac{\varepsilon_2 - \varepsilon_1}{\varepsilon_2 + 2\varepsilon_1 - V_2(\varepsilon_2 - \varepsilon_1)}, \quad (2)$$

where  $V_2$  is the normalized volume fractions of the inclusions; the total volume is  $V_1 + V_2 = 1$ . More close to the reinforced microwave substrates, textile fabrics, 3D printed and layered composites is the Wiener formula for laminar mixtures [10]

$$\frac{1}{\varepsilon_{eq} + u} = \frac{V_2}{\varepsilon_2 + u} + \frac{V_1}{\varepsilon_1 + u}; \quad 0 \leq u \leq \infty, \quad (3)$$

where the parameter  $u$  depends on the orientation between the layers, namely:

$$\frac{1}{\varepsilon_{eq}} = \frac{V_2}{\varepsilon_2} + \frac{V_1}{\varepsilon_1}; \quad u = 0; \quad (3.1)$$

$$\varepsilon_{eq} = \varepsilon_2 V_2 + \varepsilon_1 V_1; \quad u = \infty \quad (3.2); \quad u = \sqrt{\varepsilon_2 \varepsilon_1} \quad (3.3)$$

for series layers (Reuss bound) (3.1); for parallel layers (Voigt bound) (3.2) and for isotropic mixtures with randomly arranged grains (Bruggman formula) (3.3) – see the illustration curves in Fig. 2.1a,b [A52].

The effective (or equivalent) media models are very important for the characterization of the different mixed dielectrics. They present the difference between the pure parallel and pure perpendicular to the E-field direction dielectric inclusions. There exist two main ways to realize multi-component isotropic (homogenized) dielectrics with well-designed dielectric constant: 1) by random mixing (as for the foams) or 2) by constituents with similar dielectric parameters (as for same microwave substrates and woven/ knitted textile fabrics). However, in the case of 3D printing, these methods are not technologically applicable; here we should use symmetrical unit cells for the infilling medium (see IV).

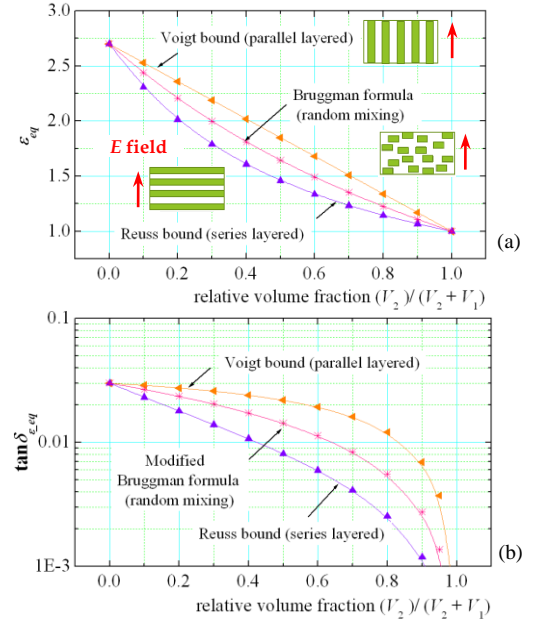


Fig. 2.1. Minimal and maximal bounds for the resultant equivalent dielectric constant (a) and dielectric loss tangent (b) of two mixed dielectrics

The next step for generalization of the concept for the EM material constants is the introducing of resonance effects in the permittivity and permeability behaviour. In the dielectric materials, the charges are displaced by an incident electric field. The amplitude is given by the restoring forces on the electrons and depends strongly on the time-variation of the field and this dipole (formed by the displaced electrons and the remaining ion) will oscillate. For frequencies around a certain frequency  $\omega_0$  the induced dipole moment might be very large and strongly depend on the frequency. This increasing interaction (called “resonance”) of the incident EM field with the structure will lead to strong scattering and absorption. The behaviour of the oscillating dipole can be described on the base of a simple driven harmonic oscillator and the solution gives the known relation between the polarization  $P$  and electric field  $E$  expressed by the electric susceptibility  $\chi_e$ , namely  $P = \varepsilon_0 \chi_e E$ . The solution to the differential equation describing forced resonance is governed by a complex Lorentzian function. Taking in mind that the electric displacement  $D$  is related to the polarization density

$P$  by  $D = \epsilon_0 E + P = \epsilon_0(1 + \chi_e)E = \epsilon_r \epsilon_0 E$ , the effective (or equivalent) resonance dielectric constant by the Lorentz model is [7, 8]:

$$\epsilon_{eq}(\omega) = 1 + \frac{\omega_p^2}{\omega_0^2 - \omega^2 - j\omega\gamma_e}; \quad \omega_p^2 = \frac{Nq^2}{\epsilon_0 m_e}, \quad (4)$$

in which  $\omega_0$  is the natural resonance frequency,  $\omega$  is the operating frequency,  $\omega_p$  is the so-called plasma frequency and  $\gamma_e$  is the damping factor in [loss/s] (here also  $N$  is the number of atoms per unit volume,  $q$  is the unit charge,  $m_e$  is the effective electron mass). This model can be generalized for multiple resonances.

By a similar way, a Lorentz model can be introduced for permeability [11]:

$$\mu_{eq}(\omega) = 1 + \frac{F\omega^2}{\omega_{m0}^2 - \omega^2 - j\omega\gamma_m}, \quad (5)$$

where now  $\omega_{m0}$  is the magnetic resonance frequency (when the magnetic element is the widely used for metamaterials' construction split-ring resonator SRR [12]),  $\gamma_m$  is the magnetic damping factor, and  $F$  is a parameter that depends on the loop gap in the SRR.

Both expressions (4, 5) show that the materials can have at some frequency intervals either positive or negative values for the effective/equivalent dielectric and magnetic constants, or even double negative values (DNG) – see examples on Fig. 2.2a,b. This approach is widely used in modern metamaterial design [13]. Due to these reasons, some other parameters, which describe the metamaterials, can have anomalous behaviour. For example, the refractive index  $n$  may obtain negative signs for some metal-containing metamaterials [8] (for isotropic and linear media the simple expression is  $n = \sqrt{\epsilon_r \mu_r}$ ).

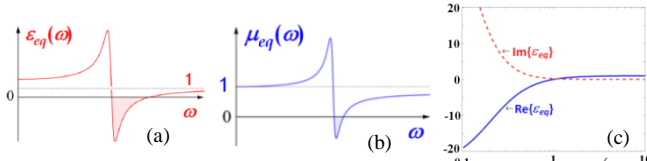


Fig. 2.2. Illustration of possible frequency behaviour of the real effective (equivalent) dielectric  $\epsilon_{eq}$  or magnetic  $\mu_{eq}$  constants for (a) artificial dielectrics and (b) artificial magnetics with resonance behaviour; (c) the real (solid blue) and imaginary (dashed red) parts of the relative permittivity as functions of frequency of sample material following the Drude model

For the special case of metals, the Lorentz model transforms into the Drude model. In metals, most electrons are free because they are not bound to nuclei (the restoring force is negligible and the natural frequency  $\omega_0 = 0$  in (4)); therefore they will oscillate harmonically under the influence of an incident EM wave and this can be described by an oscillating current density  $J = \sigma E$  (for linear media), where  $\sigma$  is the conductivity. Taking in mind the relations between the polarization  $P$ , current  $J$  and electric field  $E$  [7], we can introduce a more common definition for the relative equivalent permittivity (so-called relative generalized permittivity  $\hat{\epsilon}_{eq}(\omega)$ ):

$$\hat{\epsilon}_{eq}(\omega) = \epsilon_{eq}(\omega) - j\sigma_{eq}(\omega)/\omega, \quad (6)$$

where the equivalent complex quantity  $\epsilon_{eq}(\omega)$  measures the polarization response due to bound charges, and  $\sigma_{eq}(\omega)$  is the equivalent conductivity, taking in mind the response of the free charges. Thus, the generalized permittivity in conductors has a large imaginary part (the second term in (6)) and this means that the losses are large. But this also means that the penetration depth  $\delta$  of the EM waves into the sample surface is small. The fields attenuate rapidly within the conductor and the fields are confined to a thin surface layer; this allows the definition of surface current and surface impedance, often used by the electronics and electrical engineers. Fig. 2.2c displays the frequency behaviour of the permittivity in the Drude model. As can be seen, at low frequencies the imaginary part dominates the response. Indeed, the typical conductivity behaviour for metals at low frequencies  $\hat{\epsilon}_{dc}(\omega) \rightarrow -j\sigma_{dc}(\omega)/\omega$  is included in the Drude model in the limit  $\omega \rightarrow 0$ , and the limit for the dc conductivity is  $\sigma_{dc} = \omega_p^2 \epsilon_0 / \gamma_e$ . The Drude model is often used to describe the optical properties of noble metals, from which most optical metamaterials are made.

All the considered approximations, models and expressions above clearly show that the material constants are well determined by the overall structure of the samples and their interaction with the EM waves, by the type of components in the resultant complex mixtures, by orientation and position of the building blocks and applied technology. The specific integral character of the equivalent material constants ( $\epsilon_{eq}$ ,  $\mu_{eq}$ ) gives a potential to ensure additional information for the material properties to the results, already obtained by different local methods (e.g. spectroscopy, SEM images, scanning electron microscope, etc.) that are widely used for their characterization. In this paper, we concentrate our efforts exactly over the reliable characterization of the material constants (mainly permittivity) in the microwave range as an EM representative of the materials in different electrodynamic projects. Moreover, the EM response depends also on the material anisotropy.

### C. Anisotropy and Its Origins in the Modern Materials

The EM anisotropy of a given material can be expressed as the existence of different dielectric and magnetic constants in different directions. The reasons could be quite different. The microwave and optical engineers usually connect the anisotropic behaviour with the microwave ceramics and optical-glass lenses; this is one of the oldest known types of material anisotropy, named *crystalline anisotropy* for single- or poly-crystalline materials (optical glasses, ceramics, artificial soft and low-temperature co-fired ceramics LTCC, liquid crystals, etc.). In principle, these materials are homogeneous, but the anisotropy appears due to the existence of different crystallographic axes in the lattices and the fact that charges oscillate differently along these directions. This anisotropy is usually relatively strong. Our early investigations were connected exactly with this type of anisotropy of ceramic disks, cylinders, rings and rods by different microwave methods [A1, A2, A5-A7]. Then, the characterization of crystalline and crystalline-like materials continued by the two-resonator method [A34, A53, A56].

Another specific group of plasma/ferrite researchers identify the original concept for the material anisotropy with the electric or magnetic gyrotropy of gaseous or solid-state plasmas (gyro-electric) and ferrites (gyro-magnetic), all in external dc magnetic biasing fields. These phenomena belong to the so-called *induced anisotropy*; the dielectric and magnetic properties of such natural metamaterials have been described with non-symmetric tensors of the permittivity and permeability (including non-diagonal components, controllable by the external dc biasing magnetic field). The ferroelectric materials and films can also be associated with this group of electrically gyrotropic materials but in the external dc electric biasing field. In our early investigations, we performed a lot of attempts for difficult characterization of the microwave ferrites with different forms: disk, rod, cylinder, prism [A1, A2, A5]; we applied successfully these results in our models and methods of design of different gyrotropic devices – circulators and isolators (see the review papers [A3, A4]). Special types of investigations were devoted to ferrite and magneto-dielectric thin films [A15, A16, A23] and microwave absorbers [A10, A11, A28, A50]. Our contribution to the characterization of gaseous plasma media was connected with the development of classical and new types of hairpin resonance probes for the determination of plasma density [A27, A35, A37].

Nowadays, a new class of artificial materials appeared, for which the measured anisotropy could be considered more as an undesired property. First of all, in this group, we can add the commercial engineered reinforced substrates with many applications in the modern RF and microwave electronics. Characterization of the *dielectric anisotropy* of such popular materials is very important for the reliability of the modern design of different planar structures on high-frequency substrates, especially in the mm-wavelength range. Our research is connected mainly with the characterization of these commercial materials ([A8-A10, A12, A13, A17, A18, A20-A22, A24, A26, A30-A32, A34, A36, A41, A43, A44]). In our practice, we measured a lot of reinforced substrates from different manufacturers, which anisotropy varies in a wide range: from ~1-2 % up to 25 % (see below for this parameter) [A31]. The anisotropy of similar structures has been caused by the *spatial inhomogeneity* in different directions between the mixed reinforcing fibres net and the applied filling. To this group of anisotropic materials we can add the textile fabrics [A48] used for wearable antennas, multilayer antenna radomes [A14, A19, A25], some 3D printed dielectrics [A46, A52, A53] (see sections IV, VI).

The *controllable anisotropy* of the engineered metamaterials and “bandgap” materials (i.e. controllable dielectric constants in different directions) is another new type of artificial anisotropy [8, 14], caused by the chosen shape, geometry, size, orientation and arrangement of the unit cells, which form the “lattice” of the artificial materials. Extremely big could be the anisotropy of metamaterials with metal inclusions. Therefore, it is very similar by origin with the anisotropy, caused from the *inhomogeneity* of the reinforced and composite samples, but now this property is well-designed and fully desired, because it ensures unusual characteristics of some anisotropic metamaterial devices

[16]: invisible cloaks, wave concentrators and converters, superlenses, special sensors, etc. We already started characterization of such metamaterials with big anisotropy [A47, A51] (see section VII).

Let's consider the terminology, related to the anisotropy. In the common case, the anisotropic/gyrotropic materials are describing by full tensors; the material tensors are non-symmetrical for ferrites and plasma [8] but they will not be considered in the paper. There exist three cases of so-called dielectric anisotropy of the artificial materials, which dielectric constants can be described by diagonal tensors, namely: *biaxial* (7.1) and *uni-axial* anisotropy (7.2) or *pure isotropy* (7.3) (similar expression could be written for the magnetic constants; e.g. for ferrites, multiferoics, etc):

$$(\hat{\varepsilon}_r) = \begin{pmatrix} \varepsilon_{xx} & 0 & 0 \\ 0 & \varepsilon_{yy} & 0 \\ 0 & 0 & \varepsilon_{zz} \end{pmatrix} \quad (7.1);$$

$$(\hat{\varepsilon}_r) = \begin{pmatrix} \varepsilon_{par} & 0 & 0 \\ 0 & \varepsilon_{par} & 0 \\ 0 & 0 & \varepsilon_{perp} \end{pmatrix} \quad (7.2);$$

$$(\hat{\varepsilon}_r) = \begin{pmatrix} \varepsilon_r & 0 & 0 \\ 0 & \varepsilon_r & 0 \\ 0 & 0 & \varepsilon_r \end{pmatrix} \quad (7.3)$$

where  $\varepsilon_{xx} \neq \varepsilon_{yy} \neq \varepsilon_{zz}$ ;  $\varepsilon_{par} = \varepsilon_{xx} \approx \varepsilon_{yy}$ ;  $\varepsilon_{perp} = \varepsilon_{zz}$ ;  
 $\varepsilon_r \approx \varepsilon_{xx} \approx \varepsilon_{yy} \approx \varepsilon_{zz}$

Typical biaxial anisotropic materials are the crystals, optical glasses, liquid crystals, some nanocomposites, many metamaterials with non-symmetrical unit cells, 3D printed dielectrics, tick textile fabrics, plant and other bio-tissues, which can be described with three different scalar dielectric constants along the axes  $O_x$ ,  $O_y$  and  $O_z$ . The uni-axial anisotropy has been expressed in relatively thin structures with plane symmetry, e.g. materials like the reinforced substrates, hard or soft artificial ceramics, LTCC's, multi-layer antenna radomes, some polymers, gradient dielectrics and absorbers. The near-to-isotropic behaviour is a property of the well-homogenized and foam-like materials and metamaterials: foams, bulk plastics, injection-moulded dielectrics, non-woven substrates, foamed absorbers, etc. In the next sections of this paper, we will consider many concrete examples.

Finally, the so-called magneto-electric materials appear among modern artificial materials [7, 16]. The common issue for these materials is the magneto-electric coupling; now, the complex electric and magnetic flux densities  $\vec{D}$  and  $\vec{B}$  in the so-called bi-anisotropic magneto-electric materials can be expressed as

$$\vec{D} = (\hat{\varepsilon})\vec{E} + (\hat{\xi})\vec{B} \quad (8.1) \text{ and } \vec{B} = (\hat{\mu})\vec{H} + (\hat{\zeta})\vec{E} \quad (8.2)$$

where  $(\hat{\varepsilon})$ ,  $(\hat{\mu})$  are the permittivity and permeability tensors, while  $(\hat{\xi})$ ,  $(\hat{\zeta})$  are tensors of the corresponding magneto-electric coupling coefficients. When the parameters  $\varepsilon$ ,  $\mu$ ,  $\xi$ ,  $\zeta$  are scalars, the materials become bi-isotropic. The above

relations show that the equivalent permittivity in such materials can depend not only on the response to the E field but also on the response to the H field in the considered media (v.v. for the equivalent permeability). We already managed to characterize in our practice such samples [A51, A58-A61], but this research is in the beginning.

#### D. Numerical Methods for Estimation of the Dielectric Anisotropy of Artificial Materials

The discussions in the previous section express the significance of anisotropy for each complex material, not only for metamaterials. Therefore, it is important to predict the degree of anisotropy in different materials, but this is not possible in all cases. Full-wave analysis of anisotropic structures is possible in a few simple cases. The crystalline type of anisotropy can be bound to the lattice symmetry – isotropy for crystals with cubic symmetry; uniaxial anisotropy – with hexagonal, tetragonal symmetry; biaxial anisotropy – with monoclinic, triclinic, orthorhombic symmetry [8]. Another very popular model for crystalline anisotropy in high- $\epsilon$  ceramics is based on the lumped-element approach: the building blocks as electric dipoles can be considered at the macroscopic level as a set of parallel or series capacitors (for example see the expressions 3.1-2), but the calculated anisotropy is usually bigger than the measured one. Unfortunately, the other effective-media expressions for the resultant permittivity in different mixtures cannot give the actual anisotropy [9, 10]. There exist also attempts to bind the degree of symmetry of the unit cells for evaluation of the all-dielectric 3D printed metamaterials [8, 14]. Of course, the numerical simulations by the nowadays 3D EM simulators are also wide-spread; many microwave and optical engineers successfully apply this approach, and therefore, the big software developers pay increasing attention the new versions of the commercial 3D simulators to may fluently “cope” with the metamaterials.

In [A46, A48, A52], we proposed a numerical method for reliable prediction of the dielectric constants of artificially-constructed materials (including all-dielectric metamaterials or even samples with metal inclusions) along all three axes in the Cartesian system by resonance method in desired frequency intervals. The idea of this method is to build a well-designed unit cell, to reproduce it in a hosting isotropic substrate and to put the whole sample in a rectangular resonator (Fig. 2.3), which supports TE and TM modes with three mutually perpendicular directions of the E fields – see illustrations in Fig. 2.4. Independent extraction of the resultant dielectric constant along all three axes is possible after replacing of the bi- or uni-anisotropic sample under interest with an equivalent isotropic sample. We successfully applied the described method for many artificial samples: textile fabrics [A47], 3D printed dielectrics [A52, A54], metamaterials with surface metal inclusions [A46, A51]. Different unit cells could be used for these numerical investigations: spheres, cubes, cylinders, prisms, disks and some combinations between them, made by isotropic dielectrics or by metals. We use for a quantitative measure of the resulting dielectric constant/loss tangent anisotropy (parameters  $\Delta A_\epsilon$ ,  $\Delta A_{\tan \delta}$ ) for bi-/uni-axial anisotropy the following expressions

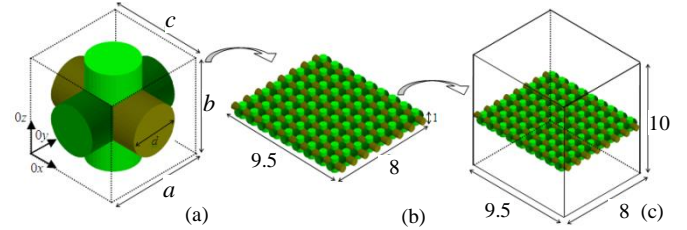


Fig. 2.3. (a) Universal unit cell with cylinders; (b) constructed artificial sample with repeated unit cells (inclusions) in a hosting isotropic substrate; (c) artificial sample in a rectangular resonator

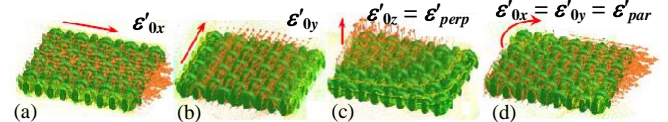


Fig. 2.4. Rectangular resonator with an artificial sample (knitted fabrics), which supports different modes with mutually perpendicular E fields along the axes: (a) 0x; (b) 0y; (c) Oz and (d) in plane 0xy

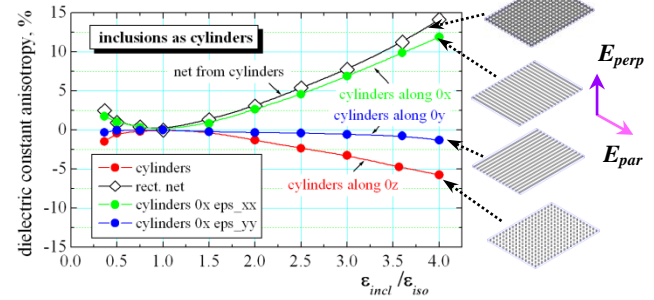


Fig. 2.5. Dielectric constant anisotropy of artificial nets from simple inclusions as regular cylinders, orientated along axes 0x, 0y, 0z or in plane 0xy; the E-fields' orientation is fixed either along x ( $E_{par}$ ) or along 0z ( $E_{perp}$ )

$$\Delta A_{\epsilon,0x/y} = 2(\epsilon'_{0x/y} - \epsilon'_{0z}) / (\epsilon'_{0x/y} + \epsilon'_{0z}), \quad (9.1)$$

$$\Delta A_{\tan \delta,0x/y} = 2(\tan \delta_{\epsilon,0x/y} - \tan \delta_{\epsilon,0z}) / (\tan \delta_{\epsilon,0x/y} + \tan \delta_{\epsilon,0z}) \quad (9.2)$$

The dependencies for  $A_\epsilon$ , % versus the ratio  $\epsilon_{incl}/\epsilon_{iso}$  in Fig. 2.5 well illustrate a simple but informative case for anisotropy prediction: inclusions as dielectric cylinders with permittivity  $\epsilon_{incl}$  orientated along the axes 0x, 0y or 0z, keeping the E fields parallel or perpendicular to the sample surface by exiting fixed mode in the rectangular resonator ( $\epsilon_{iso}$  is the permittivity of the hosting isotropic medium). The simulations show that the resultant permittivity  $\epsilon_{par,0x}$  of the artificial mixture increases along the cylinders when the E field is orientated along the same axis, in comparison to the dielectric constant  $\epsilon_{par,0y}$ , perpendicularly to the cylinder axis. This effect increases the anisotropy  $A_{\epsilon,0x}$  of the whole artificial substrate along the cylinder axis with the rise of ratio  $\epsilon_{incl}/\epsilon_{iso}$ , while the anisotropy  $A_{\epsilon,0y}$  is close to zero. The effect of anisotropy for  $\epsilon_{incl} \gg \epsilon_{iso}$  increases for a “fishnet” of cylinders. The positive  $\Delta A_\epsilon$  sign means that  $\epsilon_{par} > \epsilon_{perp}$ , while the negative sign – that  $\epsilon_{par} < \epsilon_{perp}$ . The last effect happens, when the cylinders are orientated perpendicularly to the sample. The presented above investigations have been not published yet, however, we confirmed numerically and experimentally the described rules for anisotropy of textile fabrics [A48], reinforced substrates [A31], multilayer antenna radomes [A14, A25], 3D printed dielectrics [A54], metamaterials [A46]. Similar investigations are helpful for

the design of homogenized and near-to-isotropic 3D printed dielectrics for antenna applications [A52].

### III. METHODS FOR EXPERIMENTAL CHARACTERIZATION OF DIELECTRIC PARAMETERS OF MATERIALS IN THE MICROWAVE RANGE (INCLUDING THEIR ANISOTROPY)

Nowadays, a lot of measurement methods exists for characterization of artificial materials, some of them proposed as reference ones (approved from the leading world standardization organizations as IPC, NIST, NPL [17-19]), or developed by different Universities and scientific research organizations. This is a world wealth, nevertheless that some methods can give more or less different results for the same materials. Three types of methods can be classified in the microwave range: free-space, waveguide (transmission-line) and resonance methods – Fig. 3.1a-d. The first two are considered as broadband, but less accurate methods, while the resonance methods are specified as more accurate, but narrowband ones. A good survey of the microwave methods for material characterization has been done in [20]. We consider selectively in this paper the promising methods with an accent to these, which can measure anisotropy and have been already realized in the Microwave Lab in the Faculty of Physics of Sofia University “St. Kliment Ohridski” [1, 2].

#### A. Resonance Methods

Definitely, the resonance methods are considered more accurate than the transmission-line methods [21]. The main reason is the fact that the sample under interest is a part of a bigger resonance area (Fig. 3.1d) and its dielectric and/or magnetic constants influence relatively strongly the resonance parameters of the excited modes – resonance frequency  $f_0$  and unloaded quality factor  $Q_0$  of the empty resonator, shifting them to  $f_e$  and  $Q_e$ , when the sample is placed inside (in the case of volume resonators; in other cases the sample itself could be a high-Q resonator). The big accuracy is achieved since the frequency or frequency differences can be measured with smaller errors in the microwave range, typically less than 0.01% in the X band. However, other factors can decrease the measurement accuracy, e. g. actual sample shape and sizes, sample positioning in the resonator, environmental factors, etc. Our short survey of the resonance methods is concentrated over their ability to measure the sample anisotropy, considering the expressions (9.1-9.2).

A measuring resonator can react to the sample biaxial anisotropy if it supports at least three independent modes with mutually perpendicular E (or H) fields along the Cartesian axes  $0_x$ ,  $0_y$  and  $0_z$  in a given frequency interval. A good illustration is the resonance perturbation method [22], suitable for characterization of the biaxial anisotropy of liquid crystal polymers (LCP), which have substantial potential for application in the modern microwave electronics. The method uses three waveguide modes  $TE_{011}$ ,  $TM_{120}$  and  $TE_{101}$  with mutually perpendicular E-field orientations in a non-standard rectangular cavity to extract the permittivity values  $\epsilon_{xx}$ ,  $\epsilon_{yy}$  and  $\epsilon_{zz}$ . We apply rectangular resonators made by standard waveguides that support dominant modes  $TE_{10p}$  ( $p = 1-6$ ), to extract either dielectric or magnetic parameters of microwave absorbers (Fig. 3.2).

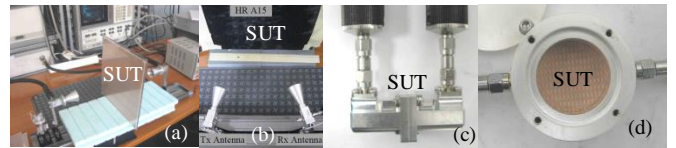


Fig. 3.1. Three popular methods used for characterization of flat samples under test (SUT): (a) free-space method in transmission regime; (b) in reflection regime; (c) waveguide method; (d) resonance method

Due to the coarse character of the known perturbation expressions [20], we apply more accurate 3D simulations.

The volume resonators also have good potential to determine the sample anisotropy, but there is no universal solution. The parallel dielectric parameters  $\epsilon_{par}/\tan\delta_{\epsilon,par}$  can be measured by TE-mode resonators (as R1 in Fig. 3.3a) (classical Courtney’s method [23], Kent’s evanescent-mode tester [24], split-cylinder resonator SCR [25], split-post dielectric resonator [26], etc.). The perpendicular parameters  $\epsilon_{perp}/\tan\delta_{\epsilon,perp}$  can be estimated by TM-mode resonators (as R2) (e.g. as in [A21, 27], reentrant cavities [28]). In fact, only a few publications have been directly dedicated to anisotropy measurements. Whispering-gallery modes with high-azimuthal index in a single dielectric resonator with fields far from the screens could be used for anisotropy measurement of ultra and extremely low-loss materials [29]. The method presented in [30] is based on resonance measurements of one prism sample in three mutually perpendicular orientations in a rectangular resonator (as in [A53, A56] for cylindrical resonators). Very important is the problem for reference determination of the proven dielectric anisotropy of the commercial microwave substrates, because the reference IPC TM-650 2.5.5.5 [17] (clamped stripline resonator test method) cannot give this parameter. The modified IPC TM-650 Bereskin’s method [31] is difficult for realization (many substrates have to be stacked horizontally and then a single sample has to be produced by a vertical cut); only a few substrate producers apply this method. Nowadays, a broadband method is proposed [32], based on numerical extraction of the parallel and perpendicular dielectric constants from data for the even and odd modes in coupled microstrip resonators printed on the substrate under test. However, the authors make a wrong conclusion about the ability to determine the parallel permittivity of a substrate (in fact, they determine the so-called design or microstrip-like value and this is proven by our measurements). Similar to the Bereskin’s method (in stripline geometry) is the method, proposed in [33] and implemented by substrate-integrated waveguide (SIW) resonators. The novelty here is the possibility to increase the working frequency up to mm-wavelength range. A common disadvantage of the methods, based on the printing of measurement resonators on the substrate under test, is the difficult extraction of the dielectric loss tangent of raw substrates by taking into account the influence of the quality of metallization (the problem is discussed in IIIC). Recently, a new TM-mode method (balanced-type circular disk resonator [34, 35]) shows big potential for characterization of the perpendicular dielectric parameters of flat samples up to 110 GHz (now reliable results have been obtained in the interval 20-70 GHz). We just started to develop this method to help substrate anisotropy measurements.

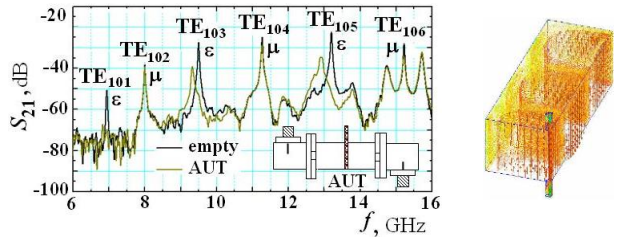


Fig. 3.2. Perturbation resonance method for determination of dielectric and magnetic parameters of microwave absorbers under test (AUT). Inset: simulated E-field distribution of the TE<sub>105</sub> mode in  $\frac{1}{2}$  part of the resonator

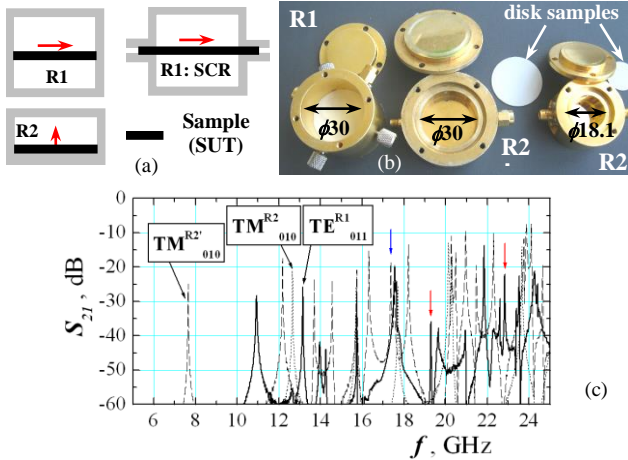


Fig. 3.3. (a) TE- (R1; SCR) and TM-mode (R2) cylinder resonators; (b) pairs with equal diameters  $\phi 30$  mm (R1&R2') or with close resonance frequencies (R1&R2); (c) mode spectrum in R1 and R2 resonators (0-25 GHz)

#### B. Characterization of the Dielectric Anisotropy by the Two-Resonator Method and Its Modifications

In 2000-2002 we first detected the dielectric anisotropy of commercial microwave substrates and developed an authorship method for its determination – the two-resonator method [A21]. Our first publications [A6, A10] have been based on a perturbation approach, but then we developed more accurate full-wave analytical models of the measurement resonators and for the extraction procedure of the complex dielectric constants of uni-axial anisotropic single and multilayer samples [A17, A21, A26]. Applying this method we managed to accumulate in a short period (2004-2008) a tremendous amount of data for the real anisotropy on many commercial substrates from different producers (used in our antenna projects [A29, A33, A38, A39, A43, A57, A61]. However, we have encountered many difficulties for a long time in trying to impose the idea of having such a feature (anisotropy) of these most spread electronic components (microwave substrates) as among the big substrate producers, as well as among the most of the users (we discuss this “story” for the substrate anisotropy in IVA).

Originally, the two-resonator method [A21, A31] is based on two consecutive measurements with/without samples of the resonance characteristics of two symmetrical modes: TE<sub>011</sub> in R1 resonator (with E fields parallel to the substrate)

and TM<sub>010</sub> in R2 resonator (E fields perpendicular to the substrate) – Fig. 3.3a and Fig. 3.4a. To achieve the best sensitivity of this method the sample is placed in the middle of R1, while it lies on the resonator bottom in R2; the chosen lower height  $H_2$  of R2 well separates the TM<sub>010</sub> and TE<sub>011</sub> resonances. The method can be realized in two options: 1) for samples with equal diameters  $D_1 = D_2$  (e.g. 30 mm), but the TM<sub>010</sub> mode has lower resonance frequency (7.65 GHz) than for TE<sub>011</sub> mode (13.15 GHz); or 2) for achieving of close resonance frequencies (e.g. in the interval 12.6-13.15 GHz), but applying resonators with different diameters ( $D_1 = 30$  mm;  $D_2 = 18.1$  mm) – see the examples in Fig. 3.3b,c. The considered here frequency band of the described method can be expanded to higher frequencies by using several selected high-order modes: e.g. TE<sub>013</sub>, TE<sub>021</sub>, TE<sub>031</sub> in R1 and TM<sub>020</sub>, TE<sub>030</sub> in R2; however, they should be well-identified in the mode spectrum (see the modes marked with arrows in Fig. 3.3c). The other way for frequency range widening is to increase or decrease the resonator (and sample) diameter. The diameter decreasing can increase the operating frequencies (e.g. for TE<sub>011</sub> in R1:  $f_1 \sim 21.8$  GHz at  $D_1 = 18.1$  mm;  $f_1 \sim 28.7$  GHz at  $D_1 = 15.0$  mm;  $f_1 \sim 39.3$  GHz at  $D_1 = 10.0$  mm; for TM<sub>010</sub> in R2:  $f_2 \sim 22.8$  GHz at  $D_2 = 10.0$  mm;  $f_2 \sim 28.5$  GHz at  $D_2 = 8.0$  mm; by higher-order modes in R1: up to 70-80 GHz; in R2: up to 65-70 GHz). However, the decreasing of resonator diameter leads to a decreasing of measurement accuracy, especially for the dielectric loss tangent, due to the smaller volume and lower Q factors in both resonators. Conversely, the diameter increasing leads to resonance frequency decrease and we managed to determine the substrate anisotropy by measurements even at 1.4-2.5 GHz [A48], but the sample sizes become too big and the accuracy again decreases. There is another way to decrease the frequency interval for anisotropy determination by small samples – to use another pair of R1/R2 resonators with naturally lower resonance frequencies based on split-coaxial resonator as R1 [A24] and reentrant resonator as R2 [A22] – see Fig. 3.4b. With this new pair of resonators, we again decreased the frequencies for determination of substrate anisotropy up to 1.7 GHz. In general, we successfully widened the applicability of two-resonator method by introducing in [A30, A31] the approach to use different pairs of measurement resonators from type R1/R2 and to obtain unique results for many commercial substrates, which was notified in [37, 38]. The third pair with split-dielectric post resonators SPDR(e/m) with TE/TM modes with added sub-

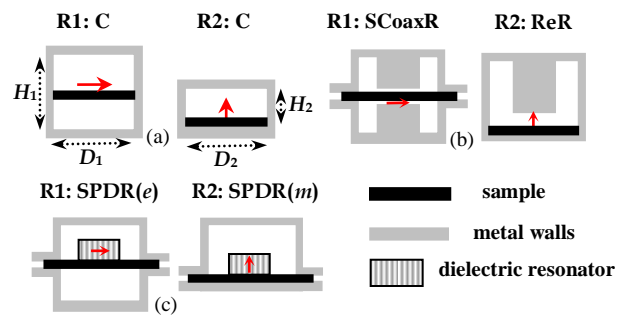


Fig. 3.4. Two-resonator method, realized by three different pairs of TE/TM resonators: (a) cylinder resonators (R1:C or R1:SCR and R2:C); (b) split coaxial resonator (R1:SCoaxR) and re-entrant resonator (R2:ReR); (c) split post dielectric resonators (R1:SPDR(e) and R2:SPDR(m))

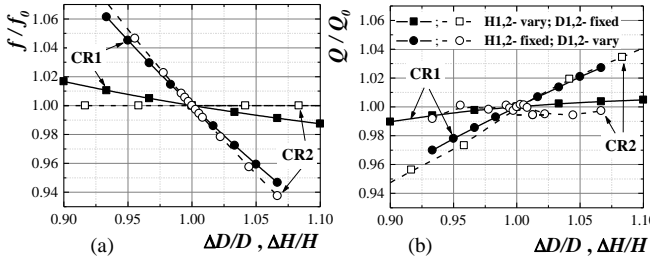


Fig. 3.5. Dependencies of the normalized resonance frequency (a) and normalized Q-factor (b) of the dominant mode in the cylinder measurement resonators CR1 and CR2

strate sample allows us preliminary to choose a frequency for measurements by the used high-Q dielectric resonators (Fig. 3.4c). We successfully applied the authorship two-resonator method for many different materials in addition to the microwave substrates, like multilayer composites, thin films, 3D printed dielectrics, textile fabrics, and even meta-materials (with less success) – details will be discussed later on.

The measurement errors of the two-resonator method have been estimated in [A21] as  $\sim 2.5\text{-}3\%$  for  $\Delta A_\epsilon$  and  $\sim 10\text{-}12\%$  for  $\Delta A_{\tan\delta\epsilon}$  in the case of multilayer materials in the Ku band (or 1.5% and 8-9% for single-layer substrates). These values fix the margins for determination of the practical isotropy of materials by the two-resonator method. A big contribution to the improvement of measurement accuracy is the concept for the equivalent parameters of measuring resonators [A30, A31]. Usually, the calculated and measured resonance parameters of the empty resonators do not fully coincide,  $f_{0\text{calc}} \neq f_{0\text{meas}}$ ,  $Q_{0\text{calc}} \neq Q_{0\text{meas}}$ . The reasons are different: size uncertainty, the influence of the coupling loops, tuning screws, eccentricity, surface cleanliness and roughness, daily temperature variations, etc. The problem can be overcome namely by the introduction of equivalent resonator dimensions and equivalent walls' conductivity. The equivalent geometrical parameters ( $D$  or  $H$ ) could be chosen on the base of a simple rule: the variation of which parameter influences more the resonant frequency of the empty cavity without any additional components? In the case of circular resonators the diameter changes "provoke" bigger variations of the resonance frequency and Q factor (see dependencies in Fig. 3.5). If we tune the selected equivalent parameters in the constructed stylized 3D models of empty resonators, we can achieve a practical coincidence between the calculated and the measured resonance parameters:  $f_{0\text{calc}} \sim f_{0\text{meas}}$ ,  $Q_{0\text{calc}} \sim Q_{0\text{meas}}$ . Thus, in the case of pair of cylinder resonators R1/R2 their 3D models include equivalent diameter  $D_{eq1,2}$  (instead  $D_{1,2}$ ), actual height  $H_{1,2}$  and equivalent wall conductivity  $\sigma_{eq1,2}$ . Additional equivalent parameters could be introduced for the other two pairs of used resonators [A31].

### C. Free-Space Method and Waveguide (Transmission-Line) Methods

The measurement setup of the free-space method (in transmission or in reflection regimes), consists of two or one horn antennas and the flat sample is placed between them or between the antenna and a reflecting screen – see Fig. 3.1a,b. The measurements of the phase delay and the losses with and without sample allow extracting the dielectric constant and dielectric loss tangent. This method is very useful for

measurements in the mm- and sub-mm-wave ranges but needs relatively big samples to avoid the diffraction effects near to the sample edge. The main problems are the reducing of the measurement errors due to multiple reflections and sample misalignment. By suitable extraction procedure, these errors could be reduced or measurements in a TDR gate could be used. Due to the TEM mode propagating in the structure, it can be used for extraction only of the parallel dielectric parameters of the sample in a transmission regime. The method is not well applicable for low-loss materials, but it is very popular for characterization of new unknown materials, including metamaterials [A51, A58, A59], composite materials as antenna radomes [A19, A25, A32] and absorbers [A28, A50, A61], all realized in our laboratory from X- to Ka-bands. An alternative of the free-space method is the resonance quasi-optical (Fabry-Perot) interferometer, realized in our laboratory in Ka-band; it can again measure the parallel dielectric parameters in mm- and sub-mm wavelength ranges even for low-loss materials.

The waveguide methods are also very popular in the dm-, cm-, mm-wavelength ranges and beyond, applying rectangular, circular or coaxial waveguides in transmission or reflection regimes. For rectangular waveguide in transmission regime, the thin sample can be placed between two waveguide flanges (as in Fig. 3.1c) or into the waveguide fitting its cross-section; the measurement of phase delay and insertion losses allows extraction of the sample dielectric parameters. Inserted in the waveguide aperture bulk samples can act as resonators in the corresponding frequency range; the extraction of the dielectric parameters is possible by measurement of the resonance frequency and Q factor. For thin samples in reflection regime, both dielectric and magnetic parameters can be extracted if the sample is placed in two fixed positions at a quarter-wavelength distance. When the sample is placed in the natural vertical position according to the wider wall of the waveguide, the method gives the parallel dielectric parameters; if the sample lies horizontally on this wall, the method extracts the perpendicular parameters. Thus, the waveguide method is one of the few relatively broadband methods, which can determine the anisotropy of the sample. Due to this reason, it is very popular for characterization of 3D printed metamaterials (e.g. see [14]), including in our laboratory [A28, A51].

The waveguide method can be also realized by planar transmission lines, printed on the substrate under interest. In this variant, it is known as the popular differential phaselength (DPL) method and it is one of the most spread methods for reliable microwave substrate characterization on the base of microstrip lines (MSL). The realization is simple:  $S_{21}$  parameters of two or more 50-Ohms MSL (or other planar lines) with different lengths have to be measured and the phase difference  $\Delta\text{ang}S_{21}$ , deg and difference between the insertion losses  $\Delta S_{21}$ , dB have to be determined for each pair of lines with length difference  $\Delta L$  (Fig. 3.6a). Then the important parameters, effective dielectric constant  $\epsilon_{eff}$  and attenuation  $\alpha$ , can be calculated by the simple expressions:

$$\epsilon_{eff} = \left( \frac{\Delta\text{ang}S_{21,c}}{360f\Delta L} \right)^2, \quad (10.1)$$

$$\alpha, \text{dB/cm} = \Delta S_{21}, \text{dB} / \Delta L, \text{cm}. \quad (10.2)$$

Fig. 3.6b,c presents an example for measured amplitude and phase  $S_{21}$  dependencies for a selected from the market commercial substrate (conditionally marked as “Substrate 3.0”) of thickness 20 mils with catalogue dielectric constant 3.0. Using totally 6 measured combinations for a set of 4 MSLs on this substrate with different thicknesses (5, 10, 20 and 30 mils) useful frequency dependencies for the effective dielectric constant and attenuation of MSL on this substrate can be obtained by (10.1-10.2) – shown in Fig. 3.7. In addition to the DPL method, other planar resonance methods are used to draw similar curves [A42]. The obtained dependencies are important for the extraction of the equivalent dielectric parameters – equivalent dielectric constant  $\epsilon_{eq}$  (in this case: MSL value  $\epsilon_{eq\_MSL}$ , shown in Fig. 3.8a) and the corresponding equivalent dielectric loss tangent  $\tan\delta_{eq}$ . However, in the last case, the imperfect metallization influences the MSL attenuation in a big degree [37]; therefore, the conductor and radiation losses have to be taken into account for more accurate extraction of  $\tan\delta_{eq}$  [A41, A55].

For more than 10 years now, the equivalent dielectric constant  $\epsilon_{eq}$  is an important parameter for reliable EM description of each reinforced substrate and each planar line printed on it. This approach allows an useful replacing of this anisotropic substrate with an isotropic equivalent practically in each RF design project, applying equivalent dielectric constant  $\epsilon_{eq}$  and equivalent dielectric loss tangent  $\tan\delta_{eq}$  (see

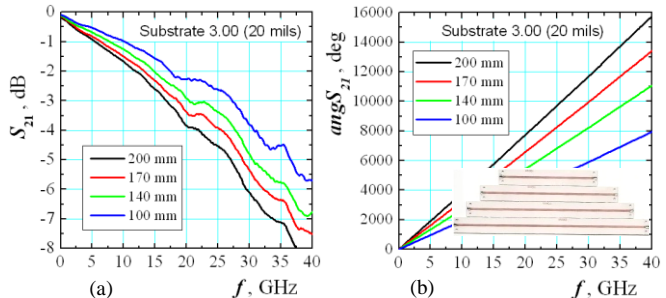


Fig. 3.6. Differential phase length (DPL) method: measured  $S_{21}$  dependencies (a) and phase delay (b); inset: four 50-Ohms microstrip lines with lengths 200, 170, 140 and 100 mm

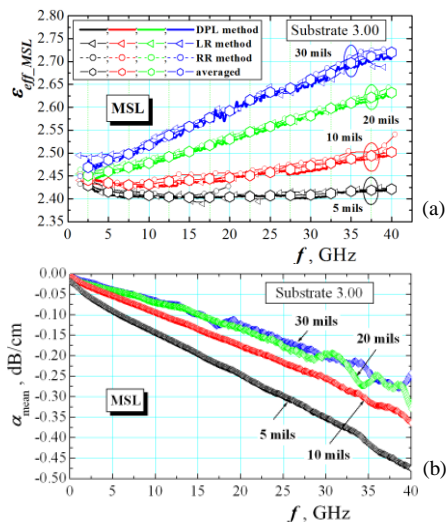


Fig. 3.7. Measured dependencies of  $\epsilon_{eff\_MSL}$  (a) and attenuation (b) by DPL and resonance methods for Substrate 3.0 with different thicknesses

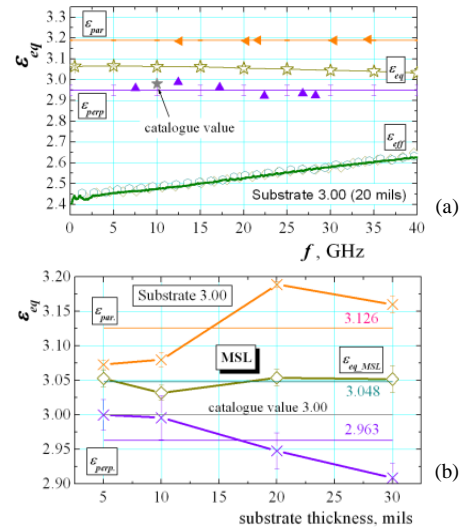


Fig. 3.8 (a) Extracted dependencies of the equivalent dielectric constant  $\epsilon_{eq\_MSL}$  of MSL compared with measured parallel and perpendicular dielectric constants,  $\epsilon_{parallel}$ ,  $\epsilon_{perp}$ ; for Substrate 3.0 (20 m); (b) parameters  $\epsilon_{parallel}$  and  $\epsilon_{perp}$ , compared with  $\epsilon_{eq\_MSL}$  for the same substrate versus the thickness

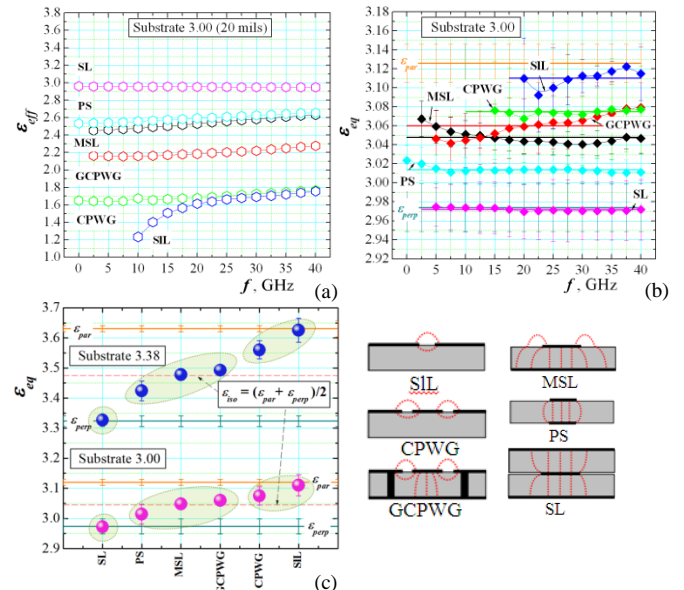


Fig. 3.9. Measured  $\epsilon_{eff}$  (a) and extracted  $\epsilon_{eq}$  (b) dependencies for six 50-Ohms planar transmission lines for Substrate 3.0 (20 mils); (c) averaged by the thickness and frequency  $\epsilon_{eq}$  values of six planar lines for Substrate 3.0 (Dk = 3) and other Substrate 3.38 (Dk = 3.38). Legend: SL – stripline; PS – paired strips; MSL – microstrip lines; CPWG – coplanar waveguide; GCPWG – grounded CPWG; SIL – slot line.

our concept described in [A31, A42]). This is an efficient approach and the leading PCB producers and developers of the 3D EM simulators started to share with the substrate users the needed information for the equivalent dielectric constant, often called “design Dk” value and usually obtained by the DPL method for MSL. Fig. 3.8b presents a useful picture for the considered Substrate 3.0 – a comparison between the measured  $\epsilon_{parallel}$ ,  $\epsilon_{perp}$  and  $\epsilon_{eq\_MSL}$  for different thickness. The results clearly show an important fact – the producers have managed to decrease the anisotropy for thin substrates, which are applicable exactly in the mm-wave-length range, where the anisotropy has a bigger influence.

The main problem is that the parameter  $\epsilon_{eq}$  of each substrate depends on the type of the printed planar line on

this substrate (see dependencies in Fig. 3.9a,b), i.e. from the concrete distribution of the parallel and perpendicular electric fields of the dominant propagation mode in a given planar line. We managed to prove for the first time this fact in our work [A31] and then developed a special concept in [A42]. It turned out that this fact is a serious inconvenience for the application of the equivalent dielectric constant approach (design Dk). However, we presented a partial solution based on the introduction of three groups of equivalent values – see the information, presented in Fig. 3.9c. The proposal is RF designers to use in their planar device projects three different values of the equivalent dielectric constant  $\epsilon_{eq}$  depending on the dominant planar structure: I – “stripline value”  $\epsilon_{eq\_SL} \sim \epsilon_{perp}$  (or process, specification Dk, applicable for stripline and SIW); II – “microstrip value”  $\epsilon_{eq\_MSL} \sim (\epsilon_{perp} + \epsilon_{par})/2$  (or design Dk, suitable for microstrip line, coupled MSL, paired strips, grounded coplanar waveguide and similar microstrip-like lines) and III – “coplanar value”  $\epsilon_{eq\_CPWG} \leq \epsilon_{par}$  (or a new coplanar design Dk, applicable for slot-based planar lines: coplanar waveguide, slot and fin-line). The first two values are already in use namely as “process” and “design” values [38, 39] (our concept only explain the origin of these values), but the third value is a new parameter – it is suitable for coplanar and slot-line based planar structures, used mostly in the integrated circuits. Many new publications confirm the usefulness of this our concept for reliable design of planar devices with equivalent dielectric constants (more details are discussed in IV).

#### D. Utilization of 3D Electromagnetic Simulators as an Auxiliary Tool for Material Characterization by Resonance Measurements

The modern material characterization needs the utilization of powerful numerical tools for obtaining accurate results after modelling of very sophisticated measuring structures. Such software instruments could be the 3D EM simulators, which demonstrate significant capabilities in the modern RF design. Considering recent publications in the area of material characterization, it is easy to establish that the 3D simulators have been successfully applied for measurement purposes, too. The ability to use commercial frequency-domain 3D simulators as auxiliary tools for accurate measurements of the substrate anisotropy based on the two-resonator method has been demonstrated for the first time in [A19]. Then, this option was developed for all types of considered resonators [A31], following few principles – simplicity, accuracy and fast simulations. Illustrative 3D models for the simplest structures, used in the two-resonator method (cylinder resonators R1 and R2), are drawn in Fig. 3.10a. Three main rules have been accepted to build these models for accurate and time-effective processing of the measured resonance parameters – 1) a stylized drawing of the resonators' body with equivalent diameters ( $D_{eq1,2}$ ), actual height  $H_{1,2}$  and equivalent wall conductivity  $\sigma_{eq1,2}$ ; 2) an optimized number of line segments for construction of the curved cylindrical surfaces (line size less than 1/16 wavelength) and 3) a suitable for the operating mode splitting (1/4 or 1/8 from the whole resonator body; Fig. 3.10b), accompanied by appropriate boundary conditions at the cut-

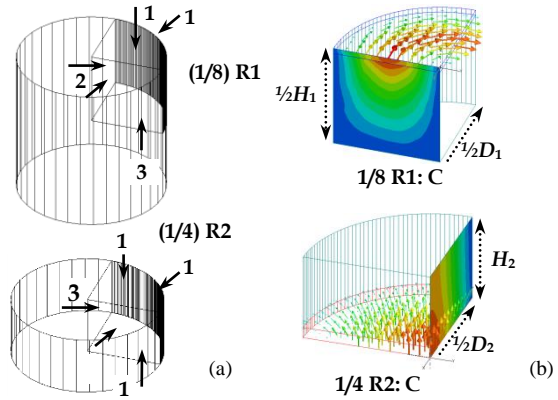


Fig. 3.10. (a) Equivalent 3D models of two cylinder resonators R1/R2 and boundary conditions (legend: 1 – finite conductivity ( $\sigma_{eq}$ ); 2 – E-field symmetry; 3 – H-field symmetry); (b) Simulated E-field scalar and vector distribution in the measurement resonators (1/8 R1 and 1/4 R2)

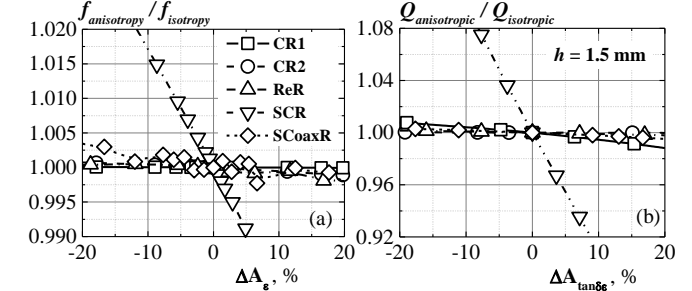


Fig. 3.11. Dependencies of the normalized resonance frequency (a) and Q-factors (b) of the used resonance modes for anisotropic and isotropic samples versus dielectric anisotropy  $\Delta A_\epsilon$ ,  $\Delta A_{\tan\delta\epsilon}$

off planes. Although the real resonators have the necessary coupling elements and holes, the resonator bodies could be introduced into the model as pure closed cylinders and this approach allows applying the Eigenmode solver of the modern 3D simulators. The utilization of the Eigenmode option for obtaining of the resonance frequency and the unloaded Q factor (notwithstanding that the modelled resonator is not fully realistic) considerably facilitates the anisotropy measurement procedure assisted by 3D simulators, if equivalent parameters have been additionally introduced and symmetrical resonator splitting has been done.

These optimized models increase the accuracy of the two-resonator methods for anisotropy measurements and allow us to evaluate the sensitivity of the corresponding resonators (with the excited TE or TM modes) to the actual sample anisotropy – see dependencies in Fig. 3.11. The analysis of the obtained results shows that the chosen modes in the different pairs of measurement resonators have very good selectivity to the corresponding dielectric constant of the sample in the resonator along a given direction with an uncertainty less than  $\pm 0.25\%$  for the normalized resonance frequency  $f_{aniso}/f_{iso}$  and less than  $\pm 0.5\%$  for the normalized Q factor  $Q_{aniso}/Q_{iso}$ , when the anisotropy varies in the intervals  $\Delta A_\epsilon$ ,  $\Delta A_{\tan\delta\epsilon} = \pm 10\%$  even for relatively thick samples (excepting for SCR).

#### E. Problems with Reliable 3D Simulations of Microstrip Lines on Anisotropic Substrates

The microwave engineers have two possibilities to take into account the material anisotropy in their numerical design

projects – to replace the real anisotropic structure with isotropic equivalent, described by the equivalent dielectric constant  $\epsilon_{eq}$ , or to use the “anisotropic material” option of the modern 3D simulators, introducing the pair of values  $\epsilon_{par}$  and  $\epsilon_{perp}$ . The concept and design accuracy applying the first option was already described above. There exist only a few papers, where the second option has been directly applied, but with not so expressed benefits (see references in [A47]).

Let's compare both options. Several 3D models have been constructed for popular planar transmission lines on an anisotropic substrate, following the accepted in the RF design standard principles for ports, radiations boxes, etc. (see the example for MSL in Fig. 3.12a). We selected one typical Substrate 3.38 with a middle anisotropy, measured by the two-resonator method in the range 5-40 GHz with parameters  $\epsilon_{par} = 3.66$ ;  $\epsilon_{perp} = 3.345$ . The corresponding equivalent dielectric constant is  $\epsilon_{eq} = 3.48$  (design value), measured by the DPL method (catalogue value is 3.38). Fig. 3.12b presents the simulated frequency  $\epsilon_{eff}$ -dependencies of a 50-Ohm MSL in two options of the used 3D simulator (in this case ANSYS ®HFSS): 1) isotropic equivalent substrate

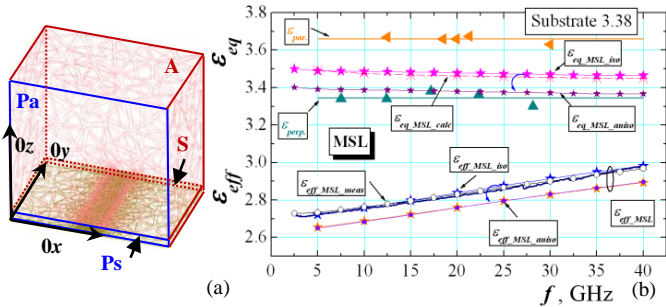


Fig. 3.12 (a) 3D model of MSL on an anisotropic substrate with selected two rectangular volumes S (substrate) and A (air above) and two  $x_0z$  planes Ps and Pa at the input port; (b) Comparison between simulated frequency dependencies of the effective  $\epsilon_{eff}$  and the corresponding equivalent  $\epsilon_{eq}$  dielectric constants of MSL on an anisotropic substrate using simulator options “isotropic or anisotropic material”

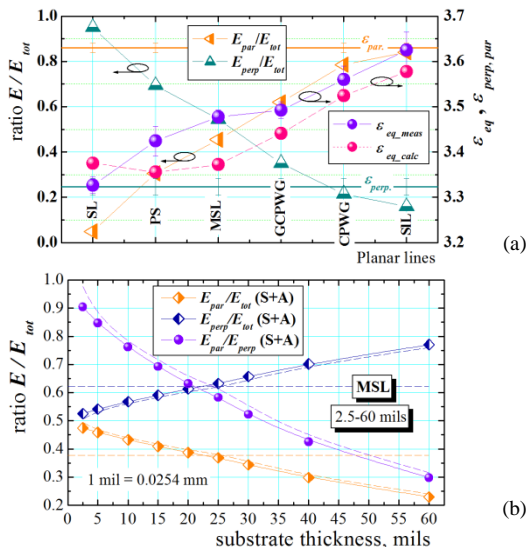


Fig. 3.13 (a) Measured and calculated  $\epsilon_{eq}$  values by simulated phase delay in several planar transmission lines and simulated normalized parallel and perpendicular E fields in these lines; (b) Distribution of normalized parallel and perpendicular electric fields in the united box volumes S+A (substrate and air box above) of 50-Ohms MSL (dashed curves – for united Ps + Pa planes on the radiation box wall – Fig. 3.12a)

with  $\epsilon_{xx} = \epsilon_{yy} = \epsilon_{zz} = \epsilon_{eq}$  and 2) anisotropic substrate with uniaxial anisotropy, namely  $\epsilon_{xx} = \epsilon_{yy} = \epsilon_{par}$ ;  $\epsilon_{zz} = \epsilon_{perp}$ . The  $\epsilon_{eq}$  values calculated by the second (anisotropic) option are visibly smaller, than the values for the isotropic case (the recalculated equivalent dielectric constant is now 3.38 instead 3.48 for MSL, i.e. 2.8%-decrease). Fig. 3.13a presents these differences for other investigated planar lines: from 0.5 up to 3 % decrease, which is not acceptable for a reliable RF design. In fact, the biggest differences appear for MSL and MSL-like lines, e.g. for coupled MSL (up to 4 % decrease, not shown). In the same time the course of the curves, representing the distribution of the normalized parallel and perpendicular electric fields,  $E_{par}/E_{tot}$  and  $E_{perp}/E_{tot}$ , in the whole structures fully correspond to the position of the measured  $\epsilon_{eq}$  values between  $\epsilon_{par}$  and  $\epsilon_{perp}$  values of each given planar line – from Fig. 3.9c. Therefore, we can try to bind the  $\epsilon_{eq}$  values directly to the field distribution. In [A46] we proposed a more accurate, field model for calculation of the  $\epsilon_{eq}$  values. For this purpose, we include in the MSL model (Fig. 3.12a) several new artificial volume and plane objects, where we can easily calculate the integrated complex E fields by the incorporated “field calculator” in the simulators. The aim is to determine both field ratios  $E_{par}/E_{tot}$  and  $E_{perp}/E_{tot}$  in these volumes or planes and to calculate  $\epsilon_{eq\_MSL}$  by the expression

$$\epsilon_{eq\_MSL} \equiv \left( \frac{E_{par}}{E_{tot}} \Big|_{MSL} \times \epsilon_{par} \Big|_{sub} + \frac{E_{perp}}{E_{tot}} \Big|_{MSL} \times \epsilon_{perp} \Big|_{sub} \right) \quad (11)$$

The obtained results are quite informative. The calculated ratio for substrate only is  $E_{par}/E_{perp} = 0.19/0.81$  in the volume S. If we determine  $\epsilon_{eq\_MSL}$  by (11) applying these ratios, the obtained dependencies are very close to the  $\epsilon_{eq\_sim\_phase}$  dependencies, obtained by the simulated phase delay (i.e. by the MSL S parameters) – see Fig. 3.12b. But if we now apply the E-field ratios in the whole structure, i. e.  $E_{par}/E_{perp} = 0.39/0.61$  in the united volumes S+A, the calculated  $\epsilon_{eq}$  values are very close to the measured values  $\epsilon_{eq\_meas}$  (or to the values, obtained by the simulator for option “equivalent isotropic substrate”). This fact is very optimistic. It points the direct connection between the calculated actual ratio  $E_{par}/E_{perp}$  for each planar structure (MSL in the considered case) and the measured equivalent dielectric constant.

The obtained positive results for the possibility to predict the actual values of the equivalent dielectric constant only on the base of the calculated near-field distribution of the parallel and perpendicular electric fields in MSL allow us to propose a reliable method for a direct determination of this important parameter without to perform any specialized time-consuming measurements. But to implement this method, we have to investigate the influence of the MSL parameters over the field distribution. Fig. 3.13b presents the most important dependences  $E_{par}/E_{tot}$  and  $E_{perp}/E_{tot}$  on the substrate thickness, which can be used directly in expression (11). According to the expectations, the parallel component of the electric field plays a bigger role for thinner substrates and v.v. Therefore, we can average the dependencies and write an approximate expression

$$\varepsilon_{eq\_MSL} \cong \left( (0.38 \pm 0.02) \times \varepsilon_{par}|_{sub} + (0.62 \pm 0.02) \times \varepsilon_{perp}|_{sub} \right), \quad (11.1)$$

which ensures the best accuracy for substrates with thickness 20-30 mils. The other MSL and substrate parameters (e.g. metallization thickness, absolute dielectric constant, losses) don't play so important role. Now, if we calculate values  $\varepsilon_{eq\_MSL\_calc}$  by (11.1), they practically coincide with the measured ones  $\varepsilon_{eq\_MSL\_iso}$  in the presented case in Fig. 3.12b.

#### IV. DIELECTRIC PROPERTIES AND ANISOTROPY OF REINFORCED, IMPREGNATED, WOVEN, KNITTED AND OTHER FIBRE MATERIALS

The dielectric mixtures based on two or more dielectrics, one part of them performed as reinforcing filaments (fibres, threads, yarns) and another part – as appropriate fillers (ceramics, PTFE, epoxy resins, air, etc.), are very popular in the modern electronics – see Fig. 4.1. This is a wide group of useful artificial materials, which can be used as substrates for printed circuit boards (PCB), reinforcing skins and foam cores for multilayer antenna radomes, textile fabrics, used for wearable antennas, self-reinforcing plastics, etc. The most spread of them is the group of reinforced PCB substrates as commercial products (considered in IVA). They consist of woven or nonwoven reinforcing fibre-glass fabrics and different fillers and the resultant homogenized structures can be used in different parts of the microwave range. Nowadays some traditional textile fabrics also can act as substrates for the popular wearable antennas in the new communication body-area networks (IVB). Another variant of the reinforced epoxy-glass laminates is applicable for antenna radomes and other radio-transparent and mechanically stable constructions (IVC). Multilayer and gradient absorbers (IVD) are artificial materials, which could be added to this group.

Of course, the question that must be answered when designing such composites is how to predict the effective/equivalent dielectric properties of the whole system? (Note that similar approaches should be applied also to the mechanical and thermal properties.) We already considered in IIB several closed-form expressions for analytical determination of the equivalent complex dielectric constant of different mixtures (early concepts [9] and some new approaches for 2D [40, 41, 42] or 3D [43] woven fabrics, including the numerical techniques [44]). To obtain the required information for the resultant dielectric mixture, it is necessary to estimate the permittivity of the separate constituents (phases) and the used mixture topology. Finally, appropriate measurements of the resultant complex dielectric constants are also necessary to be performed by destructive or nondestructive methods (some of them considered in III).

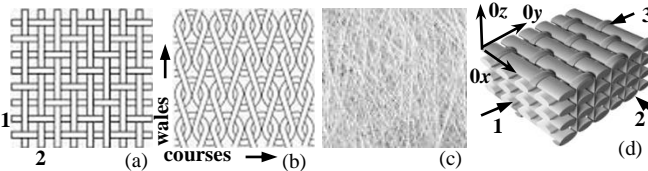


Fig. 4.1 Examples for some filament mixtures: (a) 2-D woven fabrics; (b) Jersey knitted fabrics; (c) non-woven fabrics; (d) 3D woven composites (legend: 1 – warp yarn; 2 – weft yearn; 3 – Z-yearn)

The topology of the considered reinforced dielectric mixtures (shown in Fig. 4.1) suggests the existence of artificial anisotropy, caused by the spatial inhomogeneity in the filling. We already discussed the anisotropy origin (IIC) and developed authorship methods for numerical (IID) and experimental (IIIB) determination of this parameter for such materials. We use as a measure for the degree of this anisotropy (separately for dielectric constant and dielectric loss tangent) the considered above parameters  $\Delta A_\varepsilon$ ,  $\Delta A_{\tan\delta_\varepsilon}$  defined by expressions (9.1, 9.2), where  $\varepsilon_{0x}$ ,  $\varepsilon_{0y}$  and  $\varepsilon_{0z}$  are the real dielectric constants, while  $\tan\delta_{\varepsilon,0x}$ ,  $\tan\delta_{\varepsilon,0y}$  and  $\tan\delta_{\varepsilon,0z}$  are the dielectric loss tangents (dissipation factors) along the axes  $0x$ ,  $0y$  and  $0z$  (as shown in Fig. 4.1d). The considered case refers to the biaxial anisotropy (for a pair of three different components along each axis). When the parallel components according to substrate surface coincide (i.e.  $\varepsilon_{0x}=\varepsilon_{0y}=\varepsilon_{par}$  and  $\varepsilon_{0z}=\varepsilon_{perp}$ ;  $\tan\delta_{\varepsilon,0x}=\tan\delta_{\varepsilon,0y}=\tan\delta_{\varepsilon,par}$  and  $\tan\delta_{\varepsilon,0z}=\tan\delta_{\varepsilon,perp}$ ), the uni-axial anisotropy takes place. In the next four sections, we will consider the specific features and peculiarities of the considered types of dielectric mixtures and their anisotropy.

##### A. Reinforced Commercial Substrates

The reinforced substrates are key materials in modern electronics – the basis for the realization of new devices by microwave integrated circuits (MICs) and especially for the last 5G communication standard. These materials consist of reinforcing fibre-glass fabrics and a variety of fillers – see Fig. 4.2. This mixture is a classic example for uni-axial anisotropic materials: usually, the glass fibres are high-permittivity supports, while the fillers – low-permittivity homogenizing media (with some exceptions, when the fillers are high-permittivity ceramic powders). Due to this combination of constituents the parallel dielectric constant (along the glass fibres' axes) is usually bigger than the perpendicular one, i.e.  $\varepsilon_{par} > \varepsilon_{perp}$  (the behaviour of the textile fabrics with air filling is very similar; see IVB)

The main role of the substrate is to support the metallic layout and surface-mounted components of the PCB schemes at low frequencies; however, in the microwave range, the substrate dielectric properties influence the electrodynamic behaviour of the whole printed structure. Thus, a reliable determination of the dielectric parameters of each commercial substrate by the manufacturers is very important for the consumers. The producers apply the reference IPC TM-650 2.5.5.5 test method [17] (based on clamped stripline resonator), which gives dielectric constant and dissipation factor along the  $0z$  axis (Fig. 4.2a), denoted with the popular in the datasheets symbols  $Dk$  and  $Df$  and this pair of two values is usually fully enough for many applications at lower

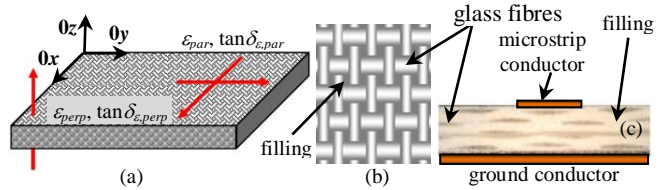


Fig. 4.2. Schematic view of the reinforced substrates: (a) substrate with uni-axial anisotropy [A21]; (b) top view (glass fibre fabrics and fillers); (c) side view of a microstrip line on a reinforced substrate

frequencies (for example, in planar schemes on the popular epoxy-glass laminate FR-4 [45], manufactured by many companies). However, at higher frequencies the anisotropy becomes important, especially for mmMICs, working in the mm-wavelength range, because the effective wavelength becomes compatible with the spatial irregularities in the reinforced substrate (well-illustrated in Fig. 4.2c).

As we mentioned above (IIIB), we maybe were the first researchers (based on our experience with ferrites and ceramics), which detected the unwanted dielectric anisotropy of several popular commercial reinforced substrates in 2000-2002 by the developed authorship two-resonator method and published the first paper [A6]. For example, we measured for a commercial substrate Ro3203 (0.254-mm thick; 10 mils) considered as pure isotropic one (reference value 3.02 [46]):  $\epsilon_{par} \sim 3.238$ ,  $\epsilon_{perp} \sim 3.036$ , equivalent dielectric constant  $\epsilon_{eq} \sim 3.111$  in the X band and dielectric anisotropy  $\Delta A_\epsilon \sim 6.4\%$  (indeed the term “equivalent dielectric constant” was firstly introduced exactly in this paper). We presented also results for other popular substrates (e.g. for the practical isotropy of Ro3003, RT Duroid 6002; useful data for Ro4003, FR-4, etc.), but due to the used perturbation approximation for TM-mode resonator, some of the obtained results were not so accurate, especially for thick substrates. Then we developed more accurate full-wave analytical models and later on effective numerical techniques of the measurement resonators and extraction procedures for determination of the parameters Dk/Df of uni-axial anisotropic single and multilayer samples by the two-resonator method ([A17, A21, A26, A31]). In a relatively short period (2004-2008) we succeeded to collect useful data for the actual anisotropy on many commercial substrates from different manufacturers and had the unique possibilities to compare and to publish some of them. In our practice, we met commercial substrates with different degree of anisotropy: 1) near-to-isotropic ( $\Delta A_\epsilon < 2-3\%$ ; non-woven substrates); 2) substrates with middle anisotropy ( $\Delta A_\epsilon \sim 5-11\%$ ; the most typical case) and 3) relatively big anisotropy ( $\Delta A_\epsilon > 15-20\%$ ) [A32]. Today, we can distribute in each group many well-known commercial products on the base of our measurements, but this information is very sensitive for the most manufacturers and we try to use in our recent publications virtual denotations instead the actual substrate names when the products are still on market. The large PCB companies continue to support an opinion that the anisotropy of part of their products is “a discrediting property” for the consumers (although it is a completely natural property for such mixtures) and they usually don’t comment the measured anisotropy effects in details, nevertheless that the degree of this anisotropy directly depends on the applied technology. Until 2006 we didn’t manage to find any information about the anisotropy of commercial substrates published in the official specifications (application notes). However, in this period, 2002-2005, we found out several articles (not cited here), presented on the largest microwave conferences (e.g. IMS), where the authors disagree with part of the used reference Dk data. For example, some of them have assumed a value of  $\sim 3.52$  for Dk of the very popular at that time substrate Ro4003 instead the catalogue value 3.38 (4.1-% increase!). They explained this decision with “better results

obtained during the simulations of MSL filters on this substrate”. It was a strange explanation for us; RF designers, who typically draw the geometrical structures of the designed planar devices in the simulators with extremely large details, frivolously start to adjust the substrate Dk value in their projects until the simulation results coincide with the measurement ones (!). For information, in this period we measured the following Dk values for Ro4003 (0.508-mm thick; 20 mils):  $\epsilon_{par} \sim 3.66$ ,  $\epsilon_{perp} \sim 3.37$  (close to catalogue value 3.38), equivalent dielectric constant exactly  $\epsilon_{eq} \sim 3.52$  for 50-Ohms microstrip lines (MSL) in the Ku band; i. e. a moderate dielectric anisotropy  $\Delta A_\epsilon \sim 8.3\%$ . Other research groups also started to show their results for anisotropy of different substrates, mentioned in IIC.

Step by step, the large PCB manufacturers accepted the problems with substrate anisotropy and offered solutions to overcome them, but without to discuss in details the source of problems. The first company, according to us, which officially began to share information for measured dielectric anisotropy of its substrate, was Taconic Headquarters Ltd., Advanced Dielectric Division. In paper [47], the authors started to discuss the dielectric anisotropy of their material TLY-5A (measured by Bereskin’s method [48]). As early as 2012, the next company that began to share results for the measured anisotropy of some of its products was Rogers Corp. Ltd. In the paper [49], the company researchers presented relatively detailed information for the anisotropy of some their substrates; even adduced a discussion for the obtained results, published earlier in our papers. They confirmed all our results, excepting data for one substrate with high-Dk. In 2013, Isola Group Ltd. also started to discuss and to solve the problems with substrate anisotropy, especially at higher frequencies (for substrates with 5G applications) and shared information for the equivalent dielectric constant [A40]. The concept for the equivalent dielectric constant, when the anisotropic substrate can be replaced with isotropic one, was more or less implemented in the datasheets. For example, Rogers Corp. (and then practically all other large PCB manufacturers: Isola Group, Taconic, ITEQ Corp., Shengyi Technology Co, etc.) started to give so-called design Dk value of each RF substrate (together with the reference technological Dk value obtained by IPC-TM-650 2.5.5.5 method) to ensure optimum simulation results. The large software developers also added the corresponding design Dk values in their material tutorials. Strictly speaking, the parameter design Dk was not well validated in the beginning, but the recent publications from the company researchers (e.g. [50]) discuss the problems of the substrate anisotropy and give unpublished data for many products. Nowadays, most of the companies present three Dk values (but not for all products): technological Dk (close to  $\epsilon_{perp}$ ); design Dk (close to  $\epsilon_{eq}$  for MSL) and a value, obtained by SPDR method (close to  $\epsilon_{par}$ ), which completely correspond to our concept for the reinforced substrates, developed since 2000 (see IIIC). This information helps to solve the problems with substrate anisotropy; nowadays, the producers try to obtain “a full 3D dielectric portrait” of their products to have better control on technology, while RF engineers would like to perform a better 3D design of their devices.

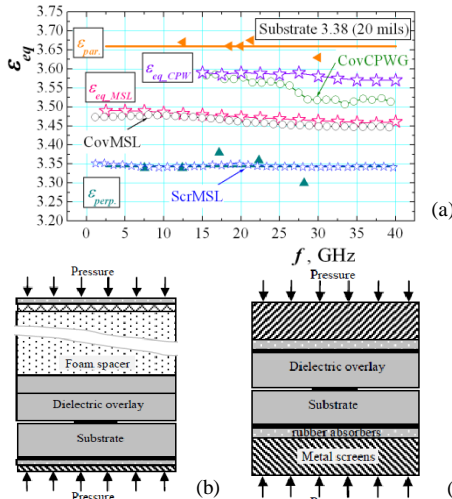


Fig. 4.3. (a) Comparison between the frequency dependencies of equivalent dielectric constant  $\epsilon_{eq}$  for uncovered and covered MSL and CPW, compared with  $\epsilon_{parallel}$  and  $\epsilon_{perp}$  values of Substrate 3.38; (b) covered MSL line resonator (side view) for direct measurement of  $\epsilon_{eq}$ ; (c) screened MSL line resonator (quasi-IPC method) for direct measurement of  $\epsilon_{perp}$  [A44]

Therefore, we can conclude that the development of measurement methods for determination of the important dielectric parameters of widespread commercial substrates, especially in the mm-wavelength range, is substantial and we continue to develop new methods (III). For example, in our paper [A44] we have presented new methods for direct measurements of the two important substrate parameters by direct determination of effective  $\epsilon_{eff}$ : design Dk (by covering of MSL with enough thick overlay from the same material) and technological Dk (by an appropriate screening of MSL) – see Fig. 4.3. The measurements of close to parallel Dk by covering of CPW were also successful [A45, A58-A62]. The last new results are related to the temperature behaviour of substrate anisotropy, which are very interesting [A66].

Of course, our main advantage in the process for characterization of all accessible on the market commercial substrates is the possibility really to obtain a full 3D “portrait” of the dielectric properties of these important materials, measuring the anisotropy by our two-resonator method [A21, A26, A31] and equivalent parameters, when these materials have been considered as isotropic ones [A31, A42]. This information can help many users to perform



Fig. 4.4. Pairs of optimized measurement resonators with different diameters: (a) TE-mode R1 (30, 18.1, 15, 10 mm) and (b) TE-mode R2 (30, 18.1, 10, 8 mm), which cover frequency range 5-39 GHz

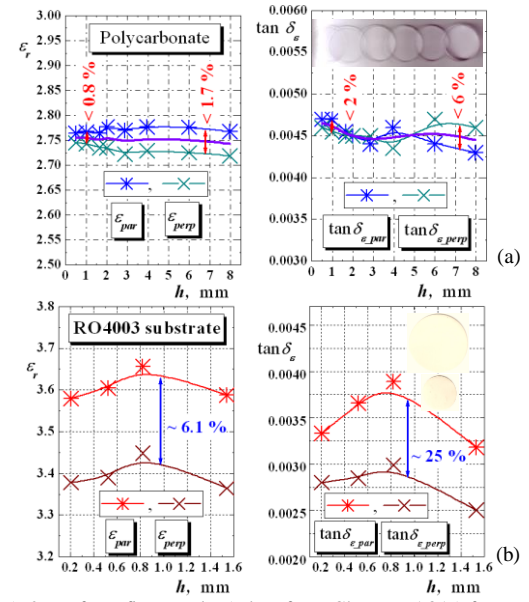


Fig. 4.5. One of our first results (taken from Chapter [A31]) for measured dielectric parameters v/s thickness of the isotropic Polycarbonate PC (a) and a popular commercial substrate Ro4003 (b)

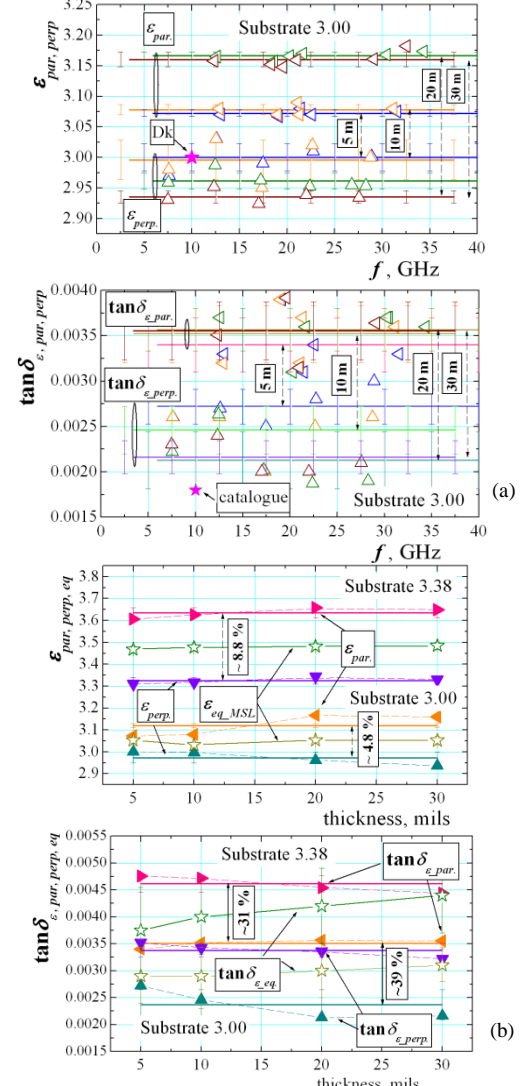


Fig. 4.6. Full ‘3D portrait’ of dielectric anisotropy of two commercial substrates conditionally marked as Substrate 3.00 (Dk = 3) and 3.38 (Dk = 3.8), versus frequency (a) and thickness (b); 1 mil = 0.0254 mm

Table 1. Measured dielectric parameters and anisotropy of several commercial substrates with practically equal or similar catalogue parameters

Substrate	$h$ , mm	parallel $\epsilon_{par}/\tan\delta_{par}$	perpendicular $\epsilon_{perp}/\tan\delta_{perp}$	equivalent $\epsilon_{eq}/\tan\delta_{eq}$	$\Delta A_\epsilon / \Delta \tan\delta_\epsilon, \%$	IPC TM 650 2.5.5.5 @ 10 GHz
Rogers Ro4003	0.510	3.67/0.0037	3.38/0.0028	3.53/0.0031	8.2/27.7	3.38/0.0027
Arlon 25N	0.520	3.57/0.0041	3.37/0.0033	3.37/0.0033	5.8/21.6	3.38/0.0025
Isola 680	0.525	3.71/0.0049	3.32/0.0042	3.32/0.0042	11.1/15.4	3.38/0.0030
Neltec NH9338	0.520	4.02/0.0051	3.14/0.0025	3.51/0.0032	24.6/68.4	3.38/0.0025
Rogers Ro3003	0.27	3.00/0.0012	2.97/0.0013	2.99/0.0013	1.0/-8.0	3.00/0.0013
Rogers Ro3203	0.26	3.18/0.0027	2.96/0.0021	3.08/0.0025	7.2/25.0	3.02/0.0016
Neltec NH9300	0.27	3.42/0.0038	2.82/0.0023	3.02/0.0023	19.4/49.2	3.00/0.0023
Arlon DiClad880	0.254	2.32/0.0016	2.15/0.00093	2.24/0.0011	7.6/53.0	2.17/0.0009

better and reliable design of different planar structures on these substrates, especially in the mm-wavelength range and the manufacturers to have better technology control of their products. Fig. 4.4 presents the photography of a set of eight TE- and TM-mode resonators, which “covers” the frequency interval 5-39 GHz by applying the fundamental modes in each resonator (and even up to 80 GHz by applying selected appropriate high-order modes). Using this measurement tool and its modifications, we managed to characterize more than 70 different substrates, accessible on the world market; a small part of the obtained results (<10 %) have been published with the actual substrate names (e.g. as in [A31]) – as in Fig. 4.5 and Table 1. The other unpublished part composes our rich database for many substrates, including the last available products. We can characterize the separate substrate materials in several ways [A36, A40]. The first two ways are based on obtaining information for the anisotropy of commercial substrates versus the frequency (as in Fig. 4.6a,b) and thickness (as in Fig. 4.6c,d or Fig. 4.5b). The set of averaged values of parameters  $\epsilon_{par}$ ,  $\epsilon_{perp}$ ,  $\epsilon_{eq}$  and  $\tan\delta_{\epsilon,par}$ ,  $\tan\delta_{\epsilon,perp}$ ,  $\tan\delta_{\epsilon,eq}$  gives valued information for each substrate and allows comparison between substrates from a specific group (like examples in Table 1), which is important for the producers and useful for the users. The last two ways for

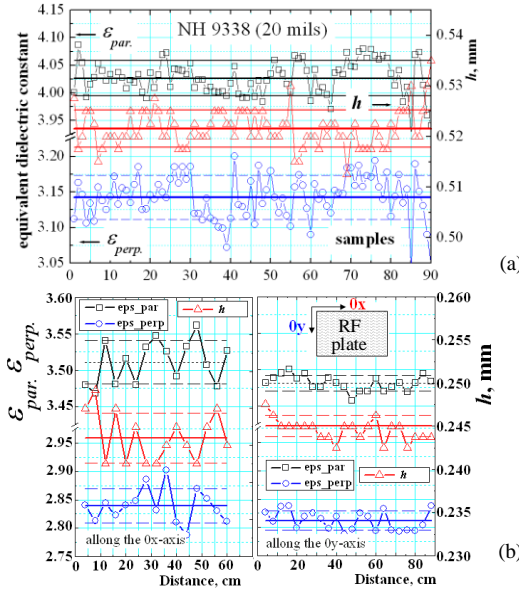
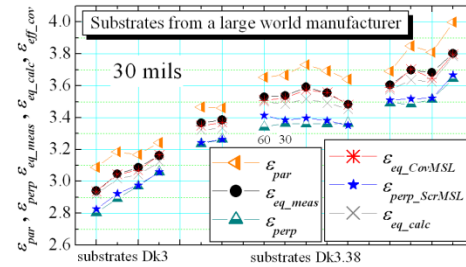


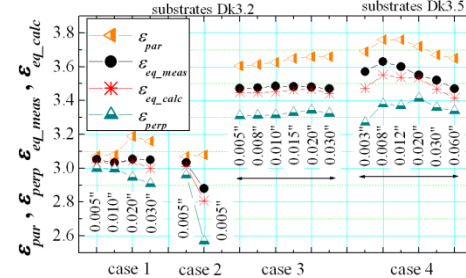
Fig. 4.7. Statistical data for substrate NH 9338 (a) and its parameters' inhomogeneity (b) [A13]

Table 2. Measured standard deviations for parameters of large-size substrate sheets [A13]

Substrate	SD $\epsilon_{par}$	SD $\epsilon_{perp}$	SD $\tan\delta_{\epsilon,par}$	SD $\tan\delta_{\epsilon,perp}$	SD $h$	Samples number	SD $Z_c$	SD $\epsilon_{eff}$	SD $\beta$	SD $\alpha$
Ro4003	$\pm 0.2$	$\pm 0.5$	$\pm 2.0$	$\pm 9.0$	$\pm 0.2$	32	$\pm 0.22$	$\pm 0.45$	$\pm 0.23$	$\pm 4.4$
NH9338	$\pm 0.8$	$\pm 1.0$	$\pm 8.5$	$\pm 13.0$	$\pm 0.7$	90	$\pm 0.52$	$\pm 0.91$	$\pm 0.45$	$\pm 6.1$



(a)



(b)

Fig. 4.8. Examples for measured parallel, perpendicular ( $\epsilon_{par}$ ,  $\epsilon_{perp}$ ) and equivalent dielectric constants ( $\epsilon_{eq}$ ) of different commercial substrates: (a) for different products of one company; (b) Comparison: case 1) low-Dk (~3.0) substrate with minimized anisotropy for small thicknesses; case 2) two low-Dk substrates with different anisotropy; cases 3, 4) family of substrates with Dk~3.38 from two different companies covering a wide thickness range 3-60 mil [A46]. Legend:  $\epsilon_{eq}$  measured by the DPL method;  $\epsilon_{eq,CovMSL}$  and  $\epsilon_{perp,ScrMSL}$  measured by the direct method presented in [A44, A45] (see Fig. 4.3);  $\epsilon_{eq,calc}$  calculated by the expression (11.1) [A46]

obtaining of substrate parameters are difficult – statistical data, extracted from a large number (50-100) of samples (as in Fig. 4.7a) and information for dielectric parameters inhomogeneity in large-size substrate sheets (Fig. 4.7b). Such data, compared for a selected extract of several concurrent substrates, are decisive for the right choice of the larger users of these materials because they show the stability of the dielectric parameters and parameters of the constructed on their base devices – e.g. impedance  $Z_c$ , propagation constant  $\beta$  and attenuation  $\alpha$  (see Table 2). Fig. 4.8 illustrates well how we can use this database for substrate parameters. A set of parameters and anisotropy of different 30-mils substrates of one producer is presented in Fig. 4.8a with typical dielectric constants 3-3.8. Fig. 4.8b (cases 1, 2) illustrates the attempts of another producer to minimize the anisotropy of low-Dk substrates with applicability in the mm-wavelength range; while Fig. 4.8b (cases 3, 4) gives a useful comparison between a family of products of two companies with similar Dk ~ 3.38 and different thicknesses.

## B. Textile Fabrics for Antenna Applications

The textile fabrics show quite similar behaviour of the dielectric properties and anisotropy like the reinforced substrates due to the structures' resemblance [51]. In our first publications on this topic [A47,A49], we presented measured by the two-resonator method dielectric anisotropy of several most popular natural and synthetic textile fabrics (see also selected results in Table 3). It turned out that the actual anisotropy  $\Delta A_\epsilon$  of textiles is small (1.5-5%) or moderate (5-9%) as the commercial microwave reinforced substrates (compare with data in Table 1). Only for more complex and multilayer artificial fabrics, the anisotropy  $\Delta A_\epsilon$  exceeds 10-12%. Then, in paper [A49] we developed 3D models for the numerical determination of dielectric anisotropy of woven

and knitted textile fabrics (Fig. 4.9) and presented useful results (part of them shown in Table 4). The information for the anisotropy of these artificial fabrics confirms the rule that the dielectric constant of these air-filled dielectric mixtures increases in the direction parallel to the axes of the fibres and decreases in the perpendicular direction (that why, different sample anisotropy  $\Delta A_\varepsilon$  appears from  $\pm 1\text{-}5\%$  up to 12-18% – last column in Table 4) (for the promising flexible PDMS

Table 3. Measured dielectric parameters and anisotropy of some classical textile fabrics (averaged values for frequency interval 0-36 GHz) [A62]. Insets at right: different disk textile samples

Textile fabric	$t, \text{mm}$	$\frac{\varepsilon_{\text{par}}}{\tan \delta_{\varepsilon, \text{par}}}$	$\frac{\varepsilon_{\text{perp}}}{\tan \delta_{\varepsilon, \text{perp}}}$	Anisotropy $\Delta A_\varepsilon / \Delta A_{\tan \delta_{\varepsilon}, \%}$
Epoxy-based waterproof fabric	0.35	1.97/0.010	1.83/0.007	7.4/30
Waterproof fabric with breathability GORE-TEX® [16]	0.20	1.53/0.006	1.38/0.004	10.3/28
Weaved silk	0.19	1.60/0.028	1.54/0.016	3.8/57
Weaved linen	0.65	1.65/0.043	1.58/0.044	4.3/-2.3
Weaved hemp fishnet	0.81	1.63/0.072	1.43/0.034	13.1/72
Natural leather	0.84	2.47/0.055	2.44/0.054	1.2/1.8
Weaved wool	2.10	1.28/0.026	1.21/0.015	5.6/54
Jersey knitted wool	5.50	1.40/0.024	1.26/0.021	10.5/13.3
Denim	0.93	1.69/0.027	1.61/0.030	4.8/-11
Cotton satin 5	0.25	1.58/0.019	1.45/0.013	8.6/38
Jersey knitted cotton	0.40	1.56/0.055	1.50/0.044	3.9/22.2

Fig. 4.9. Top and side views of 3D models of four artificial materials, made by straight or meander yarns with diameters 0.5 mm and distance between their centres 1 mm (the unit cell of samples is  $1 \times 1 \times 1.5$  mm; the unit cell has been repeated only in the Oxy plane)

Table 4. Simulated dielectric parameters and anisotropy of several artificial textile structures

No	Sample description	$\frac{\varepsilon_{\text{par}}}{\tan \delta_{\varepsilon, \text{par}}}$	$\frac{\varepsilon_{\text{perp}}}{\tan \delta_{\varepsilon, \text{perp}}}$	Anisotropy $\Delta A_\varepsilon / \Delta A_{\tan \delta_{\varepsilon}, \%}$
1	Straight cylinders along to $0x$ and $0y$ direction (fish net)	1.432/0.0020	1.205/0.0005	17.2/120
2	Meander cylinders along to $0x$ and $0y$ directions (woven symmetrical net)	1.673/0.0022	1.750/0.0025	-4.5/-12.4
3	Meander cylinders along to $0x$ direction and straight cylinder along to $0y$ directions	1.593/0.0022	1.519/0.0017	4.8/22.8
4	Jersey knitted fabric	1.726/0.0026	1.530/0.0015	12.0/53.7

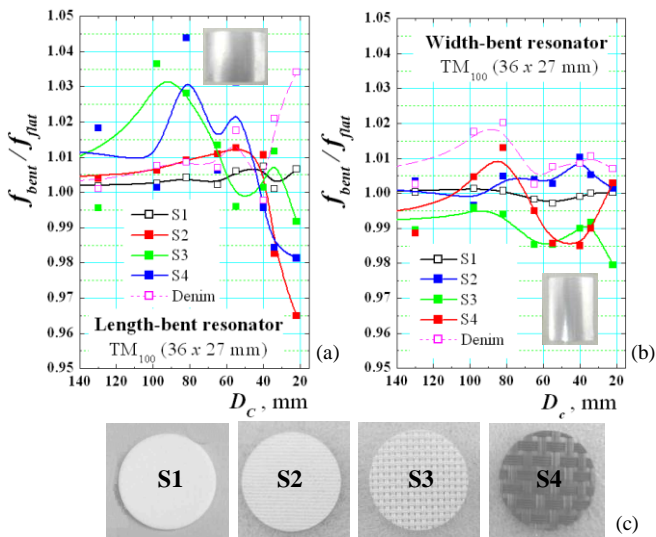


Fig. 4.10. Measured normalized resonance frequencies of length-(a) or width-bent (b) rectangular resonator 36x27 mm on substrates S1, S2, S3 and S4 (c) with measured anisotropy  $\Delta A_\varepsilon \sim 0.4; 5.7, 13.7$  and 11.3 % correspondingly [A62].

(Polydimethylsiloxane) polymer substrate,  $\Delta A_\varepsilon \sim 6.4\%$ ; more details are given in [A70, A64, A69]. These results give ideas on how to minimize the undesired anisotropy of these materials. In [A49] we investigated the behaviour of microstrip patch antennas and arrays on anisotropic textile substrates (frequency band, beamwidth, directivity and efficiency). In the recent paper [A62], we continued this research with bent microstrip rectangular resonators on selected substrates with different anisotropy. We found out that the resonance frequencies of the dominant mode in these bent structures (Fig. 4.10) depend not only on the curvature diameter  $D_C$  (obtained for pure isotropic substrates like S1) but also on the concrete anisotropy  $\Delta A_\varepsilon$  (for samples S2, S3, S4) (or combination between  $D_C$  and  $A_\varepsilon$ ), which is a completely new result (the research is still in progress [A71]).

### C. Multilayer Antenna Radomes

Antenna radomes are very important structures in the antenna design; they ensure the mechanical and weather stability of different open-air antennas and, at the same time, they should be radio-transparent in the operating frequency ranges. Therefore, the proper radome design separately from (or together with) the antenna design is an important task, because this structure adds losses and phase delay and influences the antenna beam-forming and directivity/gain. There exist two main types of radomes: thin (with thickness  $t_R$  smaller than the wavelength  $\lambda$ ) and resonance radomes (when  $t_R \sim \lambda/2$ ). The modern radomes are usually multilayer (sandwich-type) structures [52]. They consist of relatively thick middle core and two thin skin layers, which ensure the mechanical hardness. The cores are foams, wadding with air pores, honeycombs or similar low-Dk layers. On the contrary, the skins are reinforced layers: glass fabrics with resin epoxy filling, both with higher Dk. To perform reliable radome design, the dielectric properties of all radome layers have to be well determined. However, the considered structures of cores and hard skins show that they are more or less anisotropic materials. Exactly considering these needs to determine the own anisotropy of radome layers (e.g. due to the destruction of antenna circular polarization at big elevations [A65]), we developed the authorship two-resonator method for multilayer samples, as it has been described in [A21].

Fig. 4.11 presents three examples of antenna radomes. The single-layer reinforced thin radome (Fig. 4.11a) could be considered as a reinforced substrate (IVA). The popular three-layer honeycomb radome consists of rare honeycomb cells (e.g. Kevlar® paper) and two different (top and bottom) skin layers – thin glass-fibre fabrics with resin filling – Fig. 4.11b. All these samples have expressed anisotropy, illustrated in Fig. 4.12b. Based on these data we can construct different radome models – with one, three or six

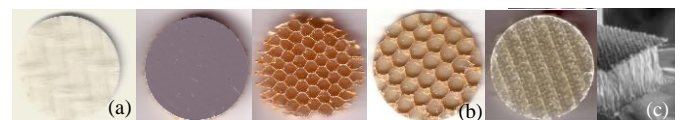


Fig. 4.11. Samples from radomes: (a) reinforced TWINTEX® fabrics woven with commingled E-glass and polypropylene filaments; (b) honeycomb radome: painted skin layer, Nomex® Kevlar-paper core and E-glass skin with glue residues [A19]; (c) Parabeam® 3D glass fabrics: reinforced 3D woven filaments with resin filling [A25]

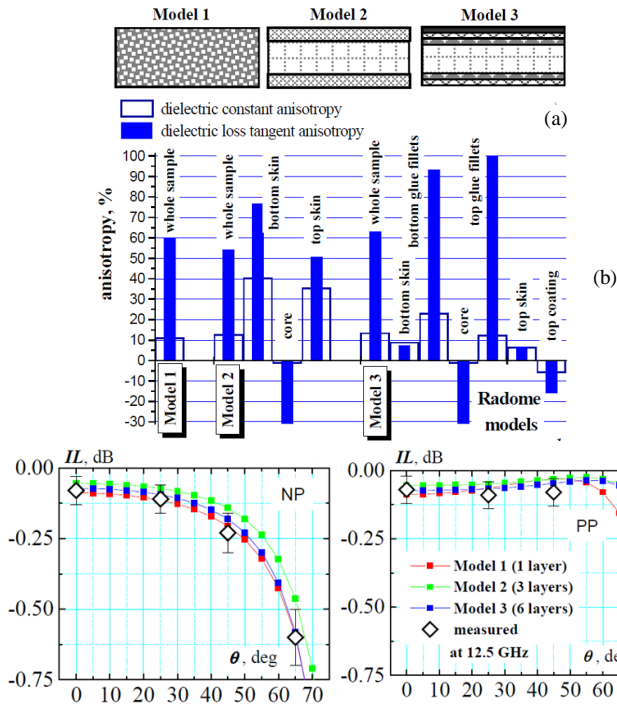


Fig. 4.12. (a) Illustrative pictures of the used radome models with 1, 3 and 6 layers; (b) dielectric anisotropy of separate layers and whole sample for each model; (c) IL-dependencies versus the incident angle  $\theta$  at 12.5 GHz for multi-layer honeycomb radome with total thickness 5.5 mm for normal (NP) and parallel (PP) polarization of the incident wave

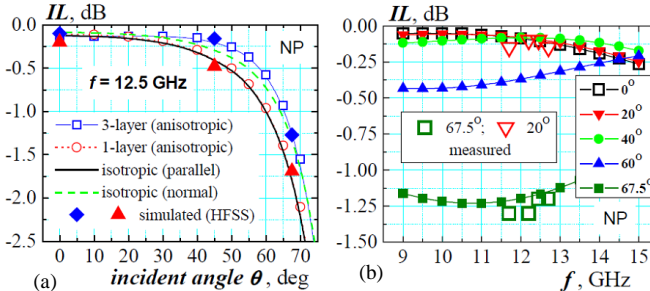


Fig. 4.13. Dependencies of the insertion losses IL in Parabeam® 3D glass radome [A25]: (a) versus the incident angle at 12.5 GHz; (b) versus the frequency at several incident angles. The results are compared with Ansoft® HFSS simulations for 1-layer and 3-layer anisotropic radome models. The measured data are obtained by measurements of the received signal in DBS-TV steerable antenna array with and without covering radome in Ku-band.

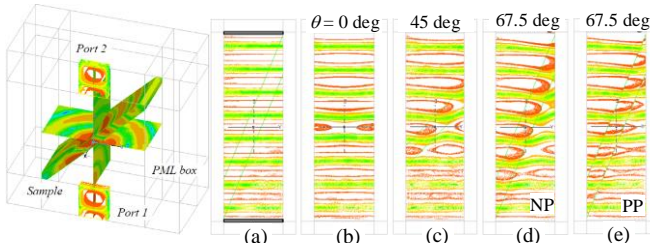


Fig. 4.14. (at left) Half part of a large simulated structure: radome sheet between two open-end waveguides; (at right) Incident (a) and total E field in PML box with radome, illuminated by plane wave – normal NP (b, c, d) and parallel PP (e) polarization

layers (Fig. 4.12a) (the last model includes two additional thin layers formed by the glue residues between the core and skins and a coating layer). We developed in our papers [A14, A19] an analytical model for determination of radome insertion (IL) and return (RL) losses of multilayer samples with anisotropy on the base of Paris' model [53] for isotropic

multilayer radomes. The comparison (Fig. 12c) between the numerical and measured IL fully confirms the validity of our theoretical radome model.

The third example is very interesting from a measurement point of view – Fig. 4.11c. We proposed for the first time in [A21, A25] the commercial ParaBeam® 3D glass fabrics to be used as an antenna radome. The specificity here is the fact that the radome body is single structure: 3D glass fabric impregnated with epoxy resin and the skin layers and core are formed by a single process. Therefore, we cannot directly measure the core parameters. For this purpose we presented in [A21] a de-embedding procedure for the extraction of dielectric parameters of the middle layer: 1) characterization of parameters of the whole sample; 2) characterization of both skin layers and 3) extraction of the parameters of the inaccessible for direct measurements 3D glass core. The measured layer anisotropy is high:  $\Delta A_e \sim 27\%$  for the top smooth skin layer;  $\sim 45.7\%$  for the rough bottom skin layer and  $-5.6\%$  for 3D glass core. With the help of the constructed radome model, we determined the IL in radome for an incident wave with normal polarization (Fig. 4.13) versus incident angle and frequency. Simulated and measured losses practically coincide. In [A25], for the first time we presented also well-developed 3D models for effective simulations for multi-layer anisotropic radomes – see illustrations in Fig. 4.14. The free-space model between two rectangular open-end waveguides gives applicable results but by very time-consuming simulations. On the contrary, stylized models with plane-wave source allow faster simulations at different incident angles with satisfactory accuracy; however, an extraction procedure has to be applied for the determination of the insertion losses and phases due to the multilayer radome [A25].

#### D. Multilayer and Gradient Absorbers

Other important materials widely used in the microwave range are the microwave absorbers. Their main role in the structures, where they have been incorporated, is to suppress the parasitic interferences, cross-talk interactions and reflections. Recently, the microwave engineers started to design the whole microwave devices together with incorporated absorbers; therefore they need to know the actual EM parameters of these materials. Usually, the microwave absorbers have been offered as foams, rubber sheets, brushed coatings or thin films with absorbing inclusions (recently absorbing metamaterials). They consist of carbon, carbonyl iron, ferrites and other high-loss inclusions; therefore, they may have as pure dielectric properties (like the carbon-containing absorbers), as well as magnetic properties [54]. In [A10, A15, A16] we presented our attempts to determine the dielectric and magnetic parameters of thin microwave absorbers. Unfortunately in this period, the commercial absorbers' producers presented in the corresponding catalogues only data for the absorbing abilities (through the sample in dB/mm), but not the actual dielectric and magnetic constants and loss tangents. In our review paper [A27] we summarized and compared the possible methods for characterization of microwave absorbers. There are no problems with pure dielectric absor-

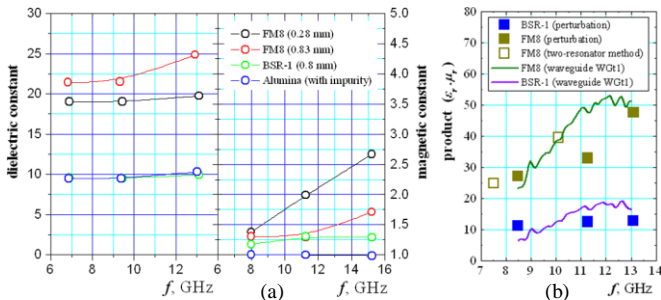


Fig. 4.15. (a) Measured dielectric and magnetic constants ( $\epsilon_r$ ,  $\mu_r$ ) of two commercial absorbers by perturbation method; (b) measured product  $\epsilon_r \times \mu_r$  by three different methods

Table 5. Extracted values of the dielectric and magnetic parameters of 30- $\mu\text{m}$  thick nano absorbers (AUT) mixed with protective lacquer L (nC – consists of nano-carbon particles of diameter  $\sim$ 3-4 nm; nF – nano-ferrite  $\text{Fe}_3\text{O}_4$  particles of diameter  $\sim$ 20-30 nm; nFnC – a mixture nF : nC = 1 : 1)

AUT + L	$\epsilon_{\text{par}}/\tan\delta_{\epsilon,\text{par}}$ (f, GHz)	$\epsilon_{\text{perp}}/\tan\delta_{\epsilon,\text{perp}}$ (f, GHz)	$\mu_{\text{par}}$ (f, GHz)	$\mu_{\text{perp}}$ (f, GHz)
nC	7.65/1.6 (12.8); 6.82/5.4 (22.1); 3.49/5.5 (32)	4.20/0.22 (7.6); 4.04/0.15 (17.5); 3.56/0.22 (27.4)		
nF	3.75/0.58 (12.8); 3.73/4.1 (22.1); 4.17/1.70 (32)	2.05/1.93 (7.6); 2.54/0.55 (17.5); 2.24/0.26 (27.4)	1.06 (20.8)	0.93 (15.7); 0.51 (24.4); 0.45 (33.8)
nFnC	8.84/3.3 (12.8); 5.82/0.25 (22.1); 2.51/0.77 (32)	2.57/0.73 (7.6); 2.67/0.08 (17.5); 2.62/0.144 (27.4)	1.16 (20.8)	1.04 (15.7); 1.50 (24.4); 2.90 (33.8)

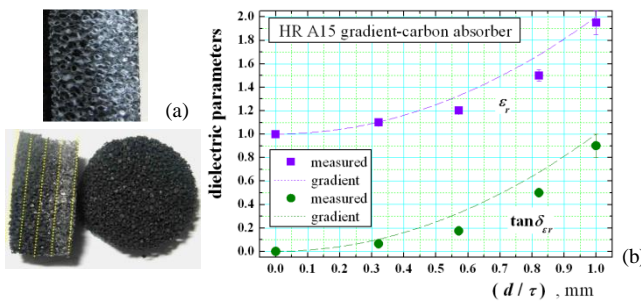


Fig. 4.16. (a) Carbon-gradient sample ECCOSORB® HR A15; (b) dependencies of the dielectric constant and dielectric loss tangent of four disk slices from 15-mm thick absorber

bers; it is difficult to separate the magnetic and dielectric properties of magneto-dielectric absorbers. The separation is relatively easy [55] by measurements of the resonance parameters of exited  $\text{TE}_{10p}$  modes in rectangular resonators with small prism samples; first modes with odd  $p$ -values (1, 3, 5) will ensure extraction of dielectric parameters  $\epsilon_r$ ,  $\tan\delta_\epsilon$ , while first modes with even  $p$ -values (2, 4, 6) – magnetic parameters  $\mu_r$ ,  $\tan\delta_\mu$ . Fig. 4.15a presents measured equivalent dielectric  $\epsilon_r$  and magnetic  $\mu_r$  constants by perturbation methods, while Fig. 4.15b compares the product  $\epsilon_r \times \mu_r$ , obtained by different measurement methods. As an example, we give the parameters of commercial rubber absorber FM8 (Collector Magma, Slovenia) in Ku band:  $\epsilon_r \sim 18.0$ ;  $\mu_r \sim 1.5$ ,  $\tan\delta_\epsilon \sim 0.2$ ;  $\tan\delta_\mu \sim 1.0$ . Thick absorber samples cannot be well characterized by resonance methods due to the big losses. However, we proposed in [A61, A67] a procedure for separate extraction of dielectric and magnetic parameters for thin nanoabsorbers by the two-resonator method using TE and TM modes with maximums of electric or magnetic fields in the place of the sample. Table 5 presents results for nano-carbon and nano-ferrite absorbers ( $\epsilon_{\text{par}}$ ,  $\tan\delta_{\epsilon,\text{par}}$  have been extracted by the help of modes  $\text{TE}_{0mn}$  with  $m = 1, 2, 3$  and  $n = 1, 3$ ;  $\epsilon_{\text{perp}}$ ,  $\tan\delta_{\epsilon,\text{perp}}$  – modes  $\text{TM}_{0m0}$  with  $m = 1, 2, 3$ ;  $\mu_{\text{par}}$  – modes  $\text{TM}_{0mn}$  with  $m = 1, 2$  and  $n = 2$ ;  $\mu_{\text{perp}}$  – modes  $\text{TE}_{0mn}$  with  $m = 1, 2, 3$  and  $n = 2, 4$ . Dielectric parameters of carbon-containing absorbers

strongly depend on the frequency, which corresponds with the results from other methods.

The last example is connected with the characterization of an innovative type of foamed absorbers with gradient carbon distribution – see illustrations in Fig. 4.16a. We performed relatively thin slices from the thick materials  $\tau \sim 14$  mm and managed to confirm this distribution as for the dielectric constant  $\epsilon_r(d) = 1 + (d/\tau)^2$ , as well as for the dielectric loss tangent  $\tan\delta_{\epsilon,r}(d) = 0 + (d/\tau)^2$  (dependencies in Fig. 4.16b). Such absorbers have considerable decreased reflectivity; we proposed in [A50] this material to be used for decreasing of the radar cross-section (RSC) of unmanned vehicles.

## V. DIELECTRIC PROPERTIES AND ANISOTROPY OF CRYSTALLINE MATERIALS

As we mentioned in IIC, the crystalline anisotropy of single- or poly-crystalline materials (glasses, ceramics, artificial soft and low-temperature co-fired ceramics LTCC, liquid crystals, ferrites, semiconductors, etc.) is one of the oldest known types of well-expressed material anisotropy. Typically, these materials are homogeneous, but the anisotropy appears due to the existence of different crystallographic axes in their lattices and the fact that charges oscillate by different manner along these directions. Our first investigations were connected exactly with this type of anisotropy of ceramic, ferrite and semiconductor disks, cylinders, rings and rods by different microwave methods [A1-A3, A5]. Then we continued with the characterization of crystalline and crystalline-like materials by the two-resonator method [A23, A34, A53, A56] and applying combinations with other broadband methods [A59, A60]. Here we will present short summarized information for these difficult for characterization materials.

### A. Crystals, Ceramics, Glasses, Semiconductors

The determination of dielectric properties of single- or poly-crystalline materials is a classical problem in the microwave frequency range [56]. There exist different methods for characterization of the dielectric properties of crystals; the most accurate are the resonance ones [20]. However, an additional circumstance for these materials is the presence of relatively strong biaxial anisotropy – different dielectric parameters along the different axes, e.g.  $\epsilon_{xx} \neq \epsilon_{yy} \neq \epsilon_{zz}$  and  $\tan\delta_{exx} \neq \tan\delta_{eyy} \neq \tan\delta_{ezz}$ . In two our papers [A53, A56] we especially applied two-resonator method for characterization of high-Dk materials like ceramics, glasses, ferrites, semiconductors, etc. These papers aimed to show the ability of this resonance method to determine the crystalline anisotropy with acceptable accuracy and how this information can be used for crystalline sample characterization.

Table 6 (part 1) presents dielectric parameters and calculated anisotropy of different ceramics, performed as disk samples, which fit the measurement resonators' diameters. They are low-loss and relatively high- $\epsilon$  materials, suitable for compact microwave integrated circuits MIC's, but the relatively big difference between the absolute values of parallel and perpendicular dielectric constants is a serious design problem. Usually  $\epsilon_{\text{par}} > \epsilon_{\text{perp}}$ ;  $\Delta A_\epsilon \sim 9\text{-}15\%$  (only for

the popular polycrystalline Alumina substrate we measure  $\epsilon_{par} < \epsilon_{perp}$ ;  $\Delta A_\epsilon \sim -7\%$ ). The attractive artificial soft ceramics (3M®Epsilam10, Rogers® Ro3010, TMM 10i), plastic substrates with high- $\epsilon$  filling, show even bigger anisotropy (7-23 %), excluding the relatively isotropic RT Duroid® 6010,  $\Delta A_\epsilon \sim 4.4\%$ ). The new class of low-temperature co-fired ceramics (LTCC), applicable in the monolithic MIC's and promising for the mm-wavelength range, also have noticeable anisotropy ( $\Delta A_\epsilon \sim 13\%$ ). In general, our results for high- $\epsilon$  ceramics are accurate, but difficult to be obtained – disk samples with fixed large diameters should be prepared, which is technologically inefficient process.

That's why, we proposed in [A53, A56] another variant of the two-resonator method for easier determination of sample anisotropy: to use separately either TE- or TM-mode resonators (R1 or R2; IIIB), but now for smaller disk or prismatic samples with different orientations parallel or perpendicular to the E fields – see the illustrations in Fig. 5.1a,b,c.

Table 6. [A56] (Part 1) Dielectric parameters and uni-axial anisotropy of ceramic samples, measured by two-resonator method (R1 & R2); (Part 2) Dielectric parameters and anisotropy of three disk samples measured by TE-mode resonator R1 in position D1 and D3 (resonator axis lies along 0z)

No	Sample; reference values			Anisotropy $\Delta A_\epsilon / \Delta A_{tan\delta_\epsilon} \%$
		$\epsilon_{par}/\tan\delta_{\epsilon,par}$	$\epsilon_{perp}/\tan\delta_{\epsilon,perp}$	
1	Alumina ( $\text{Al}_2\text{O}_3$ ) 9.8-10.7	9.65/0.0003	10.35/0.0004	-7.0/-29
2	Polycore ( $\text{Al}_2\text{O}_3 + 0.3\% \text{ MgO}$ )	10.044/0.0002	9.21/0.0003	8.7/-40
3	Sitall (glass ceramic)	8.19/0.0042	7.16/0.0038	13.4/10
4	3M ®Epsilam 10 9.8/0.0020	11.64/0.0022	9.25/0.0045	22.9/-69
5	Rogers ®TMM10i 9.9/0.0020	11.04/0.0019	10.35/0.0035	6.5/-59
6	Rogers ®Ro3010 10.2/0.0035	11.74/0.0025	10.13/0.0038	14.7/-41
7	RT Duroid® 6010 10.2/0.0023	10.71	10.252	4.4
8	ACX® LTCC 7.5/0.003	7.60/0.007	6.68/0.0075	12.9/-6.9
9	YIG Garnet 14.8: Ms 1.7 kA/cm	15.83/0.00020	13.11/0.00027	18.8/-30
<hr/>				
Part 2				
1a	Alumina ( $\text{Al}_2\text{O}_3$ ) 9.8-10.7	9.78 / 0.00080	10.20 / 0.00075	-4.2/6.5
8a	ACX® LTCC 7.5/0.003	7.66 / 0.0069	6.20 / 0.0048	21/36
10	$\text{MgTiO}_3$	14.61 / 0.00028	15.10 / 0.00018	-3.3/44

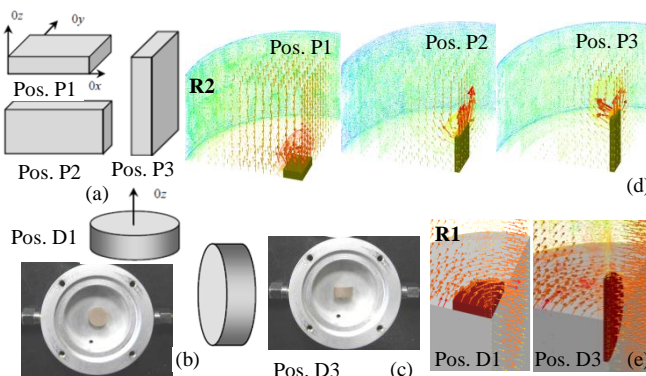


Fig. 5.1. Possible sample positions in resonators for prisms (a) and disks (b); (c) photo of samples in TM-mode resonator R2 in positions D1 and D3; (d, e) illustration of the E-field vector distribution in the measurement resonators R2 (TM<sub>010</sub> mode) and R1 (TE<sub>011</sub> mode)

Table 7. Dielectric constants and anisotropy of several prismatic samples measured by TM-mode resonator R2 in positions P1, P2 and P3 (resonator axis lies along with 0z)

No	Sample description	$\epsilon_{xx}$	$\epsilon_{yy}$	$\epsilon_{zz}$	$A_{\epsilon,xx}, \%$	$A_{\epsilon,yy}, \%$
1	Quartz (single crystal, c-axis=0z)	3.74	3.84	4.27	-13.2	-10.6
2	Quartz (fused)	4.32	4.31	4.325	-0.12	-0.35
3	Silica glass	5.15	5.23	4.30	18.0	19.5
4	Mica (multi-layer silicate)	4.87	4.70	3.00	47	44
5	Optical glass LiNbO <sub>3</sub>	32.25	29.3	22.8	34	25
6	Crystalline Si for wafer	10.75	10.15	8.125	28	22
7	Semi-isolated GaAs wafer	11.30	11.10	7.90	36	34

However, the analytical model of the measurement resonators, described in [A21, A26] cannot be used; suitable 3D models for numerical simulations have to be applied now (examples have been given in Fig. 5.1d,e). Table 6 (part 2) presents again the dielectric parameters and anisotropy of some of the disk samples in part 1, but now measured by TE-mode resonator R1 in positions D1 and D3 – the coincidence is good. The variant with prismatic samples allows us to determine the actual bi-anisotropic parameters of different high- $\epsilon$  samples. Table 7 presents the measured values  $\epsilon_{xx}$ ,  $\epsilon_{yy}$ , and  $\epsilon_{zz}$  in positions P3, P2 and P1 of several glasses and semiconductor wafers and the corresponding anisotropy  $\Delta A_{\epsilon,xy}$ . The new information from these data is the expected fact that the single crystals show bigger anisotropy than the anisotropy of the corresponding poly-crystalline sample. For example, fused and single-crystal Quartz samples have equal values for the perpendicular permittivity,  $\epsilon_{zz} \sim 4.27\text{-}4.32$  (the  $c$ -axis coincides with the resonator axis 0z), while the values for the parallel permittivity  $\epsilon_{xx}$ ,  $\epsilon_{yy}$  are different:  $\sim 3.74\text{-}3.84$  in the single crystal along the  $a$ -axes;  $\sim 4.31\text{-}4.32$  in the fused Quartz. Relatively big anisotropy we observe for the crystalline Si and semi-isolated GaAs (last two rows in Table 7).

### B. Microwave Ferrites

The microwave ferrites, e.g. spinel, garnet, and hexaferrite systems as thin or thick films, powders, bulk samples, and nowadays different multiferroic materials, are key components in the systems that send, receive, and manipulate EM signals across a wide frequency range; from VHF up to mm-wave bands [57] and they can ensure non-reciprocal behaviour. Microwave ferrites are very similar to the microwave ceramics (high dielectric constant  $\epsilon_f$  and low dielectric losses), but with this difference that they additionally possess magnetic properties – small magnetic constant ( $\mu_{dem} \leq 1$ ) and bigger magnetic losses, when no external dc magnetic field  $H_0$  has been applied (we will not consider the tensor magnetic properties in non-zero field  $H_0$ ). In our early papers [A2, A3, A5] we developed methods for

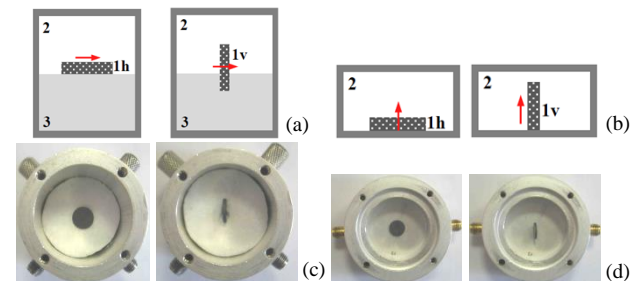


Fig. 5.2. Measurement resonators and sample position: (a) Resonator R1 with  $\text{TE}_{0mn}$  modes ( $m = 1, 2, 3, n = 1, 2, 3, 4, 5, 6$ ); (b) Resonator R2 with  $\text{TM}_{0m0}$  modes ( $m=1,2,3$ ); (c, d) Photo of R1 and R2. Legend: 1h, 1v – samples in horizontal and vertical position; 2 – resonator; 3 – support foam

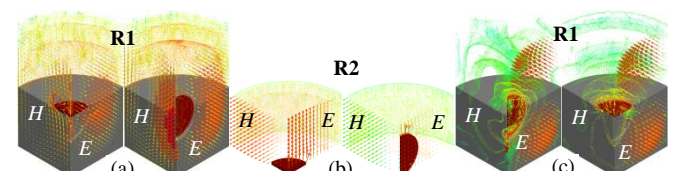


Fig. 5.3. E- and H-field distributions in resonators with samples in position 1h and 1v: (a) R1 with excited  $\text{TE}_{011}$  mode; (b) R2 with excited  $\text{TM}_{010}$  mode; (c) R1 with excited  $\text{TE}_{012}$  mode

determination of the dielectric constant  $\epsilon_f$  and saturation magnetization  $M_s$  of ferrite disks, prisms and cylinders, but calculated the demagnetized value  $\mu_{dem}$  by the known expression  $\mu_{dem} = (1/3)[1+2(1-(\gamma M_s/f)^2]^{0.5}$ , where  $\gamma = 3.5186$  MHz/(A/cm) is the gyro-magnetic ratio. Then in [A23], we began to measure the dielectric constant anisotropy of ferrites (Table 6, row 9). In our recent investigations of the Z-type hexaferrite  $\text{Sr}_3\text{Co}_2\text{Fe}_{24}\text{O}_{41}$  we managed to measure for the first time the full set of dielectric and magnetic parameters and the corresponding dielectric and magnetic anisotropy (for  $H_0=0$ ) above 3 GHz [A60]. In this case, we apply the following measurement procedure. The disk ferrite samples have been measured by the pair of resonators that support either TE<sub>0mn</sub> modes (in R1) or TM<sub>0m0</sub> modes (in R2) with samples placed in horizontal (1h) and vertical (1v) position in each resonator – see Fig. 5.2. The first several TE modes in R1 with  $m=1,2,3$  and odd  $n=1,3,5$  ensure extracting of parallel  $\epsilon_{par}$ ,  $\tan\delta_{\epsilon,par}$  (in 1h position) and perpendicular  $\epsilon_{perp}$ ,  $\tan\delta_{\epsilon,perp}$  (1v) dielectric parameters because the sample falls in the E-field maximums (Fig.4.19a), while the first TM modes with  $m=1,2,3$  – extracting of  $\epsilon_{perp}$ ,  $\tan\delta_{\epsilon,perp}$  (1h) and  $\epsilon_{par}$ ,  $\tan\delta_{\epsilon,par}$  (1v) (Fig. 5.3b). On the contrary, the first several TE modes with even  $n=2,4,6$  in R1 has minimums of the E fields and maximums of H fields in the place of sample and allow us to extract with enough accuracy the magnetic parameters: in parallel direction  $\mu_{par}$ ,  $\tan\delta_{\mu,par}$  (1v) and in perpendicular direction  $\mu_{perp}$ ,  $\tan\delta_{\mu,perp}$  (1h) (Fig. 5.3c). In fact, only TE modes with even  $n$  index have pure H-field maximum and pure E-field minimums in the place of the sample (shown in Fig. 5.4; excluding very high samples, Fig. 5.4b); the TE modes with odd  $n$  index and TM modes have mixed E and H fields in the place of the sample (illustrated in Fig. 5.3a,b). These fields exist in mutually perpendicular directions: modes, which allow  $\epsilon_{par}$  extraction, have been influenced by  $\mu_{perp}$  and v.v. That's why, the extraction procedure has been proposed as follows (the set of extracted values have been presented in Table 8). First of all, using TE modes with even  $n$  index and TM modes we determine intermediate values of the perpendicular and parallel dielectric parameters (Table 8: marked in grey) for  $\mu=1$  and

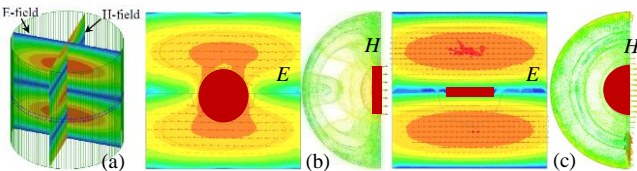


Fig. 5.4. E- and H-field distributions: a) R1 with TE<sub>112</sub> [A23]; b) R1 with TE<sub>012</sub> mode; sample in position 1v; c) R1 with TE<sub>012</sub> mode; sample in position 1h

Table 8. Extracted dielectric and magnetic parameters of hexaferrite  $\text{Sr}_3\text{Co}_2\text{Fe}_{24}\text{O}_{41}$  by the two-resonator method using different TE and TM modes for horizontally and vertically placed samples

Mode (resonance frequency, Q factor)	Sample orientation	Dielectric parameters: $\epsilon/\tan\delta_\epsilon$	Magnetic parameters: $\mu/\tan\delta_\mu$
TE <sub>011</sub> (12.4008/31.86) (13.0374/85.08)	hor. vert.	Par: 15.02/0.076 Perp: 9.03/0.25	Perp.: 0.96/0.32 Par.: 0.70/0.32
TM <sub>010</sub> (7.5620/31.86) (6.9632/194.5)	hor. vert.	Perp: 9.92/0.445 Par: 14.76/0.026	Par.: 0.70/0.30 Perp.: 0.96/0.32
TE <sub>012</sub> (15.6616/550.6) (15.6681/387.2)	hor. vert.	Par: 15.18/0.155 Perp: 7.95/0.47	Perp.: 0.92/0.70 Par.: 0.70/0.32
TE <sub>014</sub> (23.3829/963.1) (23.3907/511.0)	hor. vert.	Par: 14.20/0.070 Perp: 8.80/0.10	Perp.: 1.03/0.12 Par.: 0.73/0.40
<b>Averaged values (5-20 GHz)</b>		Par.: 14.70/0.08   Perp.: 9.30/0.15   Par.: 0.75/0.20   Perp.: 0.98/0.10 Dielectric anisotropy: 45/-61 %   Magnetic anisotropy: -27/67 %	

$\tan\delta_\mu = 0$ . Using TE modes with odd  $n$  index we determine  $\mu_{par}$ ,  $\tan\delta_{\mu,par}$  (1v) (for intermediate values  $\epsilon_{perp}$ ,  $\tan\delta_{\epsilon,perp}$ ) and  $\mu_{perp}$ ,  $\tan\delta_{\mu,perp}$  (1h) (for intermediate values  $\epsilon_{par}$ ,  $\tan\delta_{\epsilon,par}$ ). Then, with the obtained intermediate magnetic parameters we extract the corresponding final dielectric parameters and finally, we apply the same procedure for the determination of corresponding final magnetic parameters (Table 8: marked in black). Of course, there exists some uncertainty for the final obtained  $\epsilon$  and  $\mu$  parameters due to the differences between the resonance frequencies of the neighbour TE and TM modes. However, we apply additionally in [A60] a wideband method for final verifying of the frequency dependencies of ferrite material parameters (this procedure will be described later on). On the base of applied measurement methods we obtained the following averaged parameters for the considered Z-type hexaferrite  $\text{Sr}_3\text{Co}_2\text{Fe}_{24}\text{O}_{41}$  in the frequency range 5-15 GHz:  $\epsilon_{par} \sim 14.7$ ;  $\tan\delta_{\epsilon,par} \sim 0.08$ ;  $\epsilon_{perp} \sim 9.3$ ;  $\tan\delta_{\epsilon,perp} \sim 0.15$ ;  $\mu_{par} \sim 0.75$ ;  $\tan\delta_{\mu,par} \sim 0.20$ ;  $\mu_{perp} \sim 0.98$ ;  $\tan\delta_{\mu,perp} \sim 0.10$  (Table 8; last row). The measured anisotropy is relatively large, as for the dielectric parameters, as well as for the magnetic ones:  $\Delta\epsilon \sim 45\%$ ;  $\Delta\mu \sim -27\%$ .

## VI. PROPERTIES AND ANISOTROPY OF 3D-PRINTED DIELECTRICS

The opportunity for 3D printing of different dielectric, metallic or mixed artificial materials provokes nowadays a lot of new applications of these materials in the microwave devices, including antennas. The 3D printing as a modern additive technology gives also the possibility to mix two or more dielectrics in one mixture with well-designed properties for microwave applications similar like the known reinforced substrates, textile fabrics, antenna radome composites, foams, absorbers, etc. Thus, the 3D printing is practically an ideal technology for producing of a variety of anisotropic metamaterials [14], but also isotropic or anisotropic filling materials with common purposes, e.g. foam-like and substrate integrated non-radiating dielectrics, and also metallized 3D printed devices.

### A. 3D Printed Foam-Like Isotropic Dielectrics

We began to investigate in [A47] the 3D printed structures regarding possible artificial anisotropy of the resultant materials, and established some preliminary conditions for obtaining artificial isotropy – see Fig. 6.1. The conclusion is that it is easier to produce anisotropic materials by 3D printing than artificially isotropic materials. For example, designers of Luneburg lens antennas by 3D printing [58] have to produce relatively large in size complex artificial dielectrics with a specific spatial distribution of the dielectric constant but have to ensure also a practical isotropy/ homogenization (Fig. 6.1, the unit cell 1). The main condition for obtaining of an isotropic distribution of the dielectric constant is the applying of fully symmetrical unit cells along all three directions, which usually is in a contradiction with reliable mechanical properties of the whole printed body.

We discussed in our paper [A54] the possible 3D models, limitations and practical realization of artificial isotropic foam-like dielectrics by 3D printing, applying different suitable unit cells. The design strategy for the control of

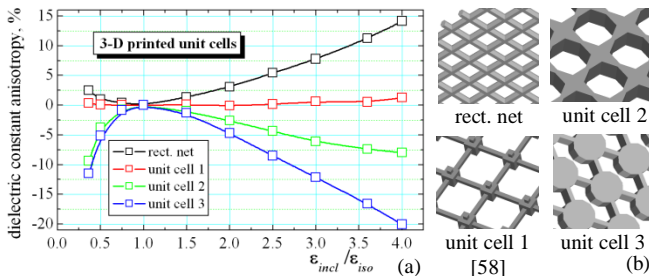


Fig. 6.1. Calculated dielectric anisotropy (a) of several 3D printed dielectrics with different unit cells (b) versus the ratio between the dielectric constants of inclusions and hosting substrate [58]

absolute values of the isotropic equivalent dielectric constant of these dielectrics has been demonstrated in Fig. 6.2 and Fig. 6.3. First of all, a suitable symmetrical unit cell can be selected with inclusions like cubes (Fig. 6.2a and [58]), spheres, prism, rhombs, cylinders or their combinations, supported by thin prismatic rods in all three directions. Then a bigger artificial substrate with appropriate dimensions has to be constructed by a repetition of the selected unit cell – Fig. 6.2b and Fig. 6.3. Finally, applying the procedure described in IID, we can calculate the equivalent (resultant) dielectric constant and loss tangent and compare with the measured values (Fig. 6.2c). The comparison for cube unit cell between our results and these in [58] is very good, at the comparison with measurement results for prism unit cell.

This technology is very effective and accurate for construction of 3D printed homogenous dielectrics with the desired dielectric constant. It is ideal now for fast and accurate 3D printing on different lenses as antennas – [58, 59]. We developed 2009 in [A29] accurate step models for an approximation of the dielectric constant gradient distribution in the Luneburg lens antennas and introduced effective 3D

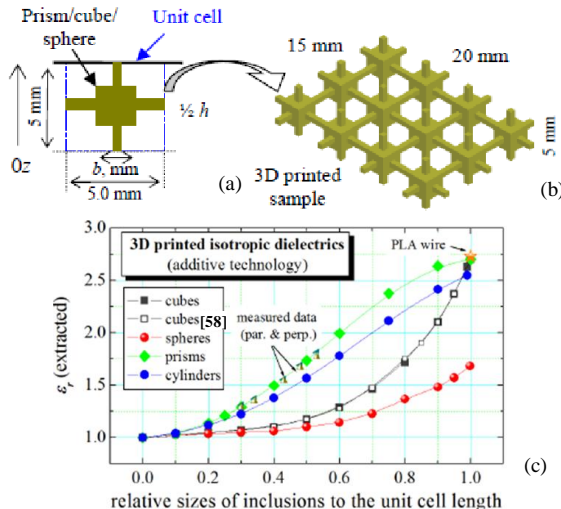


Fig. 6.2. Model of 3D printed sample: a) cubic unit cell 5×5 mm; b) whole substrate 15×20×5 mm; c) calculated and measured resultant dielectric constants by additive mixing technologies

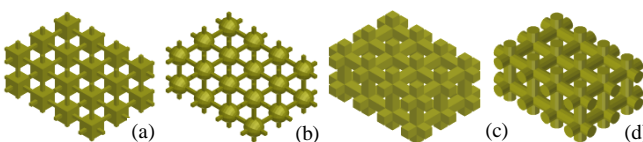


Fig. 6.3. Artificial isotropic samples constructed by unit cells with: a) cube; b) sphere; c) prism; d) cylinder

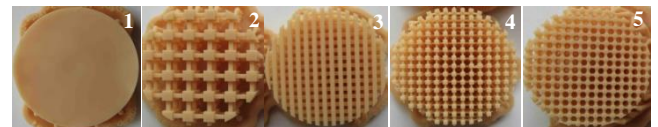


Fig. 6.4. 3D printed samples by Formlabs2® stereolithography (SLA) 3D printer applying dental model photopolymer resin FLDMBE01 (see the measurement results in Table 9)

Table 9. Measured dielectric parameters and anisotropy of 3D printed samples from Fig. 6.4

Sample description	thickness, mm	$\epsilon_{par}$	$\epsilon_{perp}$	Anisotropy $\Delta A_\epsilon$
1. Pure resin FLDMBE01	2.04	2.980	3.00	-0.67
2. Cubes 2×2 mm	7.70	1.332	1.330	0.15
3. Prisms 1×1 mm along to 0xy	9.30	1.497	1.450	3.19
4. Prisms 1×1 mm along to 0z	9.33	1.320	1.445	-9.04
5. Prisms 1×1 mm along to 0xyz	9.22	1.407	1.395	0.86

models for simulations of several variants of these promising antennas. Now we realize that these early models are fully applicable in the 3D printing of lens antennas and we have renewed our research on this topic. Fig. 6.4 presents several new 3D printed samples with controlled dielectric isotropy or anisotropy. They have been produced by Formlabs2 stereolithography (SLA) 3D printer applying photopolymer resin FLDMBE01, which ensures final size accuracy ~30  $\mu$ m.

The measurements of the dielectric parameters of these samples by the two-resonator method allow us to prove the concept for the symmetrical unit cells and foam-like dielectric behaviour. Fig. 6.5 illustrates well this concept. We constructed basic 3D net with square prisms (side 1 mm) and added new prisms with different sides (2.5 and 4 mm) and tuned length, orientated in different directions. The result is an increase of the absolute anisotropy  $\Delta A_\epsilon$ , which depends on the degree of filling, nevertheless, if its sign is positive (for horizontal orientation) or negative (for perpendicular orientation of the prisms). Only for pure cubic unit cell, the anisotropy keeps its small absolute value (the presented research is still in progress).

### B. 3D Printed Dielectrics with Non-Symmetrical Unit Cells

The 3D printers generally save time and material by making the interior of the printed object not completely solid (with low infill density). The hexagonal and rectilinear grid

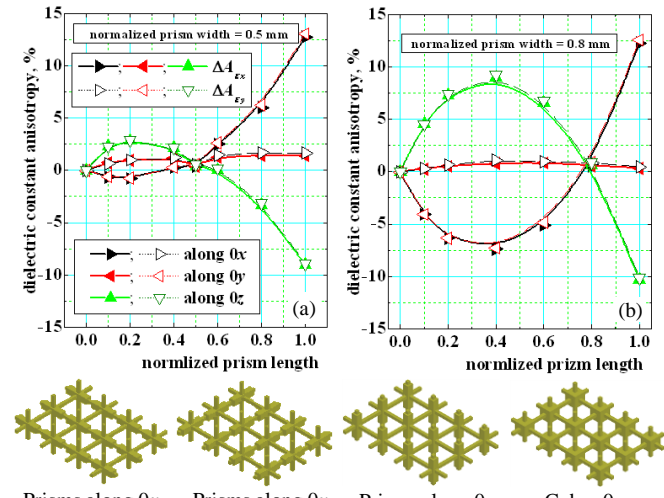


Fig. 6.5. Dielectric constant anisotropy of 3D printed nets made by prisms with different sides and lengths (both normalized to the unit-cell length 5 mm)

infill is the most common because the samples are strength and light. However, due to the poor unit-cell symmetry, the resultant anisotropy of samples with hexagon infill is relatively large for electro-dynamic purposes. Fig. 6.6a presents the dependence of uni-axial anisotropy  $\Delta A_\varepsilon$  on the outer hexagon side length  $a$  (normalized to the whole sample height  $h$ ). The sign is negative for the chosen absolute height  $h= 2$  mm; an absolute maximum appears, when the cell length is close to the height, i.e.  $a \sim h$ . In the case of mixed hexagonal-triangle filling, this maximum has been shifted for higher  $a/h$ . The anisotropy depends also on the width  $w$  of the hexagonal walls – see Fig. 6.6b; there also exists an absolute maximum for  $\Delta A_\varepsilon$  (the sign is negative for the fixed height). However, the most interesting is the  $\Delta A_\varepsilon$  dependence on the sample height  $h$  – see the corresponding curve in Fig. 6.6b for the normalized height to the hexagon length  $a$ . We can see that the anisotropy has as positive, as well as a negative sign. In our case, when the height  $h$  is about 20 % from the cell length  $a$ , the anisotropy is  $\Delta A_\varepsilon \sim 0$ . This is an important fact – the equivalent dielectric constant of the considered 3D printed dielectric depends on the sample height! It shows also how difficult is to achieve isotropy of such materials on the base of hexagonal (or other non-symmetrical) filling.

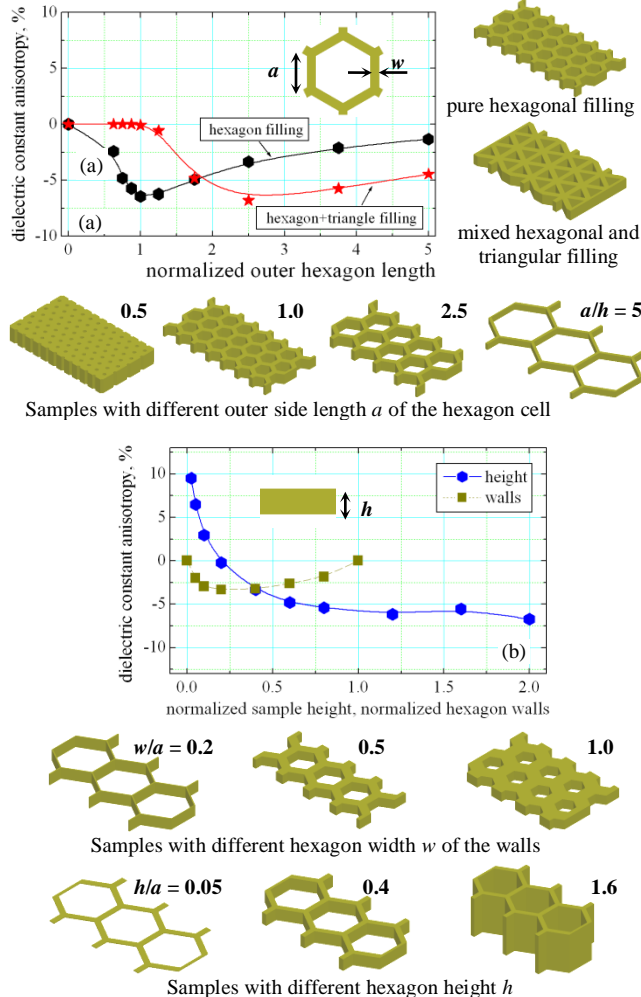


Fig. 6.6. Uniaxial anisotropy in 3D printed samples with hexagonal infill versus (a) normalized outer side length  $a$  ( $a/h$ ); (b) normalized hexagon width  $w$  and height  $h$  ( $w/a$ ;  $h/a$ )

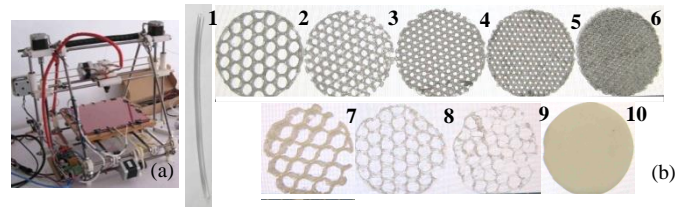


Fig. 6.7. 3D printed samples by fused deposition modelling with PLA filament applying low-cost 3D printer MakerGear® (a). Samples (b): pure PLA wire 1, samples 2-9 with infill 60-10 % and different height; dense (~100 %) 3D printed photopolymer 10 (see measurement results for samples 1-10 in Table 10)

Table 10. Measured dielectric parameters and anisotropy of 3D printed PLA samples from Fig. 6.7

Samples	$h$ , mm	$\epsilon_{par}/\tan\delta_{e,par}$	$\epsilon_{perp}/\tan\delta_{e,perp}$	Anisotropy $\Delta A_\varepsilon/\tan\delta_e\%$
1. PLA wire	$d = 2$	2.750/0.0080	2.750/0.0080	0/0
2. infill 20 %	1.85	1.310/0.00260	1.273/0.00146	2.9/56
3. 30 %	1.69	1.368/0.00287	1.328/0.00161	3.0/57
4. 40 %	1.88	1.555/0.00378	1.504/0.00229	3.3/49
5. 50 %	1.42	1.690/0.00493	1.620/0.00281	4.2/55
6. 60 %	1.68	1.810/0.00524	1.710/0.00310	5.7/178
7. 10 %	6.70	1.177/0.00158	1.216/0.00177	-3.3/-11.3
8. 10 %	1.30	1.111/0.00128	1.134/0.00093	-2.1/31
9. 10 %	0.96	1.035/0.00095	1.071/0.00052	-3.4/58
10. photopolymer 100 %	1.69	2.961/0.0049	2.960/0.0053	0.03/-7.8

We were able to prove this effect experimentally. Table 10 presents the measured dielectric parameters and anisotropy of several home-made samples from polylactic acid (PLA) polymer, applying a very low-cost 3D printer.

The photos of some produced and measured samples have been given in Fig. 6.7. Nevertheless the non-perfectly produced samples, we can see the tendency: the anisotropy  $\Delta A_\varepsilon$  increases with infill increase (3-6%; stronger for  $\Delta A_{\tan\delta_e}$ ). A negative anisotropy has been observed for samples with predominant vertically deposited walls. A dense (~100-%) 3D printed photopolymer sample shows well-expressed homogenization, which is an expectable fact. All these investigations are still in progress.

### C. Anisotropy of Substrate Integrated Nonradiative Dielectrics (SINRD)

A new class of substrate integrated nonradiative dielectrics (SINRD) has been proposed in [60]. They are ordinary substrates with a drilled pattern of air holes. The idea is to decrease the equivalent dielectric constant and dielectric loss tangent and to increase the applicability of these artificial materials in the mm-wavelength range. A similar approach can be used also for easy construction of Luneburg lens antennas, made by slices with incorporated air holes [61]. However, in these cases, we again detect the already pointed reasons for appearing of uni-axial anisotropy – directed inclusions (air cylinders in this case), placed perpendicularly to the isotropic substrate surface. We performed special research on the influence of the incorporated air holes of diameter  $d$  at distance  $L$  on the dielectric constant and anisotropy of isotropic polycarbonate (PC) substrate. As in the case of 3D printed materials with non-symmetrical (e.g. hexagonal) filling, we found out that the dielectric anisotropy of SINRD strongly depends on the air inclusions' dimensions and substrate height  $h$  – see Fig. 6.8. The anisotropy  $\Delta A_\varepsilon$  could be as with positive, as well as with negative sign for small  $L/d$  values.

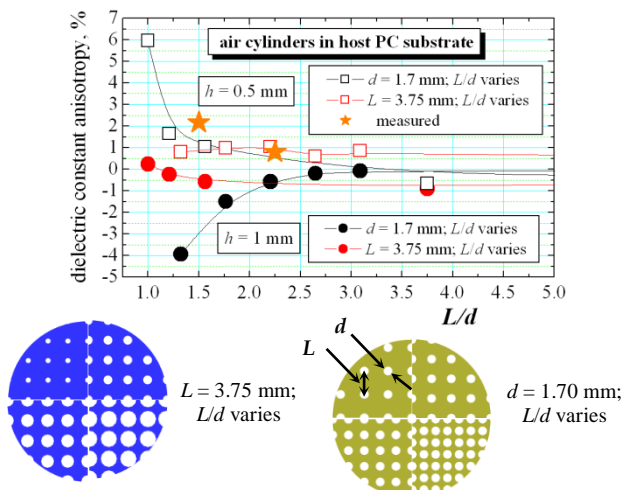


Fig. 6.8. Dielectric constant anisotropy due to the air-filled cylinders in isotropic PC substrate (SINRD)

Table 11. Measured isotropic PC and anisotropic Arlon 25N samples without/with air via holes

Samples	$h$ , mm	$\epsilon_{par}/\tan\delta_{e,par}$	$\epsilon_{perp}/\tan\delta_{e,perp}$	Anisotropy $\Delta A_e/A_{tan\delta_e}\%$
Polycarbonate (PC)	0.50	2.765/0.0050	2.764/0.0049	0.04/2.02
PC + air holes ( $d \sim 1.7$ )	0.50	2.474/0.00428	2.421/0.00409	2.17/4.54
Arlon 25N	0.513	3.645/0.00401	3.309/0.00287	9.67/33.14
Arlon 25N + air holes ( $d \sim 1.5$ )	0.513	3.413/0.00365	3.113/0.00267	9.21/31.01

We tested experimentally by the two-resonator method the influence of perpendicular air via holes in isotropic PC sample and anisotropic commercial substrate Arlon 25N (results in Table 11). The anisotropy  $\Delta A_e$  increases for isotropic PC with air holes to 2.17 %, while the anisotropy in the anisotropic substrate slightly decreases due to the incorporated isotropic (air) inclusions.

#### D. Anisotropy of Fresh Plant Tissues with Cell Structure

The dielectric anisotropy of the fresh plant tissues with cell structure can play an important role in the determination of the so-called fresh weight (FW). The nondestructive FW determination of young plant shoots, leaves, seeds, blossoms etc. is necessary for the diurnal regulation of plant growth and ensures valued information for the growing processes [62, 63]. In [A48] we managed to show that the dielectric anisotropy of these tissues is very large as in a fresh state, as well as in a dry state, probably due to the specific hexagonal cell structure (as in the case of 3D printed samples). Walnut leaves have been selected for the anisotropy test. We made disk samples from the leaves and put them in vertical or horizontal positions in resonators (Fig. 6.9a,b), which support simultaneously TE<sub>011</sub> and TM<sub>010</sub> modes (Fig. 6.9c). Due to the different water content, the resonance shifts depends on the actual sample FW and can be used for building of a calibration curve “frequency shift  $\Delta f$ , MHz – fresh weight FW, mg” by stacking together a different number of equal disk samples, smoothly increasing FW. However, we found out that the calibration curves differ for samples orientated vertically and horizontally; dependencies are given in Fig. 6.10. The reason definitely is the large leaves anisotropy. We determined the dielectric parameters of fresh and dry leaves – Table 12; both dielectric constants and anisotropy  $\Delta A_e$  decreases with the sample drying, remaining large – from 92 up to 35%. Thus, if we apply one of the obtained calibrations

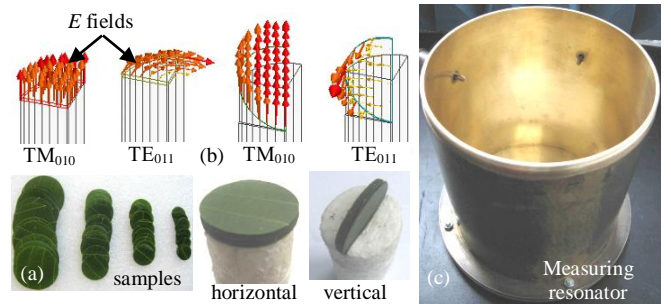


Fig. 6.9. (a) Walnut leaves and disk samples under test; (b) 3D models plant tissue of disk samples from leaves, placed horizontally and vertically on foam support in measuring cylinder resonator (c) with pair of TM<sub>010</sub> and TE<sub>011</sub> modes ( $D = 150$  mm,  $H = 172$  mm)

Table 12. Data for measured parallel and perpendicular dielectric parameters and anisotropy of samples from fresh and dry walnut leaves

Sample description	$\epsilon_{par}/\tan\delta_{e,par}$	$\epsilon_{perp}/\tan\delta_{e,perp}$	Anisotropy $\Delta A_e/A_{tan\delta_e}\%$
Immediately after the pick-up of the leaves	24.8/0.315	9.15/0.235	92/29
1.5 hours after the pick-up of the leaves	16.1/0.305	7.65/0.225	71/30
Dry leaves	2.0/0.0525	1.4/0.0275	35/63

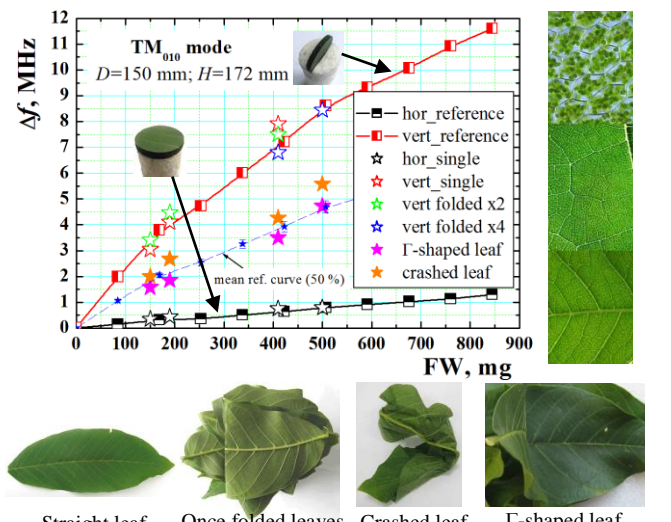


Fig. 6.10. Calibration curves for horizontal and vertical sample orientation: frequency shift v/s FW in mg for TM<sub>010</sub>-mode and positions on the plot for some unknown samples (single straight leaf, once or twice folded leaves,  $\Gamma$ -shaped or crashed walnut leaves)

curves for FW determination of plant with different leaves orientations (as in Fig. 6.11e), we will get wrong results. To prove our concept, we constructed 3D models of a fictive plant organism with three leaves (with stem) in different orientations, which have noticeable dielectric anisotropy (parallel/normal dielectric constant 35/5) – Fig. 6.11a-d. The obtained frequency shifts in MHz and recalculated relative FW are given in the insets. We can see that in both opposite cases (a, b) the shifts differ 19 times (!) for TM<sub>010</sub>. For leaves in an inclined position (c) or a mixed position (d) the shift is practically the mean value from both opposite shifts. For example, if we measure crashed or  $\Gamma$ -shaped (half of the leaf is placed vertically and the other half – horizontally) walnut leaves, the point for FW fall exactly in the middle zone between the pair of reference curves in Fig. 6.10. This fact gives a possible solution for the right prediction of the FW of the whole plant organism by nondestructive resonance method – to introduce a correction coefficient  $K$  depending on the predominant leaves' orientation in the real plant. Let

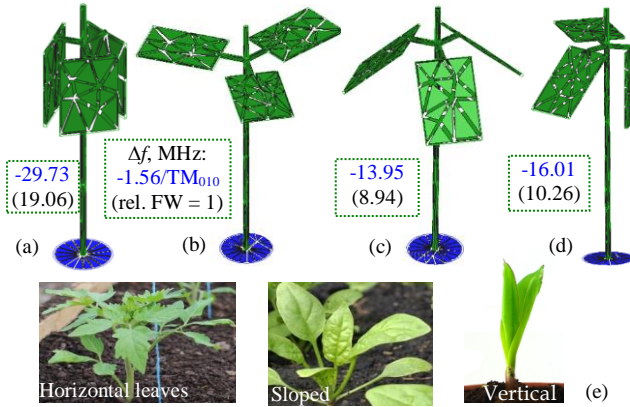


Fig. 6.11.3D models of a fictive plant organism with 3 leaves placed: (a) vertically to the resonator axis; (b) horizontally; (c) with slope 45 deg; (d) mixed position (data in boxes: frequency shift and calculated FW relative to the case (b); (e) examples for plants with different leaves orientation

the averaged relative portion of the horizontally placed leaves in the whole plant organism is  $x$  (determined by optical methods). If the frequency shifts for pure horizontal and pure vertical orientations of the plant leaves are  $\Delta f_h$  and  $\Delta f_v$ , the correction coefficient could be  $K = (1-x)\Delta f_v + x\Delta f_h$  and the actual fresh weight will be  $FW = K.FW_h$ , where  $FW_h$  is the fresh weight, which corresponds to pure horizontal orientation. For example, a mean reference curve is given in Fig. 7 for  $x = 0.5$  (50 %). Thus, for  $FW = 500$  mg of the  $\Gamma$ -shaped sample ( $x = 0.5$ ), the calculated coefficient is  $K \sim 4.61$  (the actual shift is 4.72, the measurement uncertainty is less than 2.4 %; instead ~600 % without taking the anisotropy into account). Therefore, the correction procedure allows enough accurate determination of FW taking into account of the actual plant tissue anisotropy.

## VII. DIELECTRIC PROPERTIES AND ANISOTROPY OF MICROWAVE METAMATERIALS

The engineered microwave metamaterials and photonic band-gap crystals can be designed with controllable dielectric/magnetic constants along the different directions. In this case, the artificial anisotropy is a fully desired property, which ensures unusual characteristics of some anisotropic metamaterial devices [7, 15] like invisibility cloaks, EM concentrators, EM-wave converters, etc. We will concentrate our attention on specific issues connected with experimental dielectric properties' characterization of these materials. As we already pointed in III, there exist a lot of measurement methods for material characterization, but only a few of them can determine with acceptable accuracy the artificial anisotropy. In this section, we will share our experience for anisotropy characterization of metamaterials.

### A. Metamaterials with Metal Inclusions on the Substrate Surface

We began to present the results from our research on different types of metamaterials in [A47]. Then, in the paper [A51] we discussed the results of interesting research: two selected metamaterials with metal surface inclusions on a standard substrate have been measured by different methods and the extracted values of the equivalent dielectric constants have been compared. These materials have been developed

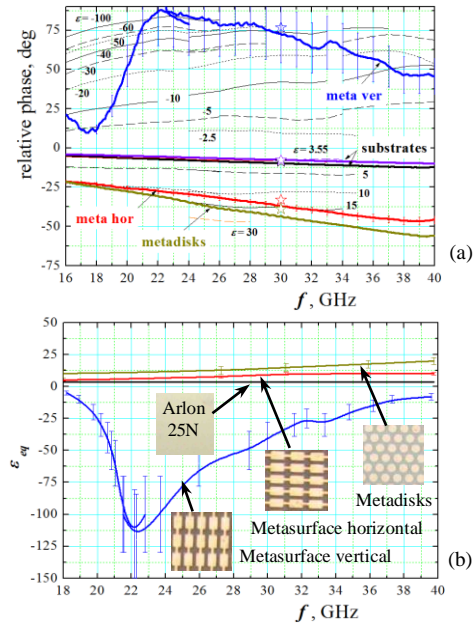


Fig. 7.1. (a) Measured relative phase delay/advance by the free-space method in K/Ka bands through two types of meta-samples with rectangular and disk metal inclusions (sample 1 “meta-disks”: symmetrical planar unit cell with disks of diameter 3 mm and distance between them 4 mm, one-side printed on Arlon 25N (6 mils); sample 2 “meta-surface”: non-symmetrical planar unit cell 3x1.5 mm two-side printed on substrate Arlon 25N (10 mils); (b) extracted values of the equivalent dielectric constants of the samples (stars – simulated by HFSS® meta-samples at 30 GHz)

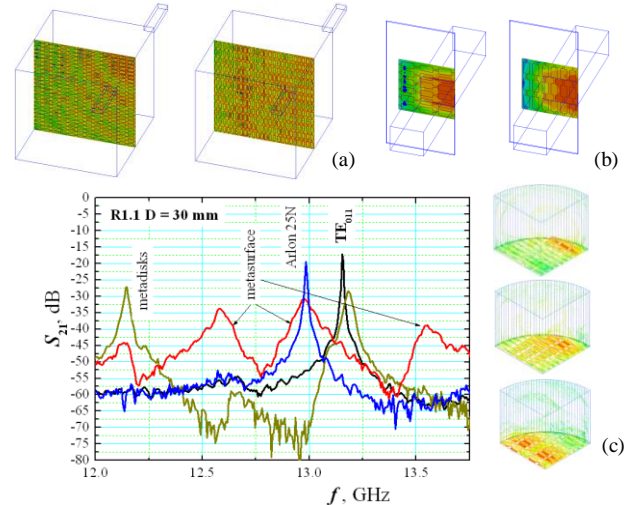


Fig. 7.2. Split 3D models for numerical  $\epsilon_{eq}$ -extraction by free-space method (a) and rectangular waveguide method (b). (c) Measured  $TE_{011}$  mode excited in a cylinder resonator with meta-samples (inset: calculated E-field distribution of parasitic multiple resonances around the  $TE_{011}$  mode)

for application in antenna radomes in the Ka-band. Fig. 7.1 presents the additional phase delay through samples' thickness, measured by a free-space method in the K/Ka-bands, and the extracted equivalent dielectric constant  $\epsilon_{eq}$  of samples, which photos have been given as insets. The first dielectric (“meta-disks”) has an increased dielectric constant in parallel directions (measured by the two-resonator method in [A49]). The second sample (“meta-surface”) placed horizontally, i.e. the rectangular unit cell is orientated perpendicularly to the electric field of the incident wave, shows similar behaviour. However, the same sample in a vertical position causes opposite phase delay (phase advance;

Fig. 7.1a) and the extracted parallel dielectric constant has a negative sign – Fig. 7.1b. The extraction has been performed by simulation of a specially constructed split 3D model of the metasamples – Fig. 7.2a. The considered samples remain the same dielectric behaviour by applying the rectangular waveguide measurement method – Fig. 7.2b, which is very popular for metamaterials (the extracted dielectric parameters have been presented in [A51]). However, the two-resonator method cannot be used for the characterization of metamaterials in all cases. Usually, the resonance measurements by TM mode resonators are normal, while the measurements by TE mode resonators sometime give multiple resonances instead one curve for a fixed mode. Fig. 7.2c illustrates this effect; due to resonance excitations in parts of the whole sample with metal inclusions a set of multiple resonance curves appears (as in the measurements, as well as in the simulations) and the right identification now is impossible. In such cases, we cannot determine the meta-sample anisotropy for negative dielectric constants; the reasons have been explained in detail in [A51, A59].

### B. Metamaterials with Controllable Filling Inclusions

In this section, we describe a successful attempt for the characterization of porous metamaterials using a combination of resonance and broadband methods [A58]. The objects of investigations are thin (6-100  $\mu\text{m}$ ) anodic aluminium oxide (AAO) layer from anodic  $\text{Al}_2\text{O}_3$  membranes with formed nano-scale air-filled pores. Such samples can be used as template matrices for incorporation into the pores of different nanostructured materials such as nanodots, nanowires and nanotubes with many nowadays applications [65, 66]. At this stage of our research, we are trying only to test the technology and the degree and type of inclusions are not well controlled. We prepared AAO samples with different relative purity (illustrated in Fig. 7.3; the purity depends on the degree of different technological contaminations). These initial investigations aim to determine for the first time in the microwave range their dielectric parameters and possible anisotropy and how the manufacturing technology influences these parameters. Table 13 presents the measured by the two-resonator method mean values of the parallel and perpendicular dielectric parameters for 4 selected samples with different purity. Definitely, samples with good purity (p1,2) have the behaviour of pure alumina ceramics with a set of air pores orientated in perpendicular directions: i.e.  $\epsilon_{\text{par}} < \epsilon_{\text{perp}} \sim 9.7\text{-}9.95$ . Thin samples with lossy inclusions (p3) have opposite behaviour  $\epsilon_{\text{par}} > \epsilon_{\text{perp}} \sim 2.8$ , while both dielectric constants increase ( $\epsilon_{\text{par}}, \epsilon_{\text{perp}} > 10.4\text{-}13.5$ ) for samples, which include irregular metal contaminations (p4). As we can conclude, in all cases the measured anisotropy is very large and this information can be used for fine technology adjustment of the porous AAO membranes.

However, such complex materials usually may have expressed frequency dependence of the dielectric parameters and anisotropy and even resonance behaviour. The applied here two-resonator method gives enough accurate information, but at fixed frequencies; to obtain informative dependencies in bigger frequency range we have to use another wideband transmission-line method (IIIC). Unfortunately, on this stage



Fig. 7.3. a) View of anodic aluminium oxide (AAO) samples with decreasing purity (p1, p2 – pure or relatively pure pores; p3 – pores with lossy magneto-dielectric contaminations; p4 – pores with metal inclusions; b) microscopic side view of nanopores of diameter 35 nm

Table 13. Dielectric parameters and anisotropy of 4 typical disk AAO samples with different thickness (mean values for the frequency range 7-15 GHz) (more information in [A58]).

Samples	$D_t, \text{mm}$ , $h_t, \mu\text{m}$	$\epsilon_{\text{par}}/\tan\delta_{\epsilon,\text{par}}$	$\epsilon_{\text{perp}}/\tan\delta_{\epsilon,\text{perp}}$	Anisotropy $\Delta A_\epsilon/A_{\tan\delta\%}$
S0 (p1)	29.7/42	5.96/-	9.68/-	-48/-
S1 (p2)	26/30	5.00/0.011	9.95/0.0005	-66/183
S2 (p3)	26/18	10.50/0.016	2.78/0.0175	116/-9
S3 (p4)	26/100	13.52/0.039	10.38/0.48	26/170

of technology, it is very difficult to print any metal layout on the considered AAO samples to form a measurable transmission line or resonator. Because of that, we applied another strategy for measurements – to obtain the needed information for the dielectric parameters, when the samples cover standard 50-Ohms planar lines: coplanar waveguide (CPW) or microstrip line (MSL) printed on a standard commercial substrate (in our case Arlon® 25N, 0.508-mm thick). We already applied this broadband method (Fig. 5.4) for a direct determination of equivalent dielectric constants of commercial substrates [A44], for metamaterials with metal surface inclusions [A51, A59], for thin nano-absorbers [A61], hexaferrites [A60] and Graphene-containing materials [A59].

In fact, the E fields of the dominant modes in both planar waveguides have mixed distribution (neither pure parallel nor pure perpendicular). The concrete proportions parallel-to-perpendicular E fields in the whole transmission lines (substrate and air space above) on 20-mils substrates have been estimated [A44] as ~38:62 in MSL and ~79:21 in CPW. Therefore, the covered CPW will extract predominantly value  $\epsilon_{eq}$  close to  $\epsilon_{\text{par}}$ , while the covered MSL – a mixed value  $\epsilon_{eq}$  between  $\epsilon_{\text{par}}$  and  $\epsilon_{\text{perp}}$ . We applied an extraction procedure for the determination of the equivalent dielectric constant  $\epsilon_{eq}$  (on the base of measured additional phase delay in CPW or MSL) and equivalent dielectric loss tangent  $\tan\delta_{\epsilon,eq}$  (only for lossy samples on the base of measured additional losses). This procedure has been developed applying simulations of well-constructed 3D models of the CPW or MSL structures (see Fig. 7.4d) with and without sample [A58]. Nevertheless, that the AAO samples have been placed on the CPW/MSL conductors under equal pressure (Fig. 7.4c), an unavoidable air gap  $g_a$  between the SUT and planar line conductors appears (Fig. 6.35a) due to different reasons: surface roughness, cleanliness, curvature, etc. However, this gap can be accurately determined by a simple way: we can preliminary measure several isotropic materials with known dielectric parameters (e.g. PTFE;  $\epsilon_r \sim 2.05$ ; Polycarbonate,  $\epsilon_r \sim 2.78$ ; Kapton®,  $\epsilon_{eq} \sim 3.16$ ). In the considered case the obtained effective air gap values are:  $g_a \sim 2.5 \pm 0.5 \mu\text{m}$  for MSL and  $g_a \sim 17.5 \pm 2.5 \mu\text{m}$  for CPW.

Fig. 7.5 gives the measured additional losses and phase delay in CPW/MSL transmission lines caused by the covering AAO sample. There are two ways to extract the dielectric parameters of AAO samples from these data: 1) to

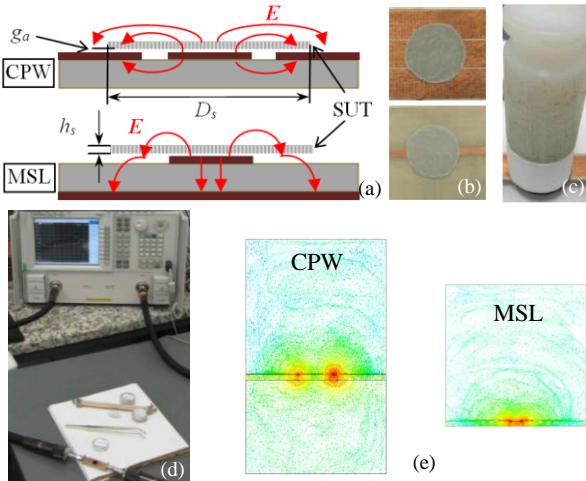


Fig. 7.4. (a) Transmission-line method: cross-section view of coplanar waveguide (CPW) and microstrip line (MSL) covered by SUT ( $E$  – electric field patterns); (b) SUT covers CPW and MSL; (c) equal pressure has been ensured for all AAO samples; (d) measurement setup with VNA; (e) Stylized 3D models of CPW and MSL and  $E$ -field distribution (red colour – strong fields; green – medium fields; blue – weak fields)

tune the equivalent parameters  $\epsilon_{eq}/\tan\delta_{\epsilon,eq}$  in the 3D models (Fig. 7.4d) until acceptable coincidence between the simulated and measured phase delay and losses (last for lossy materials only) has been reached or 2) to introduce in the 3D models the pairs of parameters  $\epsilon_{par}/\tan\delta_{\epsilon,par}$  and  $\epsilon_{perp}/\tan\delta_{\epsilon,perp}$  from the resonance measurements and to compare the simulated and measured dependencies. In this example, we selected the second way, taking the dielectric parameters from Table 13.

Samples S1,2 show behaviour as a pure dielectric (S1) or a lossy dielectric (S2) – the additional losses are relatively small and the phase delay increases almost linearly with frequency increase; the practical coincidence shows that the dielectric parameters from the resonance measurements are fully correct. However, the sample S3 has behaviour as a conductive material. This type of behaviour has been expressed with a nonlinear phase delay, which can decrease at higher frequencies and observation of very big losses. If we neglect the conductivity, the calculated losses are few dB, considerably smaller than the measured (not shown). For that reason, we have to introduce additionally to the dielectric parameters for this sample also an equivalent conductivity  $\sigma_{eq}$ . During the simulations, we vary the  $\sigma_{eq}$  values and compare the theoretical and measured dependencies simultaneously for additional losses and phases. We can observe a strong  $\sigma_{eq}$  influence for both types of curves. The procedure for such a conductive sample is as follows. First, from the dependency for additional losses in MSL structure (Fig. 7.5b) we can evaluate the equivalent conductivity  $\sigma_{eq,MSL}$  (the dielectric constant doesn't influence so much the losses). The obtained values are:  $\sigma_{eq,MSL} \sim 3-10$  S/m (for the frequency range 1-5 GHz),  $\sim 10-20$  S/m (5-10 GHz),  $\sim 20-35$  S/m (10-30 GHz),  $\sim 35-50$  S/m (30-40 GHz). The simulated values for  $\sigma_{eq,CPW}$  in CPW structure are similar (Fig. 7.5a); typically  $\sigma_{eq,CPW} \sim 35$  S/m. Now, if we consider the phase delay dependence in MSL, the combination of values  $\epsilon_{eq,MSL} \sim 9-10$  and  $\sigma_{eq,MSL} \sim 35-40$  S/m is the solution for this conductive sample S3. The phase delay dependence in CPW

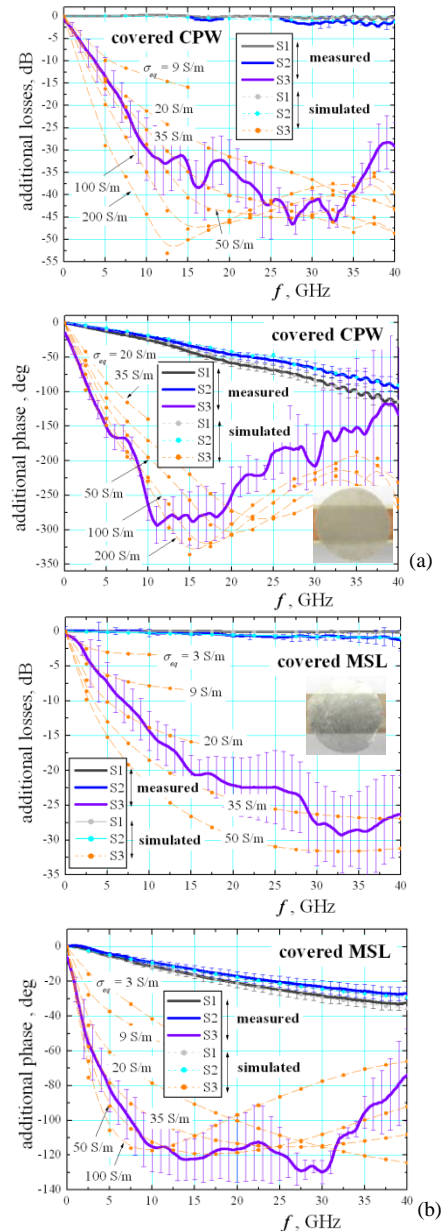


Fig. 7.5. Measured additional losses and phase delay in CPW (a) and MSL (b) transmission lines after covering by thicker AOO samples (solid curves). Theoretical dependences (dashed curves), obtained by 3D simulations with dielectric parameters from Table 13 (anisotropy option) and setting of effective air gaps  $g_a = 2.5$   $\mu$ m (MSL) and 17.5  $\mu$ m (CPW)

gives slightly different combination,  $\epsilon_{eq,CPW} \sim 11-12$  and  $\sigma_{eq,CPW} \sim 50$  S/m; the difference means that the parallel dielectric constant and conductivity are bigger.

The obtained results for the dielectric characterization of AAO samples show that the proposed combination of resonance and broadband microwave methods is working well for such complex metasamples with variety of dielectric or metal inclusions. Samples with a small amount of metallic contamination can be better characterized with high accuracy. Samples with higher conductivity are also measurable: dielectric constants and anisotropy by the resonance method and equivalent conductivity – by the broad-band transmission-line method. All these interesting and promising investigations are in progress.

### C. Carbon-Containing Materials

A good example for successful simultaneous determination of the pair of equivalent parameters  $\varepsilon_{eq}/\sigma_{eq}$  according to the Drude's model for conductive dielectrics (when the loss tangent has been neglected; expression (6)) is the characterization of several carbon-containing materials. In this section, we selected three types of samples: spectral pure Graphite, air-filled Graphite and pressed Graphene. The measured additional phase delay in CPW transmission line has been given in Fig. 7.6a, while the extracted equivalent dielectric

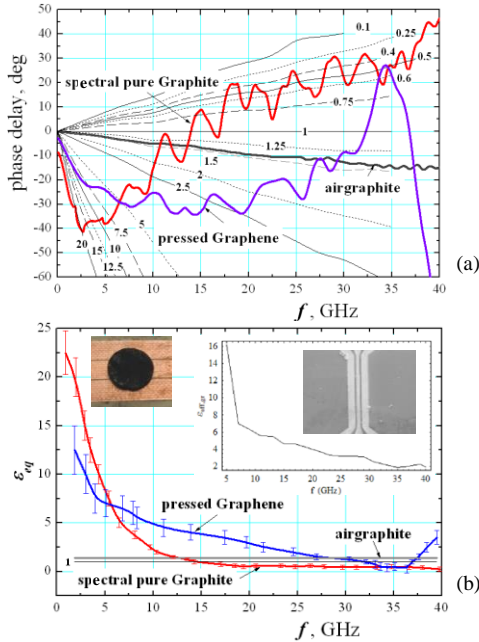


Fig. 7.6. (a) Measured relative phase delay/advance in Graphite, air-filled Graphite and pressed Graphene samples by covered CPW (sample diameter  $\sim 9$  mm; thickness 0.9 mm;  $g_a = 20 \mu\text{m}$  gap "sample-conductor"; (b) extracted  $\varepsilon_{eq}$  values (inset: dielectric constant of graphene by [66])

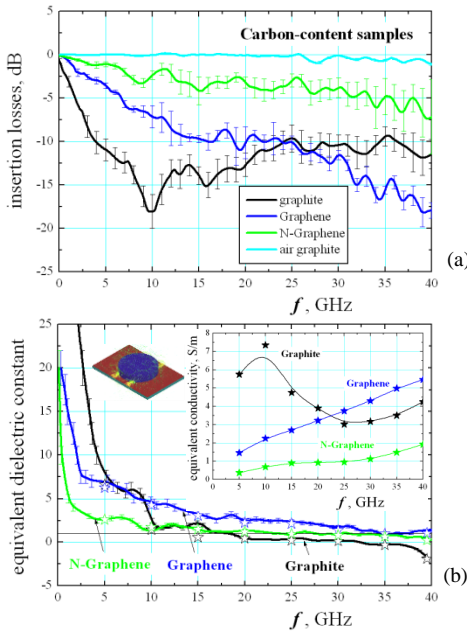


Fig. 7.7. (a) Measured additional losses in CPW with carbon-containing samples as an overlay; (b) extracted frequency dependencies of  $\varepsilon_{eq}$ ; stars: values of the equivalent dielectric constants by taking into account of the actual conductivity (inset: extracted equivalent conductivity  $\sigma_{eq}$ )

constant  $\varepsilon_{eq}$  – in Fig. 7.6b (when  $\sigma_{eq}$  has been neglected) [A51, A59]. The air-filled Graphite has the behaviour like a low-Dk dielectric;  $\varepsilon_{eq} \sim 1.4-1.5$ . However, the other materials demonstrate completely different behaviour: the phase delay at lower frequencies transforms into phase advance (positive delay). In this case, the extracted  $\varepsilon_{eq}$  values show strong frequency dependence – from 15-20 below 2 GHz up to 1 and even values below 1 for both Graphite and pressed Graphene samples. This dependence corresponds to the published results from other authors (e.g. [66]). However, the measured additional losses in CPW of these samples are very big (Fig. 7.7a) and cannot be explained with dielectric losses only; the samples have also a big equivalent conductivity  $\sigma_{eq}$ . As in the previous example, we can extract this parameter (the differences between samples are well observable; we added also the dependence for Nitrogen (N)-doped Graphene [67]; 5.5-% doping level). We established that the sensitivity and accuracy of the CPW measurement systems to the  $\sigma_{eq}$  variations are better in comparison to the MSL case; that's why we concentrate our efforts on CPW structure only. The extraction procedure is as follows. We use in the 3D models (inset in Fig. 7.7b) the initial  $\varepsilon_{eq}$  value (determined for  $\sigma_{eq} = 0$ ; Fig. 7.6b) and starting to tune the conductivity to match the simulated and measured losses at a fixed frequency, we can determine  $\sigma_{eq}$  at the same frequency. Then, simulating the phase delay/advance with the new  $\sigma_{eq}$  value at each selected frequency, we can recalculate the final  $\varepsilon_{eq}$  value – results for the extracted  $\varepsilon_{eq}/\sigma_{eq}$  dependencies are visible from Fig. 7.7b (the changes for  $\varepsilon_{eq}$  are negligible). The measured  $\sigma_{eq}$  values in the frequency range 5-40 GHz are relatively small due to the air gaps in the weakly-pressed samples.

### D. Plasmas

Plasmas (gaseous, solid-state) are such media, which also can have an expressed anisotropy of their dielectric properties depending on the realized type of plasma discharge and orientation of the external magnetic fields (if exists). In our research, we developed several hairpin probes for resonance measurements of plasma densities in different directions [A27, A37, A37]. The hairpin probe is a simple

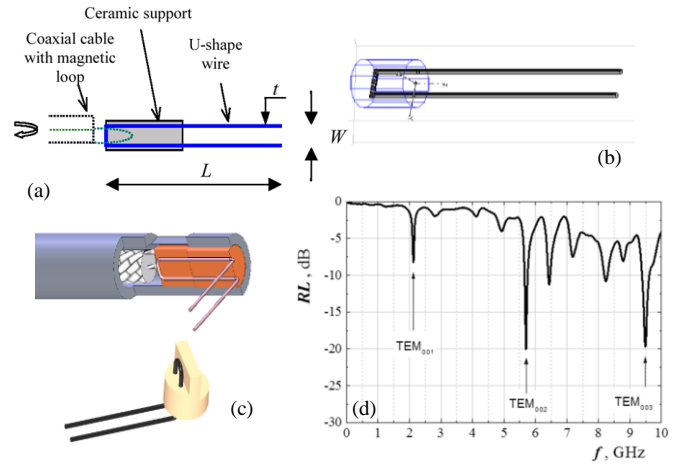


Fig. 7.8. (a) U-shape straight (180-deg) hairpin probe and (b) its 3D model in an eigenmode option of the simulator; (c) U-shaped hairpin probe orientated at 90 deg with ceramic support on the shorted end; (d) measured return losses of the hairpin probe in the air with the exciting first three TEM-mode resonances (2-10 GHz)

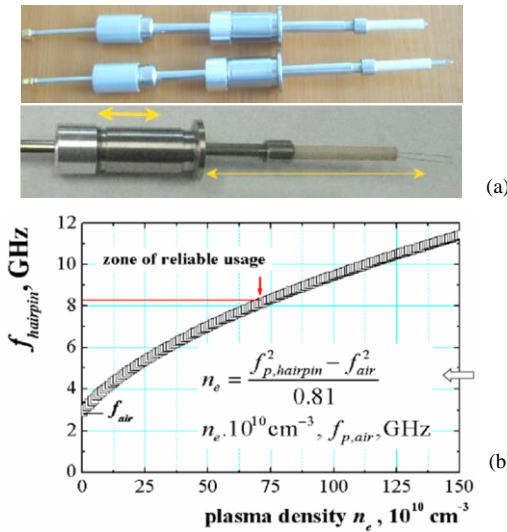


Fig. 7.9. a) Tools for mounting of the hairpin probe in the vacuumed plasma reactor; c) dependence of the hairpin resonance frequency  $f_{\text{hairpin}}$  on the plasma density  $n_e$ . Inset: expression between  $f_{\text{hairpin}}$  and  $n_e$

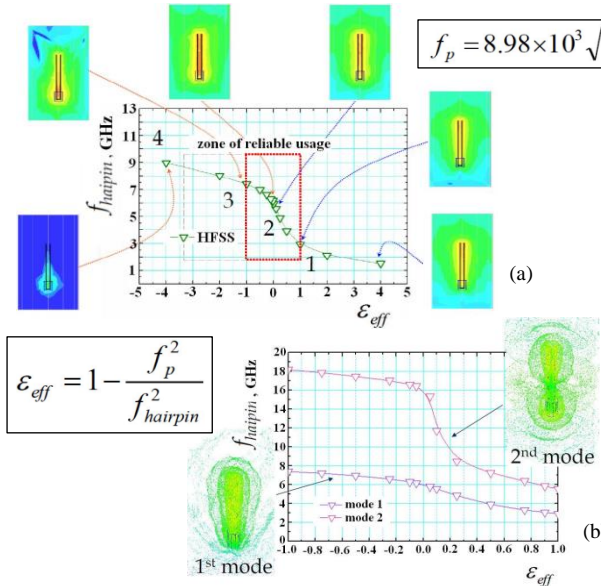


Fig. 7.10. (a) Dependence of the hairpin resonance frequency  $f_{\text{hairpin}}$  on the effective plasma permittivity  $\epsilon_{\text{eff}}$  and simulated E-field distributions in different points. Inset: expression between  $f_p$  and  $n_e$ ; (b) the same for the first two modes in the hairpin probe (Inset: expressions for the relations " $\epsilon_{\text{eff}} - f_{\text{hairpin}}, f_p$ "

quarter wavelength two-wire resonator, which can be relatively easily designed for TEM-mode operation [68, A27]. The open end of the structure ensures a maximum of the E field of the standing wave, which makes this resonance probe enough sensitive to the changes of the dielectric parameters of surrounding medium (e.g. effective plasma permittivity  $\epsilon_{p,\text{eff}}$ ). The opposite short end has a maximum of the H field, which allows to achieve a quite stable and reliable magnetic coupling between the resonator and the feeding coaxial cable using H-type coaxial loop probe – see Fig. 7.8. The main benefit of this method in comparison with the other methods for plasma density evaluation is the fact that the measurements are based on a determination of the resonance frequency  $f_{\text{hairpin}}$  instead of any absolute measurements of E-field magnitudes, which ensure better sensitivity, accuracy and measurement simplicity.

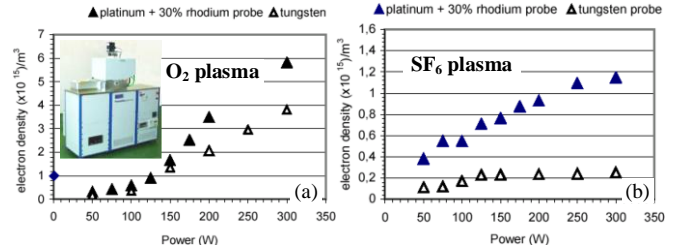


Fig. 7.11. Electron plasma density  $n_e$  versus the reactor power (W) of 100-% oxygen (O<sub>2</sub>) plasma (a) and of 100-% SF<sub>6</sub> plasma (b) at constant pressure (100 mTorr)

Fig. 7.9c illustrates the dependence of the hairpin resonance frequency  $f_{\text{hairpin}}$  on the electron plasma density  $n_e$  in a first-order approximation; similar dependence allows after calibration on air the relatively accurate determination of  $n_e$  during different plasma technological processes in vacuumed plasma reactors. The reason for existing of this dependence is the relation between the effective plasma permittivity  $\epsilon_{\text{eff}}$  and of the ratio between the plasma frequency  $f_p$  and the hairpin resonance frequency  $f_{\text{hairpin}}$  (see the inset in Fig. 7.10). In our research, we managed to determine the zone for reliable usage of this dependence (in the interval  $\epsilon_{\text{eff}} \subseteq (1, -1)$ ; see Fig. 7.10a) between the area of saturation and the fact that the sensitivity of the hairpin probe increases by using of the high-order modes (Fig. 7.10b), if they have been well identified [A35].

We developed an experimental hairpin probe [A27] for implementation in plasma reactors with aggressive gases (as in [69]) like oxygen O<sub>2</sub> and SF<sub>6</sub>. The developed probes have been incorporated in some reactors of Oxford Instruments<sup>©</sup> (see [70]). The special features of this type of hairpin probes are the type of used probe metal (Platinum + 30% Rhodium), which ensures bigger sensitivities than the conventional metals (see dependencies in Fig. 7.11) and the feeding coaxial cable filled with SiO<sub>2</sub>, which is working at relatively high temperatures in the considered plasma reactors.

#### E. Experimental Observation of Anisotropic Magneto-Dielectric Effects in a Class of Artificial Materials

In IIC, we introduced the material properties of the so-called magneto-electric materials and the possibility for their characterization. These specific materials will play increasing role as integrated tunable components in the modern microwave devices [71] due to the ability to separately control their magnetic properties by an external dc voltage and their electrical properties by an external magnetic field. However, the experimental separation of these effects is not an easy task. In our research, we already succeeded to detect magneto-dielectric effects in several artificial materials in the frequency range 2-40 GHz [A59, A63, A68]. In this paper, we will briefly describe as an example the experimental

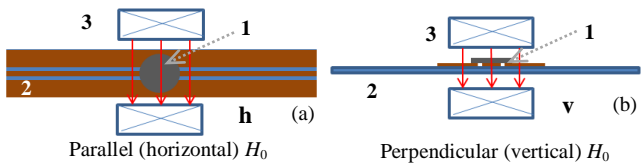


Fig. 7.12. Applied external dc magnetization of sample in parallel horizontal (a) and in perpendicular/vertical (b) direction; (c) electromagnet system. Legend: 1 – sample; 2 CPW substrate; 3 – electromagnet

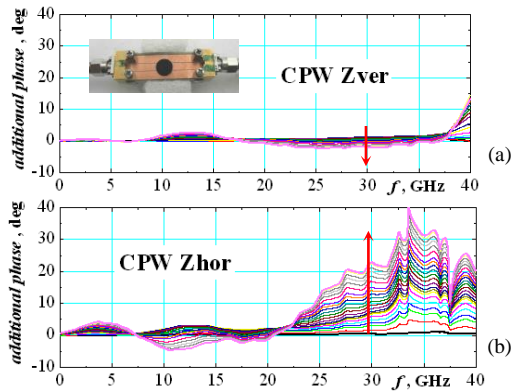


Fig. 7.13. Measured dependencies for the additional phase in CPW structure with multiferroic sample in vertical (a) and horizontal (b) magnetic field  $H_0 = 0\text{-}1.33$  kOe, normalized to values at  $H_0 = 0$  (the red arrows show the directions for  $H_0$  increasing).

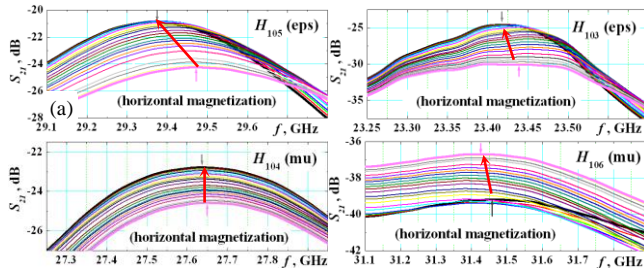


Fig. 7.14. Resonance curves of different modes in rectangular resonators (WR28) with prisms (1.22x2.07x10.16) from multi-ferroic in the centre, which have been influenced only by the dielectric (eps) (a) or magnetic (mu) (b) constants of a sample in horizontal magnetic field  $H_0 = 0\text{-}1.33$  kOe (the red arrows show the directions for  $H_0$  increasing).

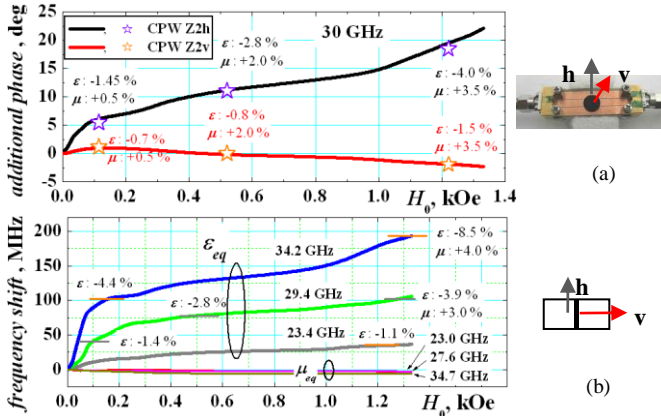


Fig. 7.15. a) Variations of the additional phase in CPW structure with multi-ferroic sample at 30 GHz v/s magnetic field  $H_0$ ; b) shift of resonance frequency of 6 TE<sub>10p</sub> modes due to magnetized multi-ferroic prism in external magnetic field  $H_0 = 0\text{-}1.33$  kOe, normalized to values at  $H_0 = 0$

verification of supposed magneto-dielectric effect in a multiferroic material Sr<sub>3</sub>Co<sub>2</sub>Fe<sub>24</sub>O<sub>41</sub> ([A60], see also VB).

In most cases, the magneto-dielectric effect in multiferroics has been measured at relatively low frequencies, (typically several hundred MHz, [72]). Only a few papers consider the characterization of this effect in the microwave range [73]. Here we describe an experimental characterization of dielectric/magnetic constants' variations of Z-type hexaferrite Sr<sub>3</sub>Co<sub>2</sub>Fe<sub>24</sub>O<sub>41</sub> in an external magnetic field. Fig. 7.12 shows the applied setup that combines measurements in the frequency range 0.01-40 GHz of CPW transmission line covered by magnetized sample by parallel or perpendicular external magnetic field  $H_0$  between 0 up to 2.4 kOe. The

samples have been directly placed on the CPW conductor and the additional losses and phases caused by the magnetized sample can be measured, when  $H_0$  increases. Fig. 7.13 a,b illustrates the differences in additional phase for  $H_0$  in both horizontal/vertical directions. The influence of the horizontal  $H_0$  is 5-6 times bigger, which clearly indicates anisotropy of the measured effect – Fig. 7.15a. However, we cannot separate in these measurements the dc magnetic field influence on the sample dielectric and magnetic constants. This information we can obtain by realized resonance perturbation measurements in a rectangular resonator with small ferrite prisms in the resonator centre. From the changes in the resonance frequencies of the excited TE<sub>10p</sub> modes (Fig. 7.14), we can separately extract the variation of the equivalent magnetic  $\mu_{eq}$  ( $p = 2, 4, 6$ ) and dielectric  $\epsilon_{eq}$  ( $p = 1, 3, 5$ ) constants of the ferroic sample. The analysis of the results in Fig. 7.15b allows us to conclude that the smaller external magnetic fields ( $H_0 \leq 0.4$  kOe) influence stronger the dielectric constant  $\epsilon_{eq}$ , while the stronger fields ( $H_0 > 0.8$  kOe) – the magnetic constant  $\mu_{eq}$ , where  $\epsilon_{eq}$  variations show a saturation. These conclusions have been confirmed by the broadband CPW measurements; see dependencies in Fig. 7.15a, where a 1.4-8.5 % variation of the material constants can be achieved in the frequency range 28-38 GHz, which is enough for possible applications as controllable delay lines. The detailed investigations of the magneto-dielectric effects in ferroic and other types of materials are still in progress [A68].

## VIII. EQUIVALENT CONDUCTIVITY OF MATERIALS

Nowadays the conductivity of materials starts to play an increasing role in the design of new RF devices, comparable with the importance of the role of the actual dielectric and magnetic parameters in the same design. The microwave engineers need to know the actual equivalent conductivity of the metals and metallization layers used in different bulk and planar devices accurately to determine the conductor losses and reflections. Moreover, today many devices are realizing with metallized injection-moulded or 3D printed dielectrics instead solid metal walls, where the equivalent conductivity depends not only on the used metal but also on the surface roughness, cleanliness, used protective layers, etc. Many new materials in modern electronics have smaller than ordinary metals but noticeable conductivity – carbon-containing materials, metasurfaces, absorbers, conductive textile fabrics, etc. In this section, we present our experience in the area of characterization of equivalent conductivity in the interval from typical values for conductive metals (e.g.  $\sim 4\text{-}6 \cdot 10^7$  S/m) up to  $10^3\text{-}10^4$  S/m by resonance methods and up to 1-10 S/m by broadband methods.

### A. Equivalent Conductivity of Metallized Plastic Samples

The nowadays technologies for creating of innovative antenna components for airborne, satellite and different 5G applications – metallized plastic details, 3D printed structures, metamaterials with metal inserts, metallized composites or textiles, etc. sharply increased the needs to characterize the actual conductivity of these materials due to the aims for more reliable 3D design. Actually, the determination of the conductivity  $\sigma_{MW}$  in the microwave range

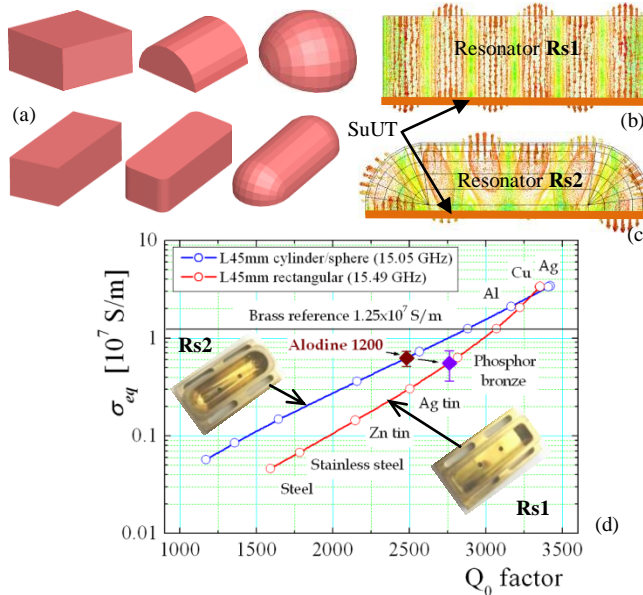


Fig. 8.1. (a) Resonators with decreasing “volume-to-bottom surface” ratio; excited  $\text{TE}_{106}$  mode in rectangular Rs1 (b) and sphere-cylindrical Rs2 (c) measurement resonators; (d) reference curves “ $\sigma_{eq}$ - $Q_0$ “ with Brass reference for determination of equivalent conductivity of surface under test (SuUT)

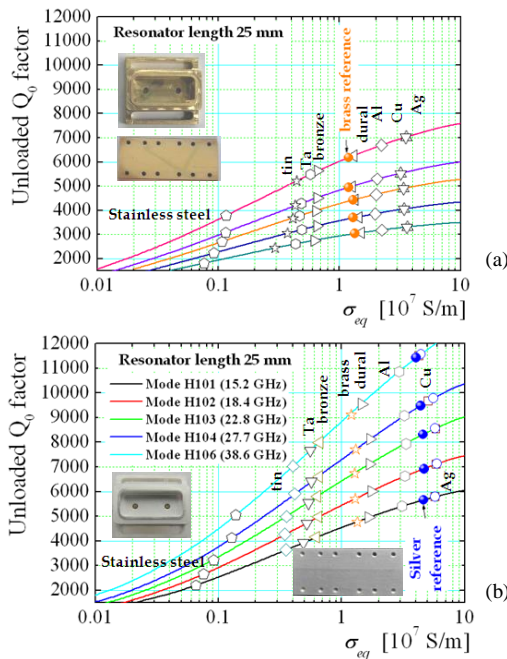


Fig. 8.2. Calibration curves “equivalent conductivity – unloaded  $Q$  factor” for the all-Brass resonator and “Brass conductivity reference” (a) and for the all-Silver resonator and “Silver conductivity reference” (b) and test values of conductivity for several known conductive materials.

(instead of the widespread dc  $\sigma_{dc}$  or optical  $\sigma_\infty$  values) is a classical problem. It is also a known fact that the so-called effective conductivity diminishes for electroplated metal surfaces [74]. It depends not only on the skin depth but additionally on the surface cleanliness, roughness, flatness, coatings, technological scratches and other surface irregularities. For this reason, we developed in [A43] an efficient microwave resonance method for determination of the useful parameter equivalent conductivity  $\sigma_{eq}$ , which better characterizes the metal surfaces in X-Ka bands and more or less differs from the dc bulk conductivity usually introduced in the 3D simulators for antenna components’

design. The idea of the method is based on the replacement of one flat surface of a selected volume resonator with the surface under test (SuUT). To increase the resonator sensitivity to the conductivity variation of SuUT, we started to search specific measuring resonators with small “volume-to-bottom surface” ratio (Fig. 8.1a). We selected two resonators – the standard rectangular resonator with excited  $\text{TE}_{10p}$  modes ( $p = 1-6$ ) (Fig. 8.1b) and a sphere-cylindrical resonator with excited similar modes (Fig. 8.1c). Applying a “Brass conductivity reference” for calibration of the measurement systems, we managed to determine with satisfying accuracy the actual equivalent conductivity  $\sigma_{eq}$  of many metallized surfaces (e.g. Alodine 1200 passivation layers over Dural surfaces; Fig. 8.1d) used in different antennas. However, the benefit of using the sphere-cylindrical measurement resonator could be minimized due to the complex E field distribution for higher modes and the “detachment” of that field from the bottom resonator wall (SuUT). Actually, the applying of a “Silver conductivity re-

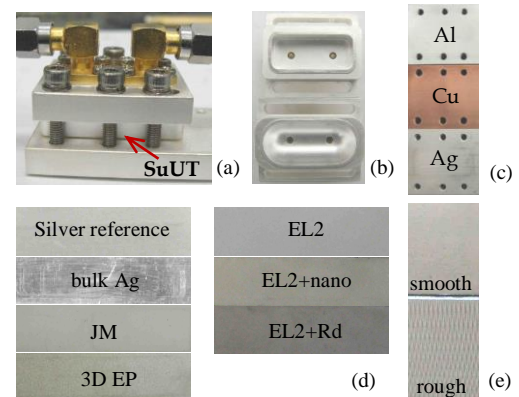


Fig. 8.3. (a) Measuring resonator with SuUT; (b) Two measuring resonators Rs1 and Rs2; (c) Reference surfaces from Al, Cu and Ag; (d) Surface view of several samples: Reference Silver EP; bulk Ag; JM – sprayed Ag nano-coating; 3D EP – electro-plated Ag on 3D printed photopolymer; EL2 – electro-less Ag; EL2+nano protective layer; EL2+Rd Rhodium protective layer; (e) smooth and rough Al surface

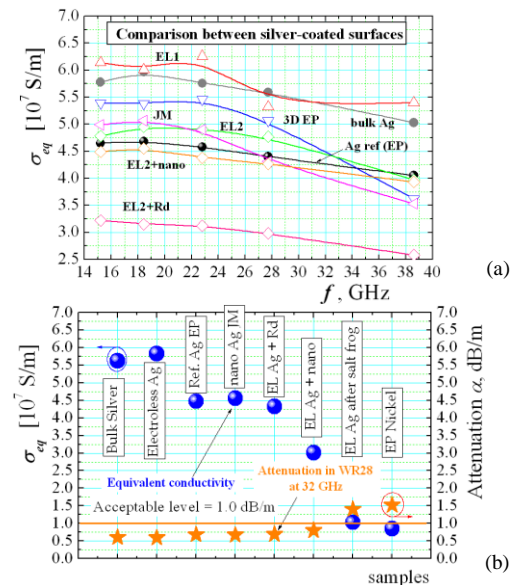


Fig. 8.4. (a) Measured equivalent conductivity  $\sigma_{eq}$  of Ag-coated samples by different technologies (see the legend in Fig. 8.3d; all Ag layers are 5-12  $\mu\text{m}$  thick); (b) Mean  $\sigma_{eq}$  (at 32 GHz) and calculated attenuation in WR28 waveguide for Ka-band for the considered samples

reference” for the measurement resonators can increase the Q factors of the excited modes twice and to additionally increase the sensitivity [A55]. The older calibration curve by the “Brass conductivity reference” covers the interval for accurate  $\sigma_{eq}$  determination from  $7.10^7$  to  $5.10^4$  S/m, while the new calibration curve by “Silver conductivity reference” covers considerable bigger interval – from  $7.10^7$  up to  $10^3$  S/m – see the set of calibration curves in Fig. 8.2. The procedure for the determination of equivalent conductivity  $\sigma_{eq}$  of SuUT is as follows. First, the unloaded Q factors of all excited TE modes have to be measured in the resonator with silver-plated walls, including the “Silver reference” as a bottom wall (instead of SuUT), Fig. 8.3a,b,c. The simulations of the 3D models for each mode (Fig. 8.1b,c) allow determining the equivalent conductivity of all resonator walls. Then the “Silver reference” has to be replaced with the corresponding SuUT and the new unloaded Q factors to be measured. The new simulations by varying the conductivity only for the SuUT allow to achieve practical coincidence between the measured and simulated Q factors and to obtain  $\sigma_{eq}$  of SuUT in the considered frequency range.

Applying this method, we succeeded to characterize the actual conductivity  $\sigma_{eq}$  of a lot of artificial metallized surfaces. First of all, we investigated the influence of the surface roughness, described by the parameter  $R_t$  – the total “peak-to-valley height” of the surface bulges. Fig. 8.3e shows two Dural surfaces: 1) “smooth” (with  $R_t < 0.05$   $\mu\text{m}$ ) and 2) “rough” (with  $R_t \sim 0.8$ - $1.6$   $\mu\text{m}$ ). We established a decrease of  $\sigma_{eq}$  with  $\sim 10$  % in Ku-band and  $\sim 25$  % in Ka-band of rough surfaces compared with the smooth surfaces of the same metal sample [A41], which proves the acceptable sensitivity of the proposed measurement method.

Fig. 8.3d illustrates the view of the top surfaces of several silver-coated plastic samples, prepared by different technology;  $\sigma_{eq}$  dependencies have been drawn in Fig. 8.4a. Acceptable values  $\sigma_{eq} = 4.6$ - $6.2$  S/m are fully realizable by electro-less (EL), electro-plated (EP) or nano-Ag-aerosols-sprayed (JM [76]) technologies. The fine surface finishing (EL1) increases the conductivity with 15-20% (EL2); the protective layers decrease  $\sigma_{eq}$  with  $\sim 10$  % (EL1 + Rhodium protective layer) or up to 35 % (EL1 + protective nanocoating). However, the importance of protective layers becomes visible in the environmental tests; an 85 % decrease of the equivalent conductivity in Ku-band was detected for pure electroless silver surface (EL1) in a salt-frog test (from 6.2 to 1.2 S/m [A55]), while the protected with Rd surface keeps value  $\sigma_{eq} \sim 4.3$  S/m. Similar measurements allow us to establish the acceptable equivalent conductivity for metallized injection-moulded or 3D printed plastics with metallization; the calculated attenuation  $\sim 1$  dB/m in WR28 waveguide for Ka-band can be satisfied for mean  $\sigma_{eq} \geq 2.5$  S/m (at 32 GHz) – see the dependencies in Fig. 8.4b.

#### B. Equivalent Conductivity of Both Sides of Metallization used for Reinforced Commercial Substrates

The determination of equivalent conductivity of copper metallization used for the microwave substrates is extremely important especially because PCB producers apply Cu folio with different roughness of both sides [76]. In the considered

in the previous section waveguide components made from metallized plastics, the losses depend on the equivalent conductivity  $\sigma_{eq}$  of the metallization top surface. Contrariwise, this role for the substrate metallization is playing from the bottom side (to the substrate) and strongly determines the transmission-line losses of printed planar structures, especially in the mm-wavelength range [77]. To minimize these losses, but to ensure acceptable adhesion of the metallization to the substrate surface, the producers apply different techniques to increase the roughness of the bottom surface, which decrease the equivalent conductivity. Our method [A55] allows accurate distinguishing of this difference – see the measured dependencies of the top and bottom sides’ conductivity  $\sigma_{eq}$  for several realistic Cu folios in Fig. 8.5a; the top surface has typically 3-5 times higher  $\sigma_{eq}$ , excepting reverse treated substrates. The reasons are well explainable. The standard technology for electro-deposited (ED) Cu folio ensures typically RMS irregularity  $R_{RMS} \sim 0.3$ - $0.4$   $\mu\text{m}$  (which better represents the surface roughness RGH) of the metal top surface (drum or resists side), while the values for the opposite backside are  $R_{RMS} \sim 1$ - $4$   $\mu\text{m}$  [76]. Only by R/A (rolled/annealed) techniques, these values can be decreased to  $R_{RMS} \sim 0.4$   $\mu\text{m}$ . The producers verified the obtained volume and surface resistivity by the IPC-TM-650 2.5.17.1 test method [78] at low frequencies. Our measurement method allows more reliable characterization of the equivalent conductivity of both metallization sides at the actual working frequencies. Fig. 8.5b shows the measured attenuation of two commercial substrates with  $Dk = 3$  with ED and LoPro® metallization and calculated values

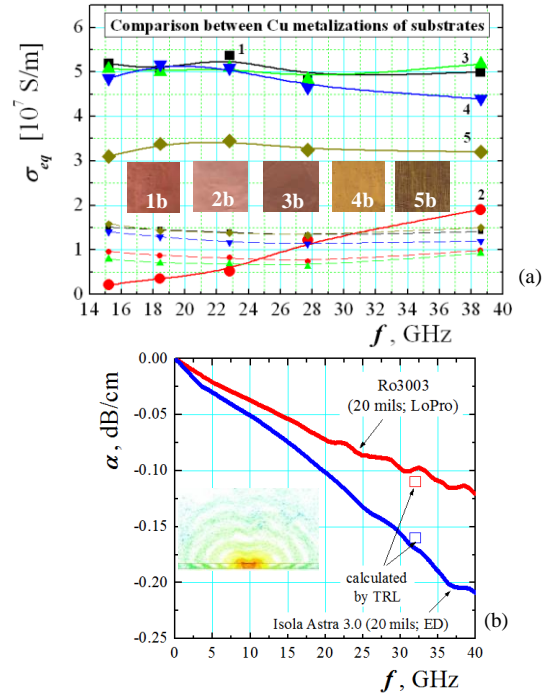
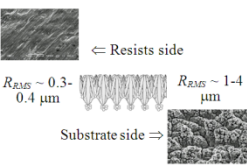


Fig. 8.5. a) Measured equivalent conductivity of copper metallization for microwave substrates; top/resist (solid curves) and bottom (dashed curves) sides (17.5- $\mu\text{m}$  thick Cu folio). Legend: 1 – Rolled/Annealed (R/A,  $R_{RMS} = 0.4$   $\mu\text{m}$ ); 2 – Reverse Treated (RTF); 3, 4 – Electro-Deposited ED with different adhesive glue; 5 – ED, additionally electro-plated (35- $\mu\text{m}$  thick). The pictures present the images of the bottom surfaces (to the substrate); b) Attenuation in 50-Ohms microstrip line on substrates with ED or LoPro® metallization, calculation by measured  $\sigma_{eq}$  (see Table 14)

Table 14. Measured equivalent conductivity  $\sigma_{eq}$  of the Copper folio for microwave substrates and calculated conductor and total losses in 50-Ohms MSL (insets: RGH of both metallization sides).

Metal type (RGH $R_{RMS}$ )	$\sigma_{eq}$ , S/m	$\alpha_C$ , dB/cm (conductor only)	$\alpha_{tot}$ , dB/cm
Ideal Cu	$5.80 \cdot 10^7$	0.041	0.065
R/A (0.4 $\mu\text{m}$ )	$5.09 \cdot 10^7$	0.044	0.067
ED LoPro (0.9 $\mu\text{m}$ )	$1.37 \cdot 10^7$	0.084	0.112
ED (2.0 $\mu\text{m}$ )	$0.63 \cdot 10^7$	0.113	0.161
RTF (1.8 $\mu\text{m}$ )	$0.79 \cdot 10^7$	0.110	0.138



at 32 GHz for the same cases by TRL calculators. The rolled/annealed (R/A) metallization used for substrates in the mm-wavelength range has better  $\sigma_{eq}$  ( $\sim 1.5 \times 10^7$  S/m) in comparison to the electro-deposited metallization ( $\sim 0.7 \times 10^7$  S/m) (Fig. 8.5a), which ensure attenuation decrease from 0.16 dB/cm to  $\sim 0.11$  dB/cm (Fig. 8.5b; Table 14).

### C. Equivalent Conductivity of Meta-Surfaces and Materials with Low Conductivity

The proposed in [A55] method for accurate characterization of equivalent conductivity even for values less than  $\sigma_{eq} < 10^5 \div 10^1$  S/m is fully applicable for different metasurfaces and materials with low conductivity. A good test of the used measurement resonators is the characterization of carbon-based samples. Fig. 8.6a shows how the measurement resonators with high Q factors allow reliable  $\sigma_{eq}$ -measurements of carbon-based samples (ordinary or carbon nanotube CNT cloths with epoxy; the CNT samples have 10 times higher  $\sigma_{eq}$   $\sim (0.2\text{-}1) \times 10^5$  S/m instead of  $\sim (0.4\text{-}1) \times 10^4$  S/m). The conductivity of the textile fabrics with different conductive fibres content is also well determinable  $\sim 10^4\text{-}5 \cdot 10^5$  S/m. Very successful could be the  $\sigma_{eq}$  characterization of meta-surfaces – a possible resonance/periodical conductivity behaviour is fully detectable and measurable for the already considered metasurface samples (compare with the dependencies for the resonance behaviour of dielectric constant in Fig. 7.1b).

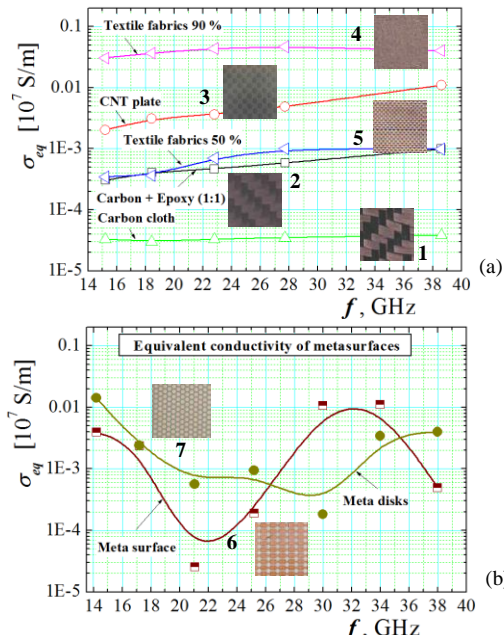


Fig. 8.6. a) Measured equivalent conductivity of low-conductive samples. Legend: 1 – pure Carbon cloth; 2 – Carbon cloth + epoxy (1:1); 3 – CNT cloth + epoxy; 4, 5 – conductive textile fabrics (90% and 50 % conductive fiber content); b) 6 – artificial metasurface; 7 – meta disks

## IX. CONCLUSIONS

In this paper, we summarize the main results from our many-years' research work devoted to the characterization of the dielectric properties of materials used in modern microwave electronics. In the first part, we prove the assumption that the well-determined complex dielectric and magnetic constants of the materials are important not only for improving the accuracy of the modern 3D design of nowadays electro-dynamic structures but also because the integral character these parameters ensure valuable information for the real material composition, structure, character of inclusions, building blocks and unit cells orientation, used technology, conditions for the material preparation, etc. We have shown that additional very useful information can be achieved when the actual anisotropy of the material constants has been determined and compared – different behaviour of their permittivity/permeability in different directions. In many standard applications (excepting usage of some metamaterials), the anisotropy of the most of artificial materials is more or less undesired properties, which decreases the accuracy for the electro-dynamic description of these materials (e.g. in the cases of reinforced substrates, wearable textile fabrics, antenna radomes, 3D printed dielectrics, etc.). However, it is important for us that nowadays most of the PCB manufacturers, EM simulators' developers and most of the material users realize the importance of the actual anisotropy of the modern materials and all of them try to solve and to take into account this property.

Our numerical models and experimental methods for characterization of the sample dielectric and magnetic properties including their anisotropy give satisfactory accuracy practically for all possible applications. The relatively full set of the implemented resonance and broadband measurement methods in our Microwave laboratory gives us the possibility for deep investigation and characterization of a variety of different materials (some of them completely new) in the nowadays electronics – microwave reinforced substrates, ceramics, multilayer composites, different dielectric mixtures, 3D printed dielectrics, textile fabrics, metamaterials, thin micro- and nano-films, carbon-containing materials, fresh and dry plant tissues, plasmas, etc.

**Acknowledgements.** The investigations have been supported by the Bulgarian National Scientific Fund under Contract No. DN-07/15/2018-19 and partially under Contract No. КП-06-Индия-7/2019 (for bent and anisotropic antenna patches and resonators and wearable antennas with metamaterials on PDMS substrates).

## REFERENCES

- [1] P. I. Dankov, *Annuaire de l'Université de Sofia "St. Kliment Ohridski", Faculté de Physique*, v. 112, 2020 (parts 1&2) (in print 2020)
- [2] P. I. Dankov, "Material Characterization in the Microwave Range, When the New Materials Become Reinforced, Composite, 3D-printed, Artificial, Nanomaterials and Metamaterials", *Asia-Pacific Microwave Conference*, Nov. 6-9, 2018, Kyoto, Japan, University Poster Exhibition, November 2018, DOI: 10.13140/RG.2.2.12158.02881
- [3] Y. Xu, Y. Fu, and H. Chen, "Electromagnetic wave propagations in conjugate meta-materials", *Optics Express*, vol. 25, no. 5, 6 March 2017, pp. 4952-4966, <https://doi.org/10.1364/OE.25.004952>

- [4] G. Singh, Rajni, A. Marwaha, "A Review of Metamaterials and its Applications", *Int. Journal of Engineering Trends and Technology (IJETT)*, vol. 19, no. 6, Jan 2015, pp. 305-310, ISSN: 2231-5381, <http://www.ijettjournal.org>
- [5] Pioneering 21<sup>st</sup> Century Electromagnetics and Photonics Laboratory, University of Texas at El Paso, College of Engineering, (Online: <http://emlab.utep.edu/research.htm>)
- [6] K. S. Cole, R. H. Cole, "Dispersion and Absorption in Dielectrics", *J. Chem. Phys.*, 9, 1941, pp. 341-351
- [7] European Commission (Directorate-General for Research, Communication Unit) (2010), "Nano-structured Metamaterials", Editor in Chief Anne F. de Baas, B-1049 Brussels, online: <http://ec.europa.eu/research/research-eu>
- [8] R. C. Rumpf, "Engineering the Dispersion and Anisotropy of Periodic Electromagnetic Structures, *Solid State Phys.* vol. 66, pp.213-300, 2015
- [9] A. Silvola, "Electromagnetic Mixing Formulas and Applications", The IEE, *Electromagnetic Waves Series 47*, 1999, London, UK
- [10] G. G. Raju, "Dielectrics in Electric Fields, Ch. 2, 2017, CRC Press, Taylor & Francis Group
- [11] A. D. Boardman, and K. Marinov, "Electromagnetic energy in a dispersive metamaterial", *Phys. Rev. B*, vol. 73, no.16, 2006, pp. 165110-1/7
- [12] P. Gay-Balmaz, O. J. F. Martin, "Electromagnetic resonances in individual and coupled split-ring resonators", *Journal of Applied Physics*, vol. 92, no. 5, 2002, pp. 2929-2936
- [13] A. Armghan, X. Hu, and M. Y. Javed, "Modeling and Simulations for Metamaterials: Emerging Research and Opportunities", *IGI Global*, 2018, DOI: 10.4018/978-1-5225-4180-6
- [14] C. R. Garcia, J. Correa, D. Espalín, J. H. Barton, R. C. Rumpf, R. Wicker, and V. Gonzalez, "3D Printing of Anisotropic Metamaterials", *PIERS Letters*, vol. 34, pp. 75-82, 2012
- [15] W.X. Jiang, J.Y. Chin and T. J. Cui, "Anisotropic metamaterial devices", *Materials Today*, vol. 12, No. 12, Dec. 2009, pp. 26-33
- [16] Handbook of Magnetic Materials, vol. 24, 2015, Ed. by K.H.J. Buschow, Ch. 3 "Advances in Magnetoelectric Materials and Their Application", <http://dx.doi.org/10.1016/bs.hmm.2015.10.001>
- [17] IPC TM-650 2.5.5.5 (1998) Test Methods Manual, <http://www.ipc.org/html/fsstandards.htm>
- [18] National Institute of Standards and Technology (NIST), USA, Reference materials, <https://www.nist.gov/mml/orm>
- [19] UK's National Measurement Institute, NPL, Electromagnetic measurements on materials, <https://www.npl.co.uk/products-services/electromagnetic-materials/>
- [20] L. F. Chen, C. K. Ong, C. P. Neo, V. V. Varadan, V. K. Varadan, "Microwave Electronics: Measurement and Material Characterization", John Wiley & Sons, Ltd., Ch. 7, 2004
- [21] J. Krupka, "Frequency domain complex permittivity measurements at microwave frequencies", *Meas. Sci. Technol.*, 17, 2006, R55–R70, doi:10.1088/0957-0233/17/6/R01
- [22] A. Gaebler, F. Goelden, S. Mueller, R. Jakoby, "Triple-Mode Cavity Perturbation Method for the Characterization of Anisotropic Media", Proc. 38<sup>th</sup> EuMC, Oct, 2008, Amsterdam, The Netherlands, pp. 909-912
- [23] W. E. Courtney, "Analysis and evaluation of a method of measuring the complex permittivity and permeability of microwave insulators," *IEEE Trans. MTT*, v. MTT-18, 8, 1970, pp. 476-485
- [24] G. Kent, "An evanescent-mode tester for ceramic dielectric substrates", *IEEE Trans. Microw. Theory Tech.*, vol. 36, no. 10, Oct. 1988, pp. 1451–1454,
- [25] M. D. Janezic and J. Baker-Jarvis, "Full-wave analysis of a split-cylinder resonator for nondestructive permittivity measurements," *IEEE Trans. Microw. Theory Tech.*, vol. 47, no. 10, pp. 2014–2020, Oct. 1999
- [26] J. Krupka, R.N. Clarke, O.C. Rochard, A.P. Gregory, "Split post dielectric resonator technique for precise measurements of laminar dielectric specimens-measurement uncertainties", Proc. 13<sup>th</sup> MIKON-2000, 22-24 May 2000, Wroclaw, Poland; DOI: 10.1109/MIKON.2000.913930
- [27] X. Zhao, C. Liu, and L. C. Shen, "Numerical analysis of a TM cavity for dielectric measurements," *IEEE Trans. Microw. Theory Tech.*, vol. 40, no. 10, pp. 1951–1958, Oct. 1992
- [28] J. Baker-Jarvis and B. F. Riddle, "Dielectric measurement using reentrant cavity", NIST, Boulder, CO, Tech. Note 1384, Nov. 1996
- [29] J. Krupka, D. Cros, M. Aubourg, and P. Giullion, "Study of whispering gallery modes in anisotropic single-crystal dielectric resonators," *IEEE Trans. Microw. Theory Tech.*, vol. 42, no. 1, pp. 56–61, Jan. 1994
- [30] G. Mumcu, K. Sertel, and J. L. Volakis, A Measurement Process to Characterize Natural and Engineered Low-Loss Uniaxial Dielectric Materials at Microwave Frequencies", *IEEE Trans. on MTT*, vol. 56, Jan. 2008, pp. 217-223, ISSN 0018-9480
- [31] A. B. Bereskin, "Microwave test fixture for determining the dielectric properties of the material", US Patent 50083088, Jan. 1992
- [32] J. C. Rautio, R. L. Carlson, B. J. Rautio, S. Arvas, "Shielded Dual-Mode Microstrip Resonator Measurement of Uniaxial Anisotropy", *IEEE Trans on MTT*, vol. 59, No. 3, pp. 748-754, March 2011
- [33] X.-C. Zhu, W. Hong, K. Wu, H.-X. Zhou, "Characterization of Substrate Anisotropy Using Substrate Integrated Waveguide Technology", Proc. *APMC'2012*, Kaohsiung, Taiwan, Dec. 2012, pp. 860-862
- [34] H. Kawabata, K. Hasuike, Y. Kobayashi, Z. Ma, "Multi-Frequency Measurements of Complex Permittivity of Dielectric Plates using Higher-Order Modes of a Balanced-Type Circular Disk Resonator", Proc. of 36<sup>th</sup> EuMC, Manchester, UK, 2006
- [35] Y. Kato, M. Horibe, "Broadband Permittivity Measurements up to 170-GHz Using Balanced-Type Circular-Disk Resonator Excited by 0.8-mm Coaxial Line", *IEEE Trans on Instrumentation and Measurement*, Volume: 68, Issue: 6, June 2019, pp. 1796-1805; DOI: 10.1109/TIM.2018.2886864
- [36] R. Sturdvant (2014), "Microwave and Millimeter-Wave Electronic Packaging", Artech House, ISBN 978-1-60807-697-0, 2014, Ch. 2
- [37] A.F. Horn III, P.A. LaFrance, J.W. Reynolds, and J. Coonrod, "The influence of test method, conductor profile and substrate anisotropy on the permittivity values required for accurate modeling of high frequency planar circuits." *Circuit World* 38, no.4, 2012, pp. 219-231
- [38] J. Coonrod, "Methods for Characterizing the dielectric constant of microwave PCB laminates", *Microwave Journal*, vol. 54, No. 5, May 2011, pp. 132-144
- [39] J. Coonrod and A. F. Horn III, "Understanding Dielectric Constant for Microwave PCB Materials", *High Frequency Design*, July 2011
- [40] E. Tuncer, "Dielectric Mixtures – Importance and Theoretical Approaches", *IEEE Electrical Insulation Magazine*, April 2013, DOI: 10.1109/MEI.2013.6648753
- [41] K. Bal, V. K. Kothari, "Permittivity of Woven Fabrics: A Comparison of Dielectric Formulas for Air-Fiber Mixture", *IEEE Transactions on Dielectrics and Electrical Insulation*, vol. 17, No. 3; 2010, pp. 881-889
- [42] Z. Li, A. Haigh, C. Soutis, A.A.P. Gibson, "X-band microwave characterization and analysis of carbon fibre-reinforced polymer composites", *Composite Structures*, 2018, DOI: 10.1016/j.comstruct.2018.09.099
- [43] Z. Li, A. Haigh, C. Soutis, A. Gibson, R. Sloan, "Dielectric constant of a three-dimensional woven glass fibre composite: analysis and measurement", *Composite Structures*, Elsevier B.V., Vol. 180, 2017, pp. 853-861
- [44] E. Tuncer, Y.V. Serdyuk, S.M. Gubanski, "Dielectric mixtures: electrical properties and modeling", *IEEE Trans. on Dielectrics and Electrical Insulation*, Vol. 9 , Issue: 5, 2002, pp. 809-828, DOI: 10.1109/TDEI.2002.103866
- [45] FR-4 Datasheets; <http://www.alldatasheet.com/datasheet-pdf/pdf/458178/FREESCALE/FR4.html>
- [46] Rogers Corp datasheet: <https://www.rogerscorp.com/acs/products/45/RO3203-RO3206-and-RO3210-Laminates.aspx>
- [47] S. J. Normyle, Application Note: The Anisotropy Of Dielectric Constant (Er) In TLY-5A Material By Bereskin", *Microwave Journal* 2006, Wireless Design Online ([http://www.taconic-add.com/pdf/technicalarticles-anisotropy\\_of\\_dielectric\\_constant\\_in\\_tly5a\\_material.pdf](http://www.taconic-add.com/pdf/technicalarticles-anisotropy_of_dielectric_constant_in_tly5a_material.pdf))
- [48] A. B. Bereskin, "Microwave test fixture for determining the dielectric properties of the material", US Patent 50083088, Jan. 1992
- [49] A. F. Horn III, P. A. LaFrance, J. W. Reynolds, and J. Coonrod, "The influence of test method, conductor profile and substrate anisotropy on the permittivity values required for accurate modeling of high frequency planar circuits." *Circuit World* 38, no.4, 2012, pp. 219-231
- [50] J. Coonrod, "Critical Aspects of Dielectric Constant Properties for High Frequency Circuit Design", *Microwave Journal* 2015, Web Seminar, Online: [www.microwavejournal.com/WebinarSlides\\_9dec15](http://www.microwavejournal.com/WebinarSlides_9dec15)
- [51] R. Salvado et. al., "Textile Materials for the Design of Wearable Antennas: A Survey", *Sensors* 2012, vol. 12, 2012, pp. 15841-15857; ISSN 1424-8220; doi:10.3390/s121115841
- [52] D.J. Kozakoff, "Analysis of Radome-Enclosed Antennas", Artech House Inc., 1997, Ch. 5
- [53] D. T. Paris, "Computer-aided radome analysis", *IEEE Trans. on Antennas and Propagation*, AP-18, pp. 7-15, Jan. 1970

- [54] J. Krupka (2006), Frequency domain complex permittivity measurements at microwave frequencies”, *IoP Publishing, Meas. Sci. Technol.* 17 R55–R70 doi:10.1088/0957-0233/17/6/R01
- [55] S. A. Ivanov, K. V. Bachev, “Measurement of the Complex Dielectric Constant, Saturation Magnetization and Linewidth of Microwave Ferrites by a Resonance Method”, *Bulg. J. Phys.* 11, 1984, pp. 513-519
- [56] P. R. Andrade, and S. P. S. Porto, “Dielectric Properties of Crystals of Order-Disorder Type”, *Annual Review of Materials Science*, 4, 287 1974, <https://doi.org/10.1146/annurev.ms.04.080174.001443>
- [57] V. G. Harris, “Modern Microwave Ferrites”, *IEEE Trans. on Magnetics* 48 No. 3, 2012, 1075-1104
- [58] M. Liang, W.-R. Ng, K.Chang, M.E.Gehm, and H. Xin, “An X-Band Luneburg Lens Antenna Fabricated by Rapid Prototyping Technology”, *IEEE MTT-S Digest 2011*, DOI: [10.1109/MWSYM.2011.5972738](https://doi.org/10.1109/MWSYM.2011.5972738)
- [59] J. Budhu, Y. Rahmat-Samii, R.E. Hodges, D.C. Hofmann, D.F. Ruffatto, K.C. Carpenter, “3D-Printed Shaped Engineered Material Inhomogeneous Lens Antennas for Next Generation Spaceborne Weather Radar Systems”, *IEEE Antenna and Wireless Prop. Letters*, v.17, No.11,2018, DOI:[10.1109/LAWP.2018.2848263](https://doi.org/10.1109/LAWP.2018.2848263)
- [60] J. Y. Cassivi, Ke Wu, Substrate integrated nonradiative dielectric waveguide, *IEEE Microwave and Wireless Components Letters*, Vol. 14 , issue 3, 2004, DOI: 10.1109/LMWC.2004.824808
- [61] S. Rondineau, M. Himdi and J. Sorieux, “A Sliced Spherical Lüneburg Lens”, *IEEE Antennas and Wireless Propagation Letters*, vol. 2, pp. 163-166, Feb. 2003
- [62] M. I. Menzel et. al., Non-invasive determination of plant biomass with microwave resonators; *Plant, Cell and Environment* 32 (2009), 368-379, doi: 10.1111/j.1365-3040.2009.01931.x
- [63] V.A. Sydoruk et. al., Design and Characterization of Microwave Cavity Resonators for Noninvasive Monitoring of Plant Water Distribution, *IEEE Trans. Microw. Theory Tech.*, MTT-64, No. 9, 2016, 2894-2904
- [64] H. O. Ali, “Review of porous anodic aluminium oxide (AAO) applications for sensors, MEMS and biomedical devices,” *Int. Journal of Surface Engineering and Coatings* 95 (6), 2017, 290-296 [doi.org/10.1080/00202967.2017.1358514]
- [65] A. M. Md Jani,D. Lasic and N. H. Voelcker, “Nanoporous anodic aluminium oxide: Advances in surface engineering and emerging applications,” *Progress in Materials Science* 58, 636–704 (2013) [<http://dx.doi.org/10.1016/j.pmatsci.2013.01.002>]
- [66] M. Dragoman et al., “The electromagnetic properties of Graphene in the microwave and millimeter-wave spectrum”, *Proc. 43rd EuMC*, 7-10 Oct 2013, Nuremberg, Germany, pp. 530-532
- [67] E. Valcheva, K. Kirilov, B. Arnaudov, N. Bundaleska, J. Henriques, S. Russev, and E. Tatarova, “Electrical conductivity of free-standing N-graphene sheets”, *AIP Conference Proceedings* 2075, 160038 (2019), <https://doi.org/10.1063/1.5091365>
- [68] R. B. Piejak, J. Al-Kuzee, and N. St. J. Braithwaite, “Hairpin resonator probe measurements in RF plasmas”, *Plasma Sources Sci. Technol.*, 14, 2005, pp.734-743
- [69] C. Scharwitz, M BoÈke, J. Winter, “Optimised Plasma Absorption Probe for the Electron Density Determination in Reactive Plasmas”, *Plasma Process. Polym.* 2008, 5
- [70] Andrew L. Goodyear, Mark Dineen, and Ligang Deng, “A Comparison of Production Plasma Etch Chemistries for InP and Related Materials”, © Oxford Instruments 2002, *Oxford Instruments Plasma Technology* (online available)
- [71] A. S. Tatarenko and M. I. Bichurin, “Microwave Magnetoelectric Devices”, *Advances in Condensed Matter Physics*, V. 2012, Hindawi Publishing Corporation, ID 286562, doi:10.1155/2012/286562
- [72] K. Ebnabbasi, Y. Chen, A Geiler, V. Harris, and C. Vittoria, “Magneto-electric effects on Sr Z-type hexaferrite at room temperature”, *J. of App. Phys.*, 111, 2012, doi: 10.1063/1.3678588
- [73] A. El Fellahi, A. Mazzamurro, J. C. Gerbedoen, Y. Dusch, O. B. Matar, P. Pernod, A. Talbi, and N. Tiercelin, “Miniaturized Coplanar Waveguide for Nanostructured Magnetostrictive Multilayer Characterization”, *MDPI Proceedings* 2018, 2, 851; doi:10.3390/proceedings2130851
- [74] A. M. Fowler, “Radio Frequency Performance of Electroplated Finishes”; *Proc. IREE Australia*, May 1970, pp. 148-164
- [75] Spray metallization by 2 aerosols in aqueous phase: <https://www.jetmetal-tech.com/technologies?lang=en>
- [76] “Copper Foils for High Frequency Materials” (2019), *Advanced Connectivity Solutions*, Rogers Corp. Chandler, AZ 85226 [www.rogerscorp.com](http://www.rogerscorp.com)
- [77] Allen F. Horn III, Patricia A. LaFrance, Christopher J. Caisse, John P. Coonrod, Bruce B. Fitts, “Effect of conductor profile structure on propagation in transmission lines,” *DesignCon2016*
- [78] IPC-TM-650 2.5.17.1 Test method “Volume and Surface Resistivity of Dielectric Materials” (metallic-clad laminates)

#### AUTHORS' REFERENCES

- [A1] S. A. Ivanov and P. I. Dankov, “Non-destructive Measurements on Ferrite Substrate Parameters”, *Proc. ISRAMIT’95*, Kiev, Ukraine, Sept. 1995, pp. 574-577
- [A2] P. I. Dankov, “Investigation of Lossy Ferrite and Semiconductor Cylinders in the mm-Wave Range”, *Proc. 13<sup>th</sup> Int. Conf. on Microwave Ferrites*, Sept. 1996, Romania, pp. 21-27
- [A3] P. I. Dankov, S. A. Ivanov, “CAD-Models for Analysis of Planar Resonance and Nonreciprocal Microwave Junctions”, *Annales de l’Université de Sofia “St. Kliment Ohridski”, Faculté de physique*, 91, 1997, pp. 5-31
- [A4] S. A. Ivanov and P. I. Dankov, “Numerical Simulation of Some Planar Microwave Gyrotropic Structures”, *Proc. 7<sup>th</sup> Int. Conf. on Mathematical Methods on Electromagnetic Theory*, Kharkov, Ukraine, June 1998, pp. 378-380
- [A5] P. I. Dankov, “Nondestructive Measurements of Gyrotropic Substrates in the cm- and the mm-Wave Range Using the Waveguide-Radial Resonator Method”, *Proc. 14<sup>th</sup> Int. Conf. on Microwave Ferrites*, Hungary, Oct. 1998, pp. 166-170
- [A6] S.A. Ivanov, P.I. Dankov, “Estimation of substrate materials for microwave application”, *2<sup>nd</sup> International Symposium of Trans Black Sea Region Applied Electromagnetism*, 2000, DOI: 10.1109/AEM.2000.943254
- [A7] P. I. Dankov, I. T. Vineshki, “Effective-Resonator Method for Nondestructive Micro-wave Measurements of Gyrotropic Materials”, *Journal of Balkan Phys. Letters*, Proc. 4<sup>th</sup> General Conf. of BPU 2000
- [A8] V. Peshlov, I. Slavkov, and P. Dankov, “Optimized Meandered Microstrip Feeds for Planar Antenna Arrays”, *Proc. European Microwave Conference*, vol. 3, EuMC-2001, Excel, London, UK, Sept. 2001, pp. 257-260
- [A9] M. Gatchev, S. Kamenopolsky, V. Boyanov, and P. Dankov, “Influence of the Milling Depth on the Microstrip Parameters in Milled PCB-Plates for Microwave Applications”, *14<sup>th</sup> Int. Conf. on Microwave, Radar and Wireless Communications MIKON’2002*, Gdansk, Poland, May 2002, pp. 189-192
- [A10] S.A. Ivanov and P.I. Dankov, “Estimation of Microwave Substrate Materials Anisotropy”, *J. Electrical Engineering*, vol. 53, No. 9s, 2002, pp. 93–96
- [A11] J. Bozmarov, R. Traykov, V. Peshlov, P. Dankov, “Application of microwave absorbers in multilayer antenna arrays”, *MIKON-2002*, v. 3, Gdansk, Poland, DOI: 10.1109/MIKON.2002.1017986
- [A12] P. Dankov, S. Kamenopolsky and V. Boyanov, “Anisotropic Substrates and Utilization of Microwave Simulators”, *14<sup>th</sup> Microcoll’2003*, Budapest, Hungary, Sept. 2003, pp. 217-220
- [A13] P. I. Dankov, “Anisotropy and Local Inhomogeneity of Dielectric Parameters of Laminated Substrates Used for Large-Size RF-Plates”, *15<sup>th</sup> Int. Conf. on Microwaves, Radar and Wireless Communications MIKON-2004*, Warsaw, Poland, May 2004, vol. 1, pp. 151-154
- [A14] V. Peshlov, S. Alexandrov and P. Dankov, “Numerical Simulations of Multilayer Radome with Anisotropic Materials”, *15<sup>th</sup> Int. Conf. on Microwaves, Radar and Wireless Communications MIKON-2004*, Warsaw, Poland, May 2004, vol. 2, pp. 562-566
- [A15] P. I. Dankov, S. M. Kolev and S. A. Ivanov, “Measurement of Dielectric Properties of Thin Nanoparticle Absorbing Films”, *17<sup>th</sup> Int. Conf. on Electromagnetic Fields and Materials EMFM-2004*, Warsaw, Poland, May 2004, pp. 89-93
- [A16] I. Nedkov, S. Kolev, P. Dankov, S. Alexandrov, “Polymer Microwave Absorber with Nanosized Ferrite and Carbon Fillers”, *Proc. IEEE Int. Spring Seminar on Electronics Technology 27<sup>th</sup> ISSE 2004*, Sofia, Bulgaria, May 2004, pp. 577-579
- [A17] P. I. Dankov, and S. A. Ivanov, “Two-Resonator Method for Measurement of Dielectric Constant Anisotropy in Multi-Layer Thin Films, Substrates and Antenna Radomes”, *34<sup>th</sup> European Microwave Conference*, Amsterdam, Holland, Oct. 2004, pp. 753-756
- [A18] P. I. Dankov, V. P. Levcheva, and V. N. Peshlov, “Utilization of 3D Simulators for Characterization of Dielectric Properties of Anisotropic Materials”, *35<sup>th</sup> European Microwave Conference*, Paris, France, Oct. 2005, pp. 515-519

# Forum for Electromagnetic Research Methods and Application Technologies (FERMAT)

- [A19] V. N. Peshlov, P. I. Dankov, B. Hadjistamov, "Models of Multilayer Antenna Radomes with Anisotropic Materials", *1<sup>st</sup> European Conference on Antennas and Propagation EuCAP'2005*, France, Nice, November 2005, No. 349840PD
- [A20] P. I. Dankov, B. Hadjistamov, and V. P. Levcheva, "Principles for Utilization of EM 3D Simulators for Measurement Purposes with Resonance Cavities", *Proc. IVth Mediterranean Microwave Symposium (MMS'2006)*, Genoa, Italy, Sept. 19-21, 2006
- [A21] P. I. Dankov, "Two-Resonator Method for Measurement of Dielectric Anisotropy in Multi-Layer Samples", *IEEE Trans. Microwave Theory Tech.*, MTT-54, April 2006, pp. 1534-1544
- [A22] B. N. Hadjistamov, V. P. Levcheva, and P. I. Dankov, "Dielectric Substrate Characterization with Re-Entrant Resonators", *Proc. Vth Mediterranean Microwave Symposium (MMS'2007)*, Budapest, Hungary, May 14-16 2007, pp. 183-186
- [A23] P. I. Dankov, V. P. Levcheva, and I. I. Arestova, "Two-Resonator Method for Characterization of High-Permittivity Dielectric and Ferrite Substrate", *Proc. ICMF'2007*, Budapest, Hungary, May 20-21, 2007, pp. 27-30
- [A24] P. I. Dankov and B. Hadjistamov, "Characterization of Microwave Substrates with Split-Cylinder and Split-Coaxial-Cylinder Resonators", *37<sup>th</sup> European Microwave Conference*, Munich, Germany, Oct. 2007, pp. 933-936
- [A25] P. I. Dankov, V. N. Peshlov, M. Gachev, "Modeling and Characterization of Multi-layer Antenna Radomes with Anisotropic Materials", *30<sup>th</sup> ESA Antenna Workshop on Antennas for Earth Observation, Telecommunications and Navigation Space Missions*, 27-30 May 2008 in Nordwijk, The Netherlands, pp. 505-508 (invited COST paper)
- [A26] V. P. Levcheva, B. N. Hadjistamov, P. I. Dankov, "Two-Resonator Method for Characterization of Dielectric Substrate Anisotropy", *Bulg. J. Phys.*, 35 (2008), pp. 33-52
- [A27] P. Dankov, P. Stefanov, V. Gueorguiev, T. Ivanov, "Hairpin-Resonator Probe and Measurement Considerations", *Journal of Physics, Conference Series*, 2008, pp. 202-209
- [A28] V. P. Levcheva, I. I. Arestova, B. R. Nikolov, and P. I. Dankov, "Characterization and Modeling of Microwave Absorbers in the RF and Antenna Projects", *Telfor Journal*, Vol. 1, No. 2, 2009, pp. 57-60
- [A29] S. R. Baev, B. N. Hadjistamov, and P. I. Dankov, "Lüneburg Lenses as Communication Antennas", *Annuaire de l'Université de Sofia "St. Kliment Ohridski"*, Faculté de Physique, 102, 2009, pp. 67-84
- [A30] P. Dankov, B. N. Hadjistamov, I. Arestova, and V. Levcheva, "Measurement of Dielectric Anisotropy of Microwave Substrates by Two-Resonator Method with Different Pairs of Resonators", *PIERS online*, vol. 5, No. 6, October 2009, pp. 501-505
- [A31] P. I. Dankov, "Dielectric Anisotropy of Modern Microwave Substrates", *Chapter 4 in "Micro-wave and Millimeter Wave Technologies from Photonic Bandgap Devices to Antenna and Applications"*, ed. by Igor Minin, In-Tech Publ., Austria, Jan. 2010, ISBN 978-953-7619-66-4
- [A32] P. I. Dankov, M. I. Kondeva, and S. R. Baev, "Influence of the Substrate Anisotropy in the Planar Antenna Simulations", ISBN: 978-1-4244-4883-8, *iWAT Conference*, Lisbon, Portugal, March 2010, DOI 10.1109/iWAT.2010.5464930
- [A33] K. Zlatkov, P. Dankov, "Detection and Reduction of EMC Problems in Microwave Antenna Feed Elements", *Microwave Review*, December 2011, ISSN 14505835, UDK 621.3.049.77, pp. 29-35
- [A34] B. N. Hadjistamov, P. I. Dankov, "Measurement of Dielectric Substrate Parameters Using Split-Post Dielectric Resonator", *Bulg. J. Phys.* 38, 2011, pp. 191-198
- [A35] P. Dankov, Z. Kiss'ovski, "Hairpin Probe Sensitivity for Determination of Plasma Density", *The XXI ESCAMPIG*, Viana do Castelo, Portugal, July 10-14 2012
- [A36] P. I. Dankov, "Material Characterization in the Microwave Range Assisted by 3D Simulators – A Modern Solution", *2<sup>nd</sup> National Congress on Physical Sciences*, Sofia, Bulgaria Sept. 2013
- [A37] P. I. Dankov, "Microwave measurement of electrical fields in different media – principles, methods and instrumentation", *Journal of Physics: Conference Series* 516 (2014) 012001 doi:10.1088/1742-6596/516/1/012001
- [A38] R. B. Borisov, K. I. Zlatkov, and P. I. Dankov, Near-field measurements using low-cost equipment for RF device characterization", *E+E Journal*, vol. 49, No. 3-4, 2014, pp. 7-12
- [A39] M. Gachev, V. Boyanov, S. Kamenopolsky, V. Peshlov, B. Marinov, and P. Dankov (2014), "On-the-Move Antenna Systems for Broad-Band Satellite Communications", DOI: 10.1109/EuCAP.2014.6902312, *8<sup>th</sup> European Conference on Antennas and Propagation (EuCAP'2014)*, The Hague, The Netherlands, 6-11 April 2014
- [A40] P. Dankov, V. Peshlov, and T. Amla, "Concept for Equivalent Dielectric Constant and Dielectric Anisotropy of Microwave Substrates and Their Applicability in the Antenna Projects", *8<sup>th</sup> Management Committee Meeting and Workshop*, Sofia, Bulgaria, Sofia University, Aula Magna, May, 18-21.05.2015
- [A41] P. Dankov, S. Kamenopolski, V. Peshlov, R. Traykov, "Determination of Surface Conductance of Metallized Plastic Antenna Elements in Ka Band", *9<sup>th</sup> Global Symposium on Millimeter Waves GSMM2016 7th ESA Workshop on Millimetre-Wave Technology and Applications*, June 6-8, 2016, Aalto University, Espoo, Finland
- [A42] P. I. Dankov, "Concept for Equivalent Dielectric Constant of Planar Transmission Lines on Anisotropic Substrates", *European Microwave Week, EuMC'2016*, London, 3-7 October 2016 pp. 158-161
- [A43] M. Gachev, and P. Dankov, „Low Profile Tracking Ground Station Antennas and Antenna Arrays for Satellite Communications“, NSS-07-0601, *7th Nano-Satellite Symposium and 4th Unisec-Global Meeting*, Hotel “Longoz” Sports and Wellness Resort “Kamchia”, Bulgaria, October 18-23, 2016
- [A44] P. I. Dankov, "A Method for Determination of Equivalent Dielectric Constant of Planar Transmission Lines on Anisotropic Substrates with Dielectric Overlay", *Int. Workshop on Antenna Technology iWAT2017*, Athens, 1-3March 2017, pp.61-64
- [A45] P. I. Dankov, "A Method for Determination of Equivalent Dielectric Constant of Planar Transmission Lines on Anisotropic Substrates with Dielectric Overlay"; *FERMAT*, Vo. 22, Communication 9, Jul.-Aug., 2017; <https://www.e-fermat.org/communication/dankov-comm-iwat2017-2017-vol22-jul-aug-009> (see [A41])
- [A46] P. I. Dankov, „Problems with Reliable 3D Simulations of Microstrip Lines on Anisotropic Substrates“, *Proc. IEEE MTT-S International Conference on Numerical Electromagnetic and Multiphysics Modeling and Optimization for RF, Microwave, and Terahertz Applications (NEMO)*, May 2017; DOI: 10.1109/NEMO.2017.7964199
- [A47] P. I. Dankov, „Uniaxial Anisotropy Estimation of the Modern Artificial Dielectrics for Antenna Applications“, *Proc. IEEE MTT-S Int. Microwave Workshop Series on Advanced Materials and Processes*, Pavia, Italy, 20-22 September 2017
- [A48] P. I. Dankov, "Characterization of Dielectric Anisotropy of Small Samples from Plant Fresh and Dry Biomass by Microwave Resonance Method", *Proc. 47<sup>th</sup> European Microwave Conference*, 10-12 October 2017, Nuremberg, Germany, pp. 954-957
- [A49] P. I. Dankov, M. I. Tsatsova, and V. P. Levcheva, "Investigation of Uniaxial Dielectric Anisotropy of Textile Fabrics and Its Influence over the Wearable Antennas' Behaviour", *Proc. of PIERS'2017*, Singapore, 19-22 Nov. 2017
- [A50] P. I. Dankov, and I. I. Iliev, "Characterization and Modeling of Gradient-Carbon Absorber Layers Suitable for Radar Cross Section Reduction of UAVs", *Proc. of PIERS'2017*, Singapore, 19-22 Nov. 2017
- [A51] P. I. Dankov, "Experimental Characterization of Positive and Negative Dielectric Constants and Artificial Anisotropy of Metamaterials in the Microwave Range", *8<sup>th</sup> Int. Workshop and Summer School on Plasma Physics (IWSPP'2018)*, Kiten, Bulgaria, (invited paper, online); *Journal of Physics: Conf. Series*, IOP Publishing, 2020
- [A52] P. I. Dankov, "Characterization of Dielectric Properties, Resultant Isotropy and Anisotropy of 3D Printed Dielectrics", *Proc. 48<sup>th</sup> EuMC*, Madrid, Spain, Sept. 2018
- [A53] V. Levcheva, P. Dankov, "Measurement of Uni- and Bi-Axial Dielectric Anisotropy of Crystalline Samples by Microwave Resonance Method", *Bulg. J. Phys.*, v. 45 (2018), pp. 264-274
- [A54] P. Dankov, V. Levcheva, and M. Iliev, "Practical Isotropy and Anisotropy of 3D Printed Artificial Foam-Like Dielectrics with Antenna Applications", *Metamaterials'2018 (12th International Congress on Artificial Materials for Novel Wave Phenomena)*, Espoo, Finland, 27-31 Aug. 2018
- [A55] P. Dankov, R. Traykov, V. Peshlov, and S. Kamenopolski, "Equivalent Conductivity Characterization of Silver-Coated Plastic Antenna Components in Ku, K and Ka Bands", *Asia-Pacific Microwave Conference APMC2018*, November 6-9 2018, Kyoto, Japan
- [A56] P. I. Dankov, M. T. Iliev, V. P. Levcheva, "Biaxial dielectric anisotropy of crystalline materials and its characterization by resonance

- microwave methods”, *Bulgarian Chemical Communications*, Vol. 50 (Special Issue F), December 2018, pp. 126-134
- [A57] M. Gachev, and P. Dankov, „Microwaves in Bulgaria”, *1<sup>st</sup> European Microwave Conference in Central Europe*, 13-15 May 2019, Prague , Czech Republic)
- [A58] P. Dankov; B. Tzaneva; V. Videkov, “Microwave characteristics of thin Al<sub>2</sub>O<sub>3</sub> membranes as metasamples for optical applications”, *SPIE Conference Proceeding*, Proceedings Volume 11332, International Conference on Quantum, Nonlinear, and Nanophotonics (ICQNN 2019)
- [A59] P. I. Dankov, “Characterization of Dielectric Properties of Conductive Materials by Coplanar Waveguide Method”, *IEEE 19th Mediterranean Microwave Symposium*, Tunisia, Nov.2019, IEEE Xplore DOI: 10.1109/MMS48040.2019.9157262
- [A60] P. Dankov, S. Kolev, T. Koutzarova, “Dielectric and magnetic properties of hexaferrite Sr<sub>3</sub>Co<sub>2</sub>Fe<sub>24</sub>O<sub>41</sub> thin samples in the microwave range”, *VIET2019*, Sept. 2019, Sozopol, Bulgaria, IOP Publishing, *J. Phys.: Conf. Ser.* 1492 (2020) 012048; doi:10.1088/1742-6596/1492/1/012048
- [A61] P. Dankov, V. Levcheva, S. Kolev, and T. Koutzarova, “Characterization of multilayer nano-absorbers”, *VIET2019*, Sept. 2019, Sozopol, Bulgaria IOP Publishing, *J. Phys.: Conf. Ser.* 1492 (2020) 012047; doi:10.1088/1742-6596/1492/1/012047
- [A62] P. Dankov, V. Levcheva, P. Sharma, “Influence of Dielectric Anisotropy and Bending on Wearable Textile Antenna Properties”, *iWAT2020*, Feb. 2020, Bucharest, Romania, Available: IEEE Xplore
- [A63] P. Dankov (2020), “Anisotropy of artificial materials and how to characterize it” - *COST Action CA18223 SyMat Meeting* – Prague, Feb. 2020 (online)
- [A64] P. K. Sharma, N. Gupta, and P. I. Dankov, “Wideband Transmission Line Characterization of Polydimethylsiloxane (PDMS) as a Wearable Antenna Substrate”, *IEEE CONECCT’2020*, July 2-4 2020, Bangalore, India (virtual); Available: IEEE Xplore
- [A65] P. Dankov, Y. Zhelev, and I. Slavkov, “Problems with Antenna Radome Behaviour at Low Elevation Directions”, Proc. *XI National Conference with International Participation "Electronica 2020"*, July 23-24, 2020, Sofia, Bulgaria (virtual), Available: IEEE Xplore
- [A66] P. Dankov, V. Levcheva, and M. Iliev, “Characterization of Dielectric Anisotropy of Reinforced Substrates at Different Temperatures”, Proc. *XI National Conference with International Participation "Electronica 2020"*, July 23-24, 2020, Sofia, Bulgaria (virtual), Available: IEEE Xplore
- [A67] V. Levcheva, and P. Dankov, “Characterization of Microwave Absorbers, Including Multilayer Nanoabsorbers”, Proc. *22<sup>nd</sup> Int. Conf. MM&T2020*, 29 Aug. - 1 Sept. 2020, Burgas, Bulgaria (to be published in *Journal of Materials, Methods & Technologies* (ISSN 1314-7269)
- [A68] P. Dankov, and V. Levcheva, “Investigation of Artificial Meta-materials and Multilayer Nanocomposites in External Magnetic Field”, Proc. *22<sup>nd</sup> Int. Conf. MM&T2020*, 29 Aug. - 1 Sept. 2020, Burgas, Bulgaria (to be published in *Journal of Materials, Methods & Technologies* (ISSN 1314-7269)
- [A69] N. Gupta, P. Sharma, P. Dankov, “Characterization of Polydimethylsiloxane (PDMS) as a Wearable Antenna Substrate using Resonance and Planar Structure Methods”, *International Journal of Electronics and Communications*, AEUE\_2020\_1595, 2020 (accepted)
- [A70] P. I. Dankov, P. K. Sharma, and N. Gupta, “Characterization of Polydimethylsiloxane (PDMS) as a Flexible Polymer Substrate for Wearable Antennas and Sensors”, *IEEE Trans. Antennas Propag.*, (prepared for submission, Sept. 2020)
- [A71] P. I. Dankov, P. K. Sharma, and N. Gupta, “Numerical and Experimental Investigation of the Competitive Impacts of Dielectric Anisotropy and Substrate Curvature on Planar Radiators and Sensors”, *Sensors 2020*, (prepared for a special edition, Nov. 2020)



Plamen I. Dankov is an Assoc. Professor in Faculty of Physics, Sofia University, Bulgaria and materials' characterization consultant of several international companies. His educational activities are in the area of microwave and wireless technique, microwave measurements, antennas, aerospace engineering. He is a chair of two MSc programs in the area of Wireless networks and devices and Aerospace engineering and communications. His research interests include microwave material characterization, microwave gyroscopic devices, antenna and antenna arrays, EMC problems, microwave measurements, 3D electromagnetic simulations, small satellites, etc. He has more than 150 scientific and popular publications and 3 books in these areas. Dr. P. Dankov is IEEE Member in 4 Societies: MTT, A&P, I&M, Aerospace. He was a member of General Assembly of EuMA and representative of Group 8 (2013-2016). He is a POC of UNISEC Global in Japan and Secretary of UNISEC Bulgaria in the area of University small satellites.